Monitoring the dynamics of the Agulhas Current System off Port Edward, Kwazulu-Natal.

By

Gavin Shaun Louw

Thesis submitted in fulfilment of the requirements for the degree

Master of Technology: Oceanography

in the Faculty of Applied Sciences

at the Cape Peninsula University of Technology

Supervisor:

Associate Professor Mike Roberts

Co-supervisor:

Dr Conrad Sparks

Cape Town

Date submitted: October 2014

Table of Contents

Declaration

I, Gavin Shaun Louw, declare that the contents of this thesis represent my own unaided work, and that the thesis has not previously been submitted for academic examination towards any qualification. Furthermore, it represents my own opinions and not necessarily those of the Cape Peninsula University of Technology.

_____   _____

Signed   **Date**

Abstract

In order to validate remote sensing products and to provide data for model assimilation, a real-time monitoring line consisting of three moorings was deployed across the Agulhas Current off Port Edward, South Africa. This deployment formed part of a Technology and Human Resource for Industry Programme (THRIP) funded initiative to develop a real-time mooring system capable of measuring ocean parameters in the Agulhas Current during 2011.

The slope and offshore moorings displayed a distinct stratified regime within the Agulhas Current, a northeastward flowing Agulhas Undercurrent and the southwestward flowing Agulhas Current. Three major reversal events, with northeastward currents occurred on 23 July, 02 September and on 11 October 2011. All current reversals caused a decrease in current velocity. The Agulhas Undercurrent was a persistent feature and average velocities between the line of moorings ranged between 13.38 cm/s and 15.52 cm/s. The results obtained from the mooring systems were consistent in terms of velocity, direction and hydrographic properties of the Agulhas Current as described in previous literature. The low directional variability in the surface layers at the offshore mooring and dominant southwestward flow, except during reversal events indicate the strong influence of the Agulhas Current in this region. The inshore mooring showed less occurrences of the Agulhas Undercurrent if northward flow in the bottom layers was to be considered as signs of the Agulhas Undercurrent.

General current characteristics as well as the characterisation of the mesoscale features affecting the coast off Port Edward was accomplished through the use of the *in situ* moorings. All current reversals encountered were associated with the process of vortex shedding from the Natal Bight. These events may be related to the shedding of the Durban Cyclonic Eddy from its origin in the Natal Bight. Data from the offshore mooring suggested that for monitoring Agulhas Current core dynamics, it was ideally placed as highest surface velocities were measured by this mooring system. The slope mooring recorded highest velocities within the Agulhas Undercurrent and was thus ideally placed to measure the Agulhas Undercurrent's core. Shelf dynamics were under the influence of the Agulhas Current and northerly current reversals and were aptly recorded by the inshore mooring which was placed on the continental shelf, close to the shelf break.

Acknowledgements

List of Figures

List of Abbreviations

AAIW: Antarctic Intermediate Water

ADCP: Acoustic Doppler Current Profilers

AADW: Antarctic Deep Water

AUCE: Agulhas Undercurrent Experiment

CCAR: Colorado Centre for Astrodynamic Research

CNES: Centre National d'etudes spatiales (National Centre for Space Studies)

CTD: Conductivity Temperature Depth

DT: Delayed Time

DVS: Doppler Volume Samplers

Envisat: Environmental satellite

IMOS: The Integrated Marine Observing System

INCOIS: Indian National Centre for Ocean Information Systems

IndOOS: Indian Ocean Observing System

ITSW: Indian Tropical Surface Waters

MRSU: The Marine Remote Sensing Unit

MSLA: Mean Sea Level Anomaly

NADW: North Atlantic Deep Water

NIDW: North Indian Deep Water

NRF: National Research Foundation

ODV: Ocean Data View

RAMA: The Research Moored Array for African – Asian – Australian Monsoon Analysis and
        prediction

RSW: Red Sea Water

S-ADCP: Ship-mounted Acoustic Doppler Current Profiler

SAR: Synthetic Aperture Radar

SAR-Africa: Synthetic Aperture Radar for Africa

SICW: South Indian Ocean Central Water

SISSW: South Indian Subtropical Surface Water

SOTN: The Seychelles Ocean Temperature Network

SSHA: Sea Surface Height Anomaly

SST: Sea Surface Temperature

Sverdrup (Sv): Measurement of volume transport – i.e. 15 x 106 / m^3 = 15 Sv

SWIO: South Western Indian Ocean

THRIP: Technology and Human Resource for Industry Programme

T-S: Temperature-Salinity

TSW: Tropical Surface Water

UTR: Underwater temperature recorder

WIOCOS: Western Indian Ocean Coastal Observing System

Chapter 1: Introduction

1.1 Background

The Agulhas Current is a western boundary current of the Indian Ocean subtropical gyre, flowing in a southwestward direction along the east coast of South Africa. This current exhibits remarkable stability, compared to the Kuroshio and Gulf Stream, for such a swift flowing western boundary current. The Agulhas Current has been extensively studied in the past (Harris, 1972; Biastoch & Krauss, 1999; Lutjeharms *et al.*, 2001; Lutjeharms, 2006). Its general flow characteristics, volume transport, benthic structure, chemical composition and biological nature have all been well documented by numerous authors (Meyer *et al.*, 2002; Bryden *et al.*, 2005; Lutjeharms, 2007; Vousden *et al.*, 2008). A new challenge facing regional scientists and engineers is to constantly monitor changes and predict conditions within the oceanic environment in real-time.

The oceanic environment is inhospitable, harsh and unrelenting, making the need to monitor and forecast of utmost importance. Economic, commercial, fisheries and environmental management, disasters, maintaining the safety of vessels at sea and people in coastal environments and weather predictions are some of the more important activities requiring regular and reliable ocean monitoring (Roberts *et al.*, 2011). The major difficulty in ocean-state prediction is the complexity of the various spatial and temporal scales driving the variability in the regional and coastal environment (Veitch and Backeberg, 2011). The high cost and dangers involved in going to sea makes it almost impossible to completely and comprehensively cover the entire ocean, even on a regional scale, with *in situ* monitoring platforms. By deploying *in situ* platforms at key locations and inserting these data sets into numerical models, interpolation generated in these models may overcome the spatio-temporal limitations of sampling the ocean through ship-based operations. Numerical models have now become major tools in operational oceanography (Hoguane, 2011; Veitch and Backeberg, 2011). The goal of disseminating ocean forecasts generated through the use of ocean models is to ultimately generate general interest in the state of the ocean to the same level to that of meteorological weather forecasts (Veitch and Backeberg, 2011).

A combination of multi-parametric, real-time measurements and numerical models are needed to produce suitable forecast products for the end-user (Nittis *et al.*, 2006). According

to Rao *et al*., (2008), the availability of real-time ocean data is important for decision support systems that provide oceanic information and advisory services for climate predictability, both in the short- and long-term. To produce oceanographic data at near real-time (or 'now-time') rates requires many interlinking systems and processes to be integrated and function as a whole. Figure 1.1 illustrates the processes involved in displaying oceanographic measurements in real-time to the end-user. *In situ* data such as current velocity and direction are collected by an array of instruments, e.g. Acoustic Doppler Current Profilers (ADCP's) and Doppler Volume Samplers (DVS's), providing scientists with real-time oceanic measurements. These data sets are analysed and error checked in order to be inserted into numerical models for ocean state prediction purposes (Figure 1.1). The level of acceptance of these predictions by society is highly dependent on the accuracy of the *in situ* data and by the accuracy of the predictions obtained from numerical model analysis.
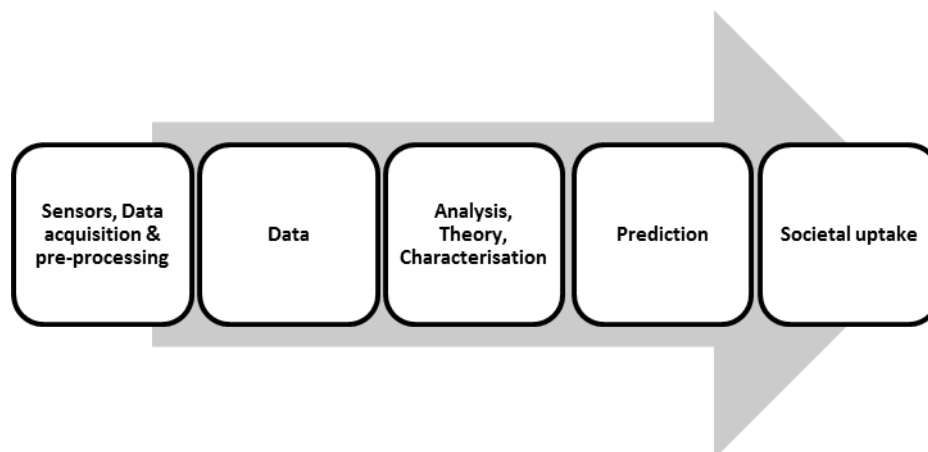
Figure 1.1: The processes involved in developing an operational forecast end-user product**.**

Decreasing the gap between modelled outputs and the true state of the oceanic system requires many *in situ* and/or remotely sensed data sources. Currently, numerous international and regional sampling and monitoring initiatives are operational within the Indian Ocean (Rao *et al.,* 2008; McPhaden, 2009; McPhaden *et al.*, 2009; Robinson *et al.*, 2009). Some of these monitoring projects within the Indian Ocean and their area of coverage are presented in Figure 1.2. According to McPhaden (2009), the major research topics that drive the operational undertakings in the Indian Ocean are listed as the following:

a) Seasonal monsoons

b) Severe weather events and cyclones

c) Intraseasonal Madden Julian Oscillations

d) Interannual variations affecting the Indian Ocean Dipole

e) Decadal variability within the Indian Ocean and warming trends
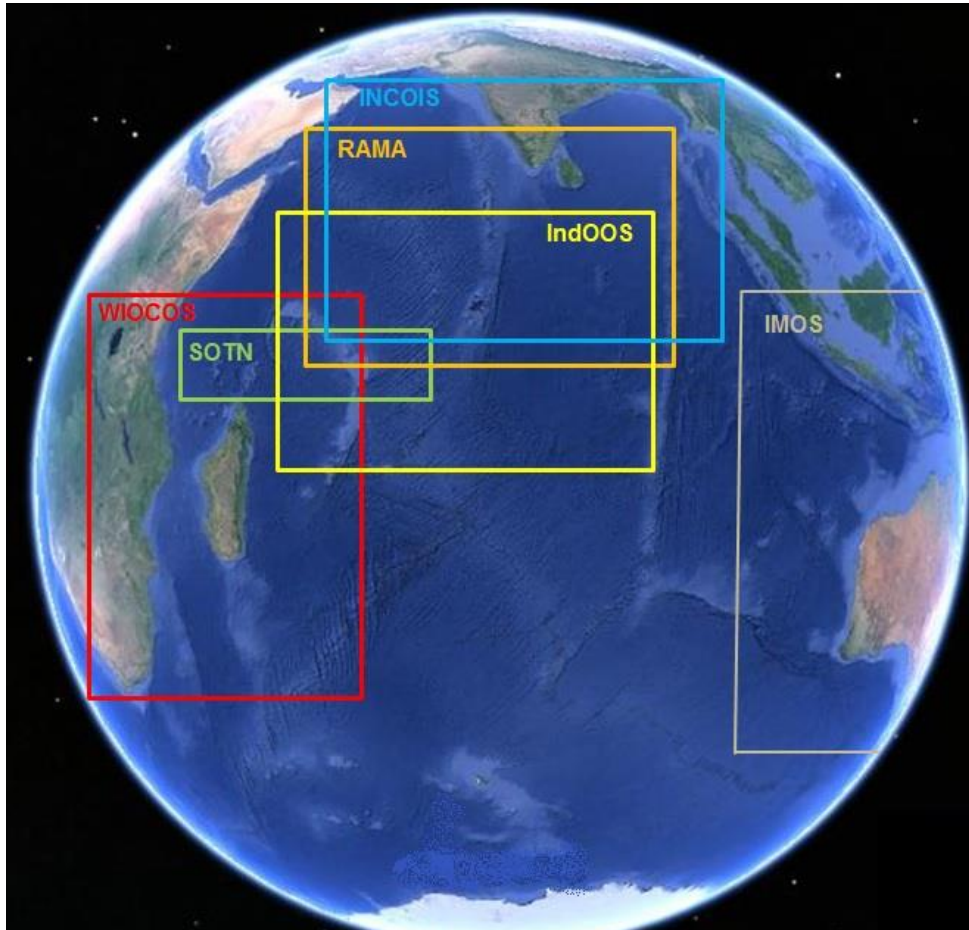
Figure 1.2: Multi-national monitoring projects within in Indian Ocean:

━ Western Indian Ocean Coastal Observing System (WIOCOS)

━ The Seychelles Ocean Temperature Network (SOTN)

━ The Research Moored Array for African – Asian – Australian Monsoon Analysis and Prediction (RAMA)

━ Indian Ocean Observing System (IndOOS)

━ Indian National Centre for Ocean Information Systems (INCOIS)

━ The Integrated Marine Observing System (IMOS)

The Western Indian Ocean Coastal Observing System (WIOCOS) (Figure 1.2) was started in 1990 using simple self-recording underwater temperature recorders (UTR's) attached to a 70 kg cement block. This monitoring project has grown and now covers the region between Kenya, the Seychelles and South Africa in the south western Indian Ocean. Due to the

difficulties of maintaining moorings in strong, deep currents such as the Agulhas Current, many attempts have been made to develop remotely sensed technology to measure current speed and direction. The latest form of satellite measurement technology utilizes radar signals to measure ocean roughness (Rouault *et al.*, 2009). The Marine Remote Sensing Unit (MRSU) at the University of Cape Town piloted a programme known as SAR-Africa (Synthetic Aperture Radar for Africa) which aims to develop a sustainable research and operational capacity for marine synthetic aperture radar applications in southern Africa (Rouault *et al.*, 2009). The SAR sensor, situated on Envisat (Environmental satellite), measures the ocean's surface roughness and provides information on wind, waves, currents, surface films (such as oil spills) and sea ice. These oceanic features detectable by SAR-Africa may prove to be invaluable as an operational tool, as they allow for the detection of oil spills, ship surveillance, sea-state monitoring and storm predictions.

1.2   Rationale and key questions

The SAR-Africa programme requires validation of satellite sensors and improvement of algorithms (Rouault *et al.*, 2009), and therefore requires *in situ* surface velocity and direction measurements to be collected and transmitted in real-time (Figure 1.3). The more *in situ* data points available for model assimilation, the greater the accuracy of the model predictions. Although these moorings do not measure the surface currents, combining *in situ* observations with satellite data and ocean models creates a comprehensive 3D picture of the ocean, thereby advancing our knowledge of oceanographic processes. Port Edward is situated on one of the ground tracks of Envisat and by deploying an *in situ* platform here, it would act as a point of reference for the remotely sensed oceanic currents. In order to validate the remote sensing products and to provide data for model assimilation, a real-time monitoring line consisting of three moorings was deployed across the Agulhas Current off Port Edward, South Africa. This project formed part of the National Research Foundation (NRF) project as part of the Technology and Human Resource for Industry Programme (THRIP) to stimulate innovation in South Africa and was an initiative to develop a real-time mooring system capable of measuring ocean parameters in the Agulhas Current. This line of moorings off Port Edward will aid in increasing the operational capacity of South Africa, adding to the collective understanding of the Indian Ocean on a regional and basin scale.

Accurate characterization of the measurements provided by these moorings is paramount for societal uptake and future scientific endeavours. For this reason, the aim of this thesis is to investigate the data obtained from the mooring line off Port Edward from July 2011 to December 2011 and to determine whether key characteristics of the Agulhas Current system are accurately and adequately captured. To achieve this aim, the following key questions were addressed;

1. Do the moorings capture the 'permanent' ocean currents, viz. the Agulhas Current and the Agulhas Undercurrent
2. Are the moorings able to capture the transient features of the system, viz. Natal Pulses and Durban Eddies.
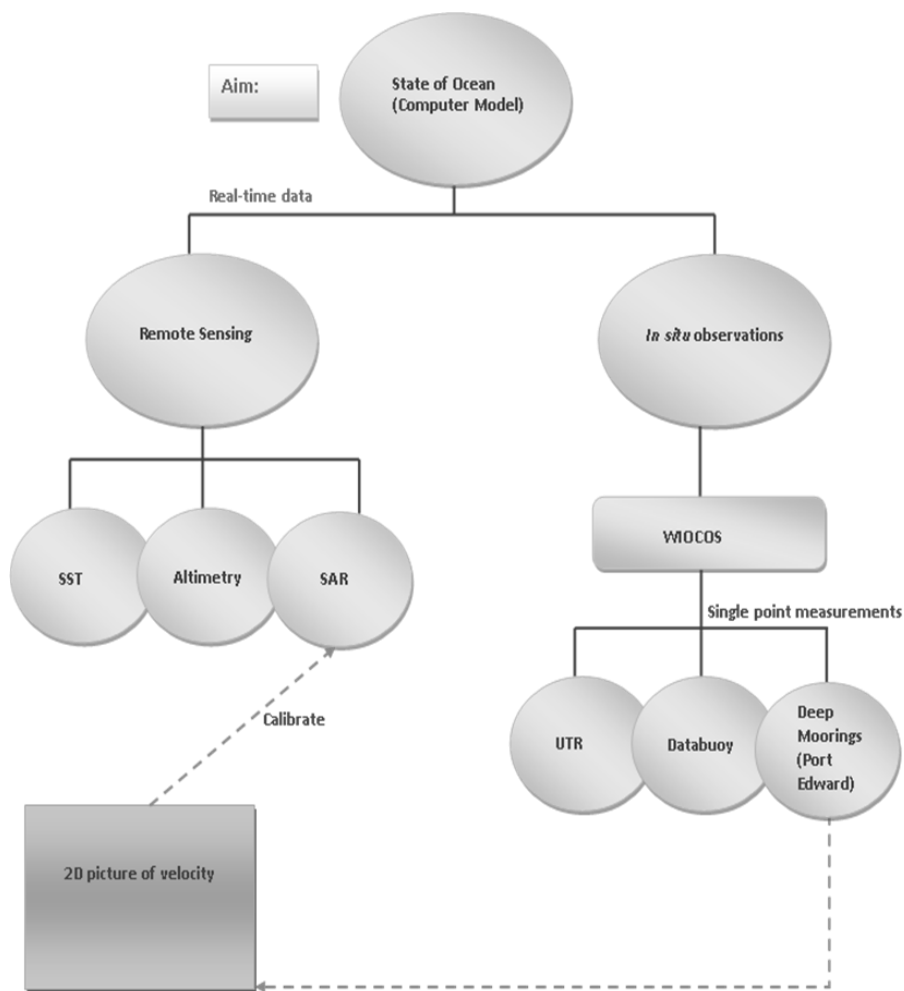
Figure 1.3: Illustration of the system required to monitor and predict the state of the ocean. Remotely sensed parameters (sea surface temperature (SST), altimetry and synthetic aperture radar (SAR) form one set of requirements for oceanographic model parameterization. The *in situ* platforms are used to calibrate satellite sensors, improve algorithms and increase model output accuracies.

Chapter 2: Literature Review

This review was not intended to be an exhaustive one, and therefore detailed descriptions of the meteorological and geological characteristics of Port Edward have not been included. While it is known that high frequency atmospheric forcing induces high frequency variability in surface currents (Lutjeharms, 2006), the main aim of this thesis was to describe the macroscale (Agulhas Current and Agulhas Undercurrent) and mesoscale (Durban eddies and Natal Pulses) oceanographic features within the region, and thus the short timescale wind-induced variations have been ignored.

2.1   The Agulhas Current

The Agulhas Current (Figure 2.1) is a warm, fast-moving western boundary current on the western side of the wind-driven, large-scale south Indian Ocean gyre system (Eden and Olbers, 2010). Originating at approximately 27° S, it flows poleward along the east coast of South Africa and extends to a depth of approximately 2000 m (Lutjeharms *et al.,* 2001). According to Lutjeharms (2001), the Agulhas Current has three sources, namely, the Mozambique Channel Drift (~13 % of the overall flow), the East Madagascar Current (~30 % of overall flow) and the re-circulation in the South Western Indian Ocean subgyre (~57 % of overall flow). The Agulhas Current does not exhibit clear seasonal variations in surface velocity, which suggests that there is no strong relationship between the Agulhas Current and the monsoonal regime in the north western Indian Ocean (Lutjeharms, 2006). Conversely, Krug and Tournadre (2012) discovered through the use of numerical ocean models that the Agulhas Current possesses an annual cycle in its volume transport.

Compared to other western boundary currents (e.g. the Gulf Stream and the Kuroshio Current), the Agulhas Current is extremely stable, mainly due to the steering and stabilising effect of the steep continental slope (de Ruijter *et al.*, 1999; Roberts *et al.*, 2010). The continental shelf on the east coast of South Africa is narrow and has a steep gradient (Roberts *et al.*, 2010). The shelf edge is defined by the 50 m depth contour north of Cape St Lucia (Figure 2.2) and by the 100 m depth contour southwards to Port Alfred (Roberts *et al.*, 2010). Between Cape St Lucia and Durban (Figure 2.2) the shelf widens to 45 km and this region is known as the Kwazulu-Natal Bight (Shillington, 1992). South of the Natal Bight the

shelf narrows and the Agulhas Current moves inshore. Further south, the shelf starts to widen near Port St John's to eventually form the Agulhas Bank (Roberts *et al.*, 2010).
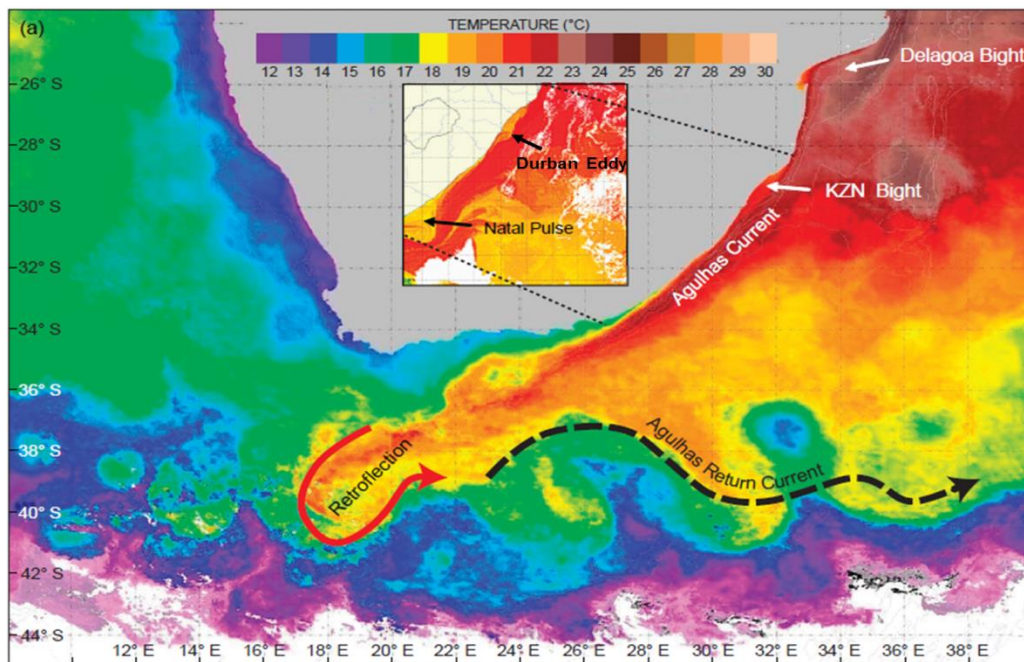
Figure 2.1: The greater Agulhas Current system. Indicated are the major features found within this western boundary current system: the Agulhas Current, the Agulhas Retroflection and the Agulhas Return Current. The inset illustrates a Natal Pulse and Durban Eddy (after Roberts *et al.*, 2010).

According to Schumann (1981), the core of the Agulhas Current is believed to be situated 40-50 km offshore of the shelf edge. The core possesses a mean velocity of between 140 cm/s and 160 cm/s, and a peak velocity of 260 cm/s (Lutjeharms *et al.*, 2001; Schumann, 1981). The Agulhas possesses an estimated volume transport of roughly 70 Sv which increases as the current moves south (Gründlingh, 1980; Bryden *et al.*, 2005). Although the Agulhas Current is very stable in its trajectory, it occasionally meanders along the coast. Deviations within its path are due to the irregular occurrence of mesoscale eddies, Natal Pulses and Durban break-away eddies (Roberts *et al.*, 2010). Mesoscale eddies enter the Agulhas Current through two of its source regions, via the Mozambique Channel and from an eastward direction, past the southern tip of Madagascar (Lutjeharms, 2006). It is believed that meanders in the East Madagascar Current may cause the shedding of rings, which feed into the Agulhas Current near the Natal Bight region (Lutjeharms, 2006). Eddies from the Mozambique Channel may have diameters of more than 300 km, extend all the way to the seafloor and have a southward net transport of 15 Sv (Lutjeharms, 2006).

Natal Pulses and Durban break-away eddies originate in the northern Agulhas Current, in the Kwazulu-Natal Bight (Roberts *et al.*, 2010). An onshore and northward, counter current flow results as part of a quasi-permanent cyclonic gyre known as the Durban cyclonic eddy (Schumann, 1981). Natal Pulses and Durban eddies are discussed in greater detail in sections 2.2 and 2.3 respectively.
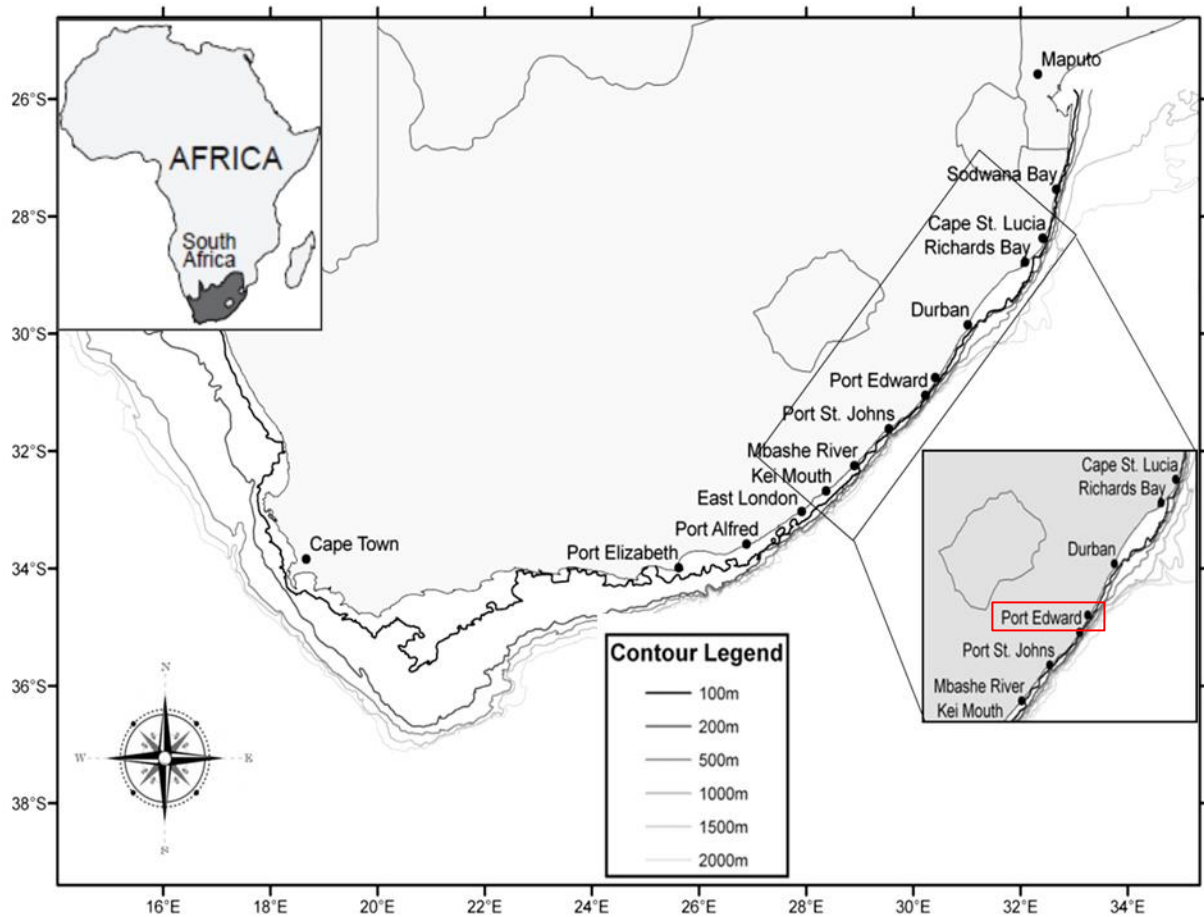
Figure 2.2: The South African coast, highlighting the Port Edward region where the moorings were deployed (Taken from Roberts *et al.*, 2010).

The Agulhas Current's upper layer consists of tropical and sub-tropical water of the South Western Indian type which travels poleward (Lutjeharms *et al.,* 2001), extending to a depth of approximately 200 m (Schumann, 1998). Below the upper layers, throughout the South Western Indian Ocean (SWIO) South Indian Ocean Central Water (SICW) is found, which extends to a depth of 800 m (Schumann, 1998). The Antarctic Intermediate Water (AAIW) is found below the SICW and occurs at approximately 1200 m (Lutjeharms *et al.*, 2000). At similar depths as AAIW, Red Sea Water (RSW) is also found and it derives its characteristic

high salinity values from the excessive evaporation in its place of origin, the Red Sea (Lutjeharms, 2006). The North Indian Deep Water (NIDW) is found at approximately 1500 m depth, with the North Atlantic Deep Water (NADW) and the Antarctic Deep Water (AADW) occupying the lower levels of the water column in the Agulhas Current system (Schumann, 1998).

2.2   The Natal Pulse

The Agulhas Current does not deviate from its mean path by more than ±15 km, but irregular exceptions to this rule do occur (Lutjeharms and Connell, 1989) in the form of large meanders (Lutjeharms and Roberts, 1988). These large meanders are known as Natal Pulses (Lutjeharms and Connell, 1989) and were found to occur between 17% and 23% of the time (Gründlingh, 1983; Lutjeharms and Roberts, 1988; Lutjeharms and Connell, 1989). They travel south, away from their origin in the Kwazulu-Natal Bight, on the shoreward boundary of the Agulhas Current, and according to Lutjeharms and Roberts (1988) and van Leeuwen *et al.* (2000) these Natal Pulses move along the coast at approximately 20 km/day. The formation of the Natal Pulse occurs at irregular intervals varying between 50 to 240 days between pulses (de Ruijter *et al.*, 1999) and occurs at an average frequency of 4 to 6 pulses per year (Bryden *et al.*, 2005; Lutjeharms, 2006). The azimuthal speed of the cyclone embedded within the Natal Pulse ranges from 50 cm/s at 1200 m to 85 cm/s at 300 m (Lutjeharms, 2006). As the Natal Pulse propagates downstream, it grows larger in its seaward extent. Lutjeharms and Roberts (1988) and de Ruijter *et al.* (1999) proposed a number of triggering mechanisms for the formation of Natal Pulses. The first mechanism was through the shedding of topographically induced, coastally trapped lee eddies in the north of the Kwazulu-Natal Bight which is energetically driven by the Agulhas Current. These eddies escape through the process of vortex shedding from their point of origin. Secondly, Natal Pulses may form through the adsorption of deep-sea eddies on the offshore border of the Agulhas Current (Tsugawa and Hasumi, 2010). Finally, their formation may be due to barotropic instability within the baroclinic Agulhas Current.

Natal Pulses may affect the trajectory of the Agulhas Current considerably (Lutjeharms and de Ruijter, 1996) and are a cause for early retroflection in the southern Agulhas region (Lutjeharms and van Ballegooyen, 1988). The Natal Pulse contributes to the shedding of Agulhas rings further downstream (van Leeuwen *et al.*, 2000), are a form of leakage of warm salty water into the south Atlantic and changes the dynamics of the entire water column

along its path (Rouault and Penven, 2011). Lutjeharms *et al.* (2001) also attributed certain aspects of the coastal circulation in the northern Agulhas to be under the influence of these periodic Natal Pulses which drive localized upwelling (Bryden *et al.*, 2005) and transport particles and larvae from the northern to the southern part of the region.

2.3   The Durban cyclonic eddy

On the shoreward side of the Agulhas Current, in the area surrounding Durban, a quasi-permanent northeastward flowing current exists (Lutjeharms *et al.*, 2000). This flow is part of a cyclonic eddy which is known as the Durban cyclonic eddy (Figure 2.3). The Durban cyclonic eddy is the major cause of northeastward flow throughout the water column off Durban (Lutjeharms, 2006). Roberts *et al.* (2010) reported that this eddy was formed by the interaction of the Agulhas Current and a bathymetric feature between the 100 and 500 m depth contour known as a subsurface 'bight'. Roberts *et al.* (2010) added that these eddies were shed roughly every 15 days and moved in a southwestward direction downstream and did not grow in offshore extent, but rather flattened and elongated against the shelf to form lateral waves at roughly 34° S.
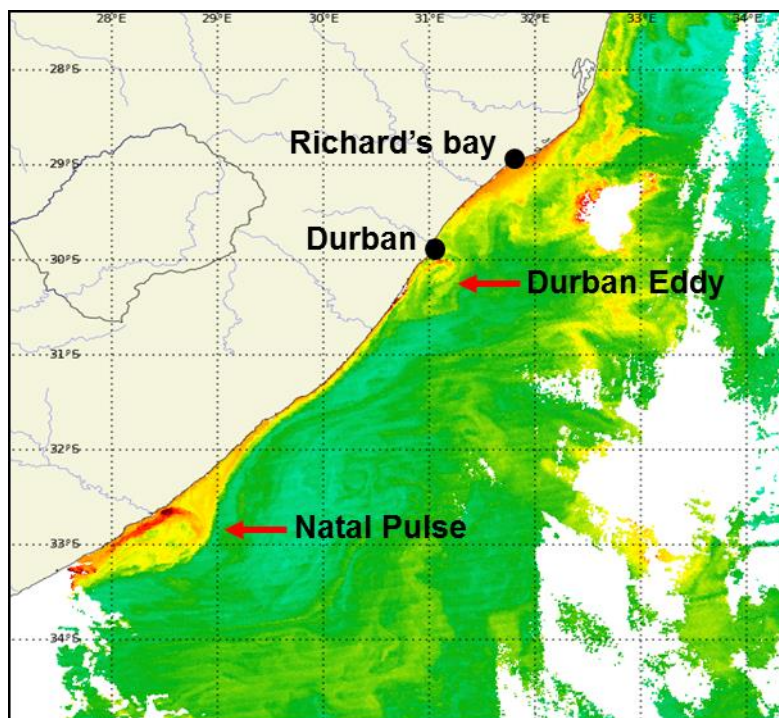
Figure 2.3: Satellite image of chlorophyll-*a* distribution in the Agulhas Current on 15 June 2011, indicating the presence of the Durban cyclonic eddy. A Natal Pulse is also indicated. Source: The Marine Remote Sensing Unit (MRSU) at the University of Cape Town (UCT).

2.4   The Agulhas Undercurrent

The Agulhas Undercurrent was first measured in 1995 (Beal, 2009). It was shown to have a volume flux of 4.2 Sv, travelling equatorward and according to Bryden and Beal (2001), Arhan *et al.* (2003) and van Aken *et al.* (2004), it carries NADW from the Southeast Atlantic to the interior of the Indian Ocean. The depth at which the undercurrent was found was extremely variable with a core displaying maximum velocities at 1200 m depths (Beal, 2009). This undercurrent forms a vital part in potential ventilation of deep Indian Ocean water (Beal & Bryden, 1997). Bryden *et al.* (2005) stated that the undercurrent is a persistent feature and displayed a peak velocity of 30 cm/s.

In 2003, the Agulhas Current and Agulhas Undercurrent were studied through a series of hydrographic and direct velocity measurements during the Agulhas Undercurrent Experiment (AUCE) (Beal, 2009). The findings of this research are illustrated in Figure 2.4, which represents a snapshot of the mean velocity structure of the Agulhas Current and Agulhas Undercurrent. Results showed the Agulhas Undercurrent on the continental slope as it flowed in a northeastward direction with an intermediate core and a second core below 2000 m (Beal, 2009).

Slope-attached undercurrents have been found in the Mozambique Channel (de Ruijter *et al.*, 2002) and under the southern branch of the East Madagascar Current (Nauw *et al.,* 2008), both areas being source regions of the Agulhas Current. Research conducted by Biastoch *et al.* (2009) revealed possible connections between these undercurrent regimes and the Agulhas Undercurrent. According to de Ruijter *et al.* (2002), the Mozambique Undercurrent may be a direct continuation of the Agulhas Undercurrent. Methods used by Biastoch *et al.* (2009) in identifying the Agulhas Undercurrent were adopted for this thesis and they were: (i) all northward flow across a section (mooring line), (ii) northward flow below 1000 m, (iii) northward flow inshore of the Agulhas Current, and (iv) northward flow inshore and below 1000 m.
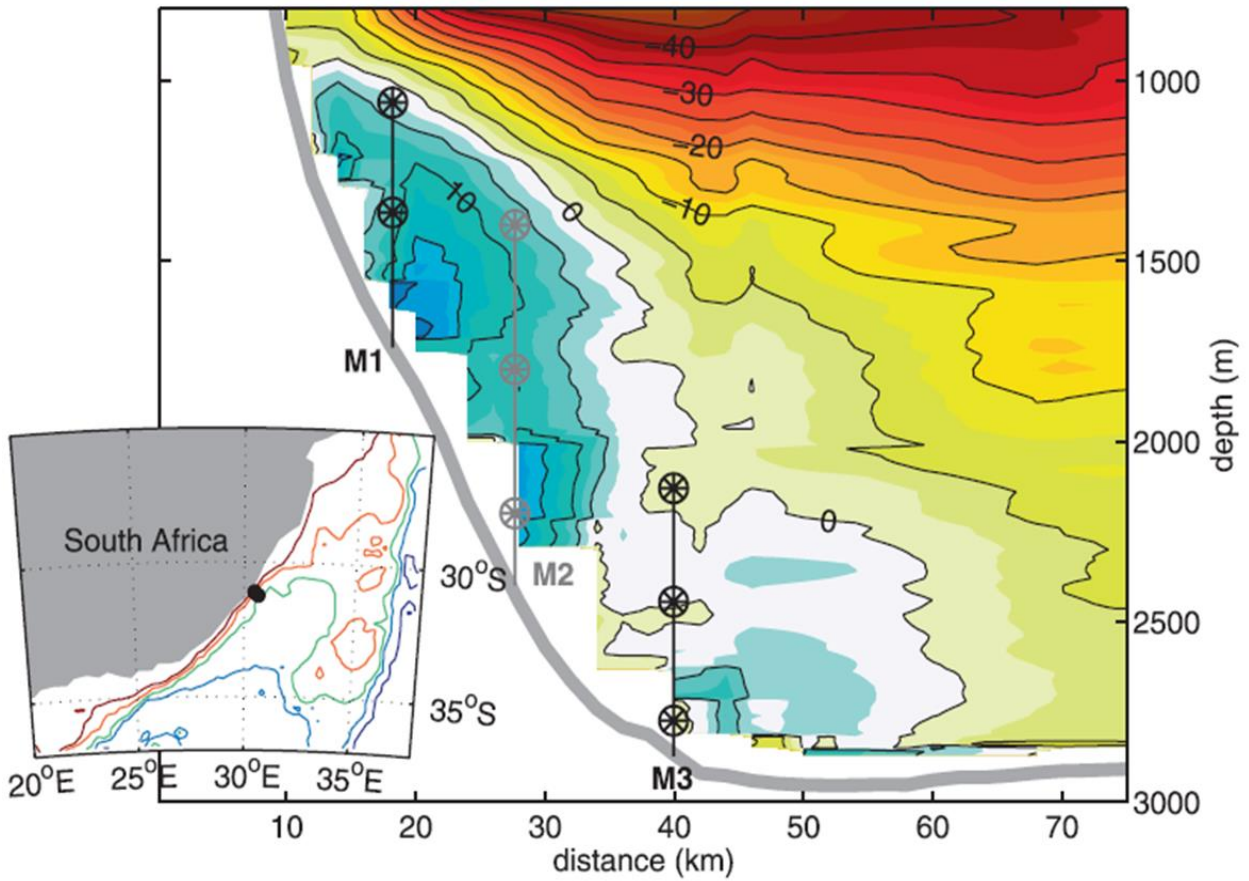
Figure 2.4: Illustration depicting the positions of the Agulhas Undercurrent Experiment (AUCE) moorings in relation to the Agulhas Undercurrent (white to blue) and the Agulhas Current (red to orange) (Beal, 2009). The colour contours represent current velocity from strong (red) to weaker (blue) values. Inset: Position of the AUCE moorings (black dot) in relation to the South African coast.

Chapter 3: Data and Methods

3.1   Study area

This study was conducted on the east coast of South Africa offshore of Port Edward (Figure 2.2). This site was chosen because the area directly south of Port Edward has historically been used as a site for studying the Agulhas Current (Beal, 2009; Beal and Bryden, 1997). Roberts *et al.* (2010) and Beal and Bryden (1997) further stated that the core of the Agulhas Current was closest to the shelf edge off Port Edward. An additional reason for the choice of study site was that the moorings line would follow an existing ground track of the SAR satellite.

To determine the positions of the moorings a bathymetric survey of the continental slope off Port Edward was done onboard the RS *Algoa* in March 2010. The results are shown in Figure 3.1. The dashed lines represent the survey transect lines, covering the shelf edge, down the continental slope and towards the foot of the slope. The bathymetric survey was conducted in order to identify any irregular, hazardous features which needed to be avoided during mooring deployment. Based on the results obtained from the survey, the moorings were deployed as shown in Figure 3.1.   The deployed mooring transect line was perpendicular to the coast and stretched from the continental shelf to the 2000 m depth contour. The 200 m mooring was 9.5 km from the coast, the 1000 m mooring was 13 km and the 2000 m mooring, 26 km.
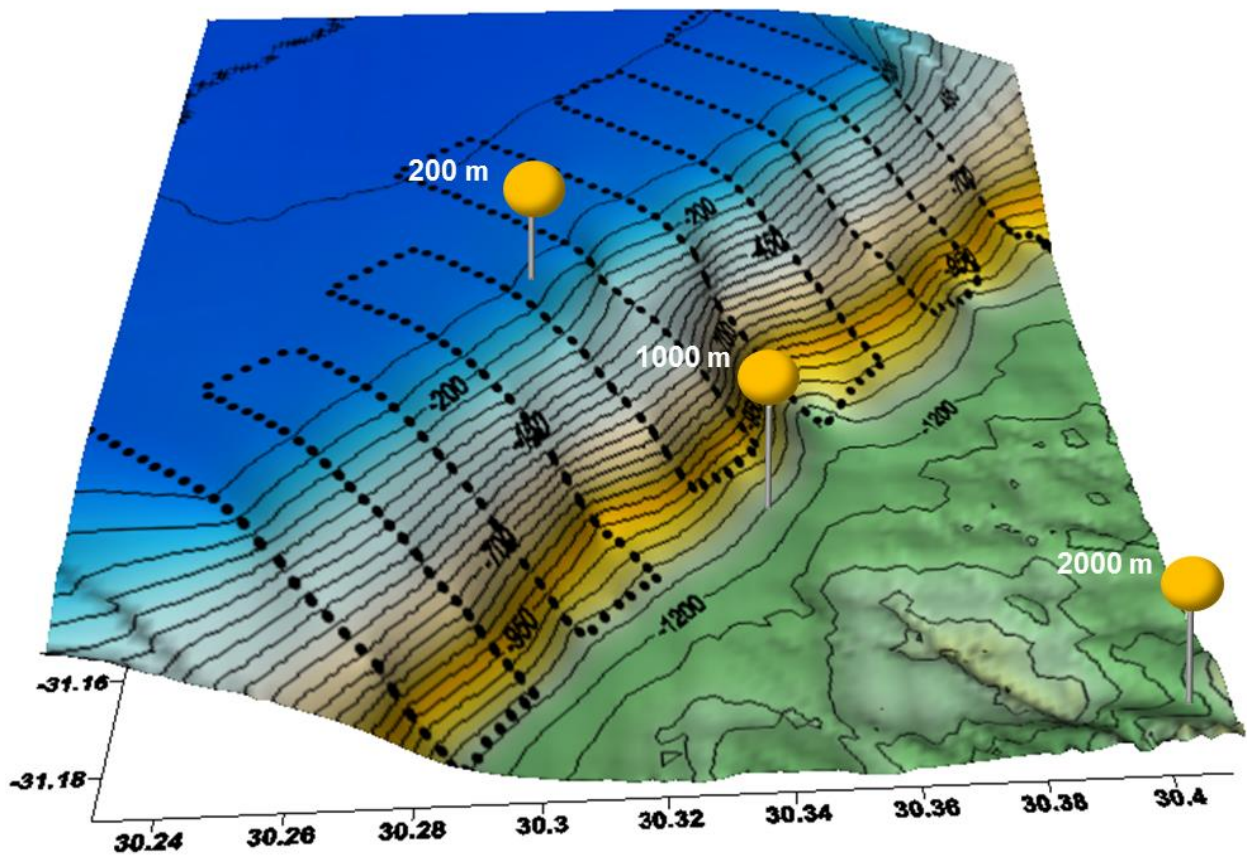
Figure 3.1: Bathymetry survey conducted by the *RS Algoa* during September 2010 depicting the mooring positions.

3.2 Mooring design

The mooring line comprised two sub-surface floats positioned at 500 m depth in a total water depth of 1000 m and 2000 m and a shallower mooring placed at a depth of 200 m (Figure 3.2). The 1000 m and 2000 m moorings had two oppositely facing (upward and downward) ADCP's. The 1000 m mooring was accompanied by a surface float for real-time data transmission. For simplicity, the 200 m mooring will be referred to as the inshore mooring, the 1000 m mooring will be referred to as the slope mooring and the 2000 m mooring will be known as the offshore mooring.
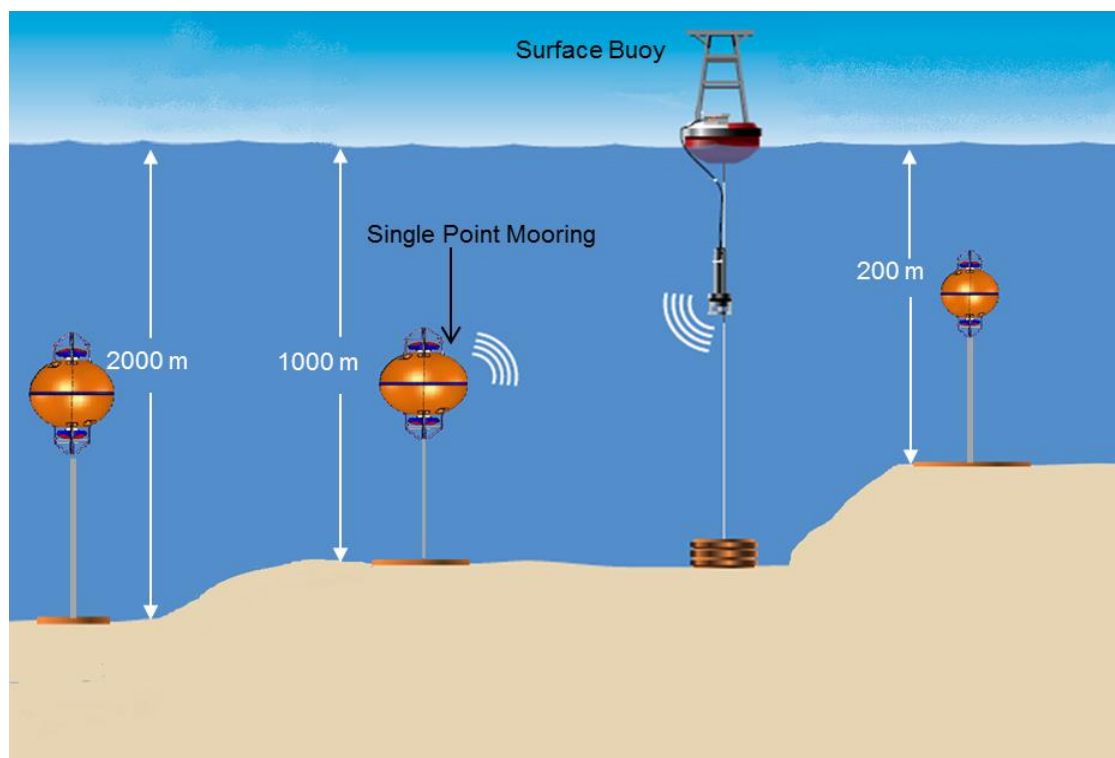
Figure 3.2: Shows the overall configuration of the mooring systems

Inshore Mooring

The inshore mooring was situated at -31° 06' 32'' S , 30° 18' 26'' E and it comprised a 150 kHz upward facing ADCP in a 36 inch Flotation Technologies® buoy deployed during July 2011 (Figure 3.3). The ADCP was configured to record data every 60 minutes with an ensemble size of 120 pings (one ping per second) and thus had an ensemble duration of

120 seconds. The mooring was deployed in 217 m water depth and the transducer depth was 210 m with a blank distance of 3.5 m above the transducer face. The water column was sampled using 44 bins, each bin being 5 m in length. The combined distance covered by the 44 bins was 220 m, exceeding the total water depth. This was done to account for tidal height and potential draw down effects of the current on the mooring system. Measurements taken in the air were discarded during data analysis. The magnetic variation was set to 0° during pre-deployment setup and corrected manually upon mooring recovery.
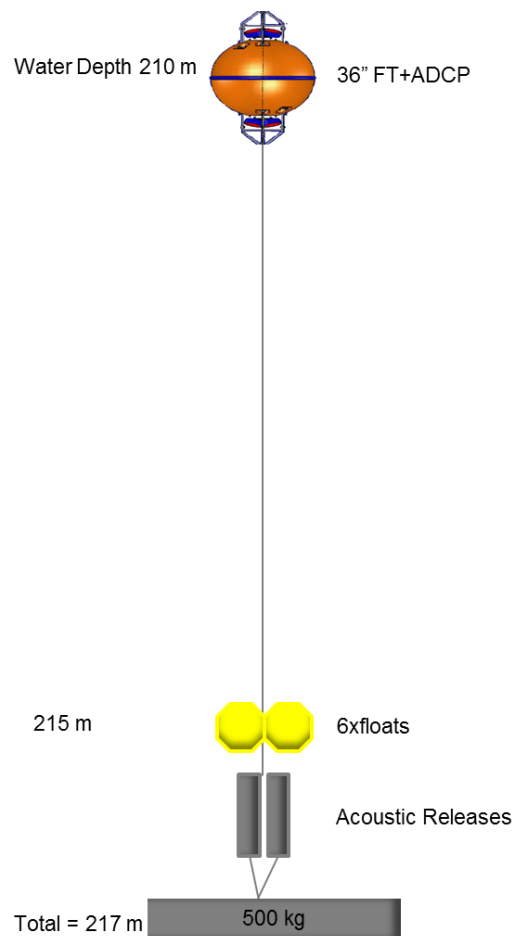
Figure 3.3: Simplified illustration of the inshore mooring system. The mooring consisted of one 36" float housing a ADCP. The water depth indicated at the top of the figure is the water depth at which the ADCP was situated.

The slope mooring consisted of two opposing (upward and downward facing) 75 kHz ADCP's installed in a 76" Flotation Technologies® buoy deployed during June 2011 (Figure 3.4). Each ADCP was setup to measure 500 m of the total water depth of 1 000 m. The sub-surface float provided the sea temperature at 500 m and current profile data. The ADCP's were configured to record every 60 minutes with an ensemble size of 25 pings (one ping per second) and thus an ensemble duration of 25 s. The transducer was situated at ~500 m with a blank distance of 8 m above the transducer face. The water column was sampled using 20 bins for each ADCP, each bin being 30 m long. The magnetic variation of the ADCPs compass is always set at 0° and corrected manually after the data had been downloaded via the buoys.
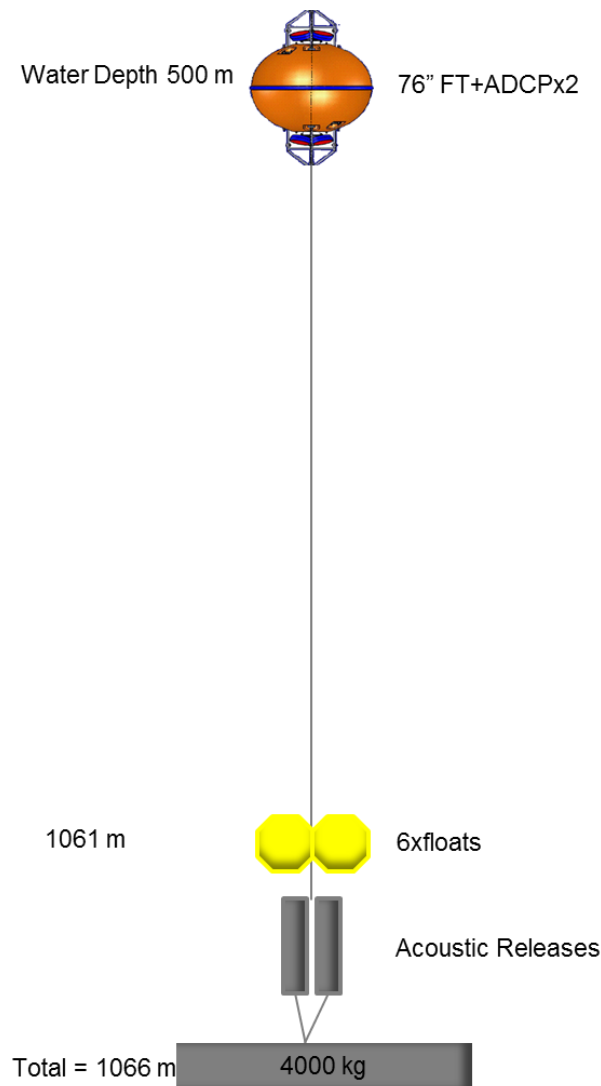
Figure 3.4: Simplified illustration of the slope mooring system. The mooring consisted of one 76" float housing two ADCPs. The water depth indicated at the top of the figure is the water depth at which the ADCP was situated.

<u>Offshore Mooring</u>

Two 49" Flotation Technology buoys each housed a 75 kHz ADCP, one upward looking and one downward looking, similar to that of the slope mooring and was deployed during July 2011. The offshore mooring was designed with a 1500 m long mooring cable, positioning it at a depth of 500 m and was not setup to supply real-time data (Figure 3.5). Data were collected manually after instrument recovery and analysed. The 75 kHz ADCP has a maximum range of 600 m and approaching that maximum, data quality may have been compromised. To compensate for the decay in data quality as distances reach the maximum operating range of the ADCP and to measure currents all the way to the seafloor, five single point DVS's were evenly spaced along the lower 1500 m of cable. Each DVS provided current measurements for 5 m of the water column and divided the 5 m into five 1 m bins. Hydrographic data (temperature and salinity) was supplied by five mini conductivity temperature depth instruments (CTD) referred to as a SBE MicroCat ® which were attached evenly along the mooring line. As anomalies within the Agulhas Current move across the line of moorings their internal dynamics may be described through temperature and salinity analysis via the attached SBE MicroCat hydrographic instruments.

In swift flowing currents, moorings have a tendency to be pulled down by the current to deeper depths and this is known as current induced mooring draw-down. This would have implications on the various bin depths. The offshore mooring had the largest current induced mooring draw-down of between 50 and 100 m. The effect of mooring draw-down by the current would affect the depths at which measurements were taken (especially the depth of the surface bin) at that point in time, by being pulled down to deeper depths with more marked effects as the current approached maximum velocities. These effects are not critical for data analysis and the processed data will be considered as correct for depth profile velocity, direction and temperature analysis obtained from these ADCP's.

DVS 1 was within the range of the offshore moorings 'good' bin and was omitted from the results, thus only DVS 2 to 5 were used in data analysis (Figure 3.5).
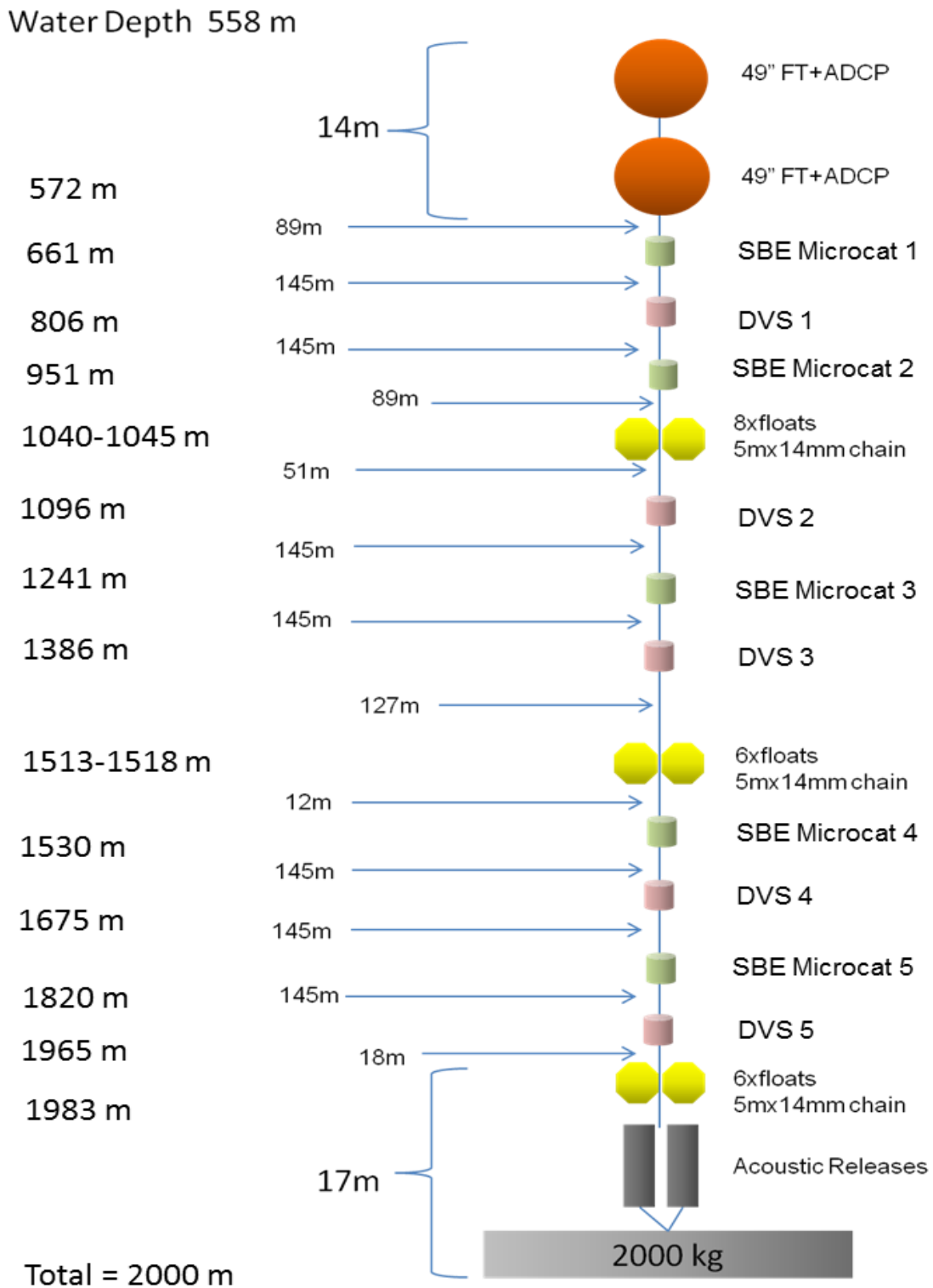
Figure 3.5: Simplified illustration of the offshore mooring system. The mooring consisted of two 49" floats housing one ADCP each and a series of instruments (SBE MicroCat and DVS ADCP) along the mooring line. The indicated depths to the left of the figure are the specific depths at which each instrument was installed. The water depth indicated at the top of the figure is the water depth at which the ADCPs were situated.

3.3   Data processing and quality control

The ADCP data was downloaded using the WinSC software which was provided by the ADCP manufacturers, Teledyne®. Unprocessed data (binary data) from all five ADCP's were converted to ASCII format for processing in Microsoft Excel® and a local in-house processing programme known as ADAS used for graphical analysis. The slope mooring was deployed on 23 May 2011, earlier than the inshore and offshore moorings and for purposes of uniformity, data analysis started from 21 July 2011 (deployment date of the inshore and offshore moorings) to 04 December 2011 (date of moorings' recovery), except for the inshore mooring which stopped recording data on 07 October 2011. Data was corrected to true north by applying a magnetic variation of -26.23° (26.23° W) for the Port Edward area. During processing, bins with data loss in excess of 25 % were discarded as the percentage data loss exceeded the cut-off threshold of 25%. In the processing programme ADAS, bins with errors in excess of 25% were not computable.

Surface bins used for each mooring differed in depth due to the unpredictable nature of various natural processes and instrument technology limitations. The percentage data loss in the bins closest to surface or sea-bed determined whether or not it may have been used in processing. For the inshore mooring only data from the first 37 bins were used, discarding the last seven bins (Figure 3.6). The inshore mooring's last good bin and the bin chosen to represent surface measurements was at 20.9 m depth. This mooring stopped recording data on 7 October 2011 due to technical malfunction.

For the upward looking ADCP on the slope mooring, the last five bins were discarded (Figure 3.7a) and the last good bin was at 49.9 m depth. Data from bins 16, 17, 18, 19 and 20 for the downward looking ADCP on the same mooring were discarded (Figure 3.7b) due to a high percentage of erroneous readings caused by the usual environmental inhibitors of acoustic signal transmission (side-lobe interference, multi-path interference and reflection from the ocean surface and bottom) and instrument limitations.   Bin 15, at an average depth of 960 m, was used as the last 'good' bin of the downward looking ADCP at the slope mooring.

The upward and downward looking ADCP's of the offshore mooring made use of the first 13 and 19 bins respectively, discarding the last seven bins of the upward looking ADCP (Figure 3.8a) and the last bin of the downward looking ADCP (Figure 3.8b). The depth of the

surface bin (bin 13) at the offshore mooring had an average depth of 96 m. The average depth of the bottom bin of the offshore mooring was at 1090 m depth.
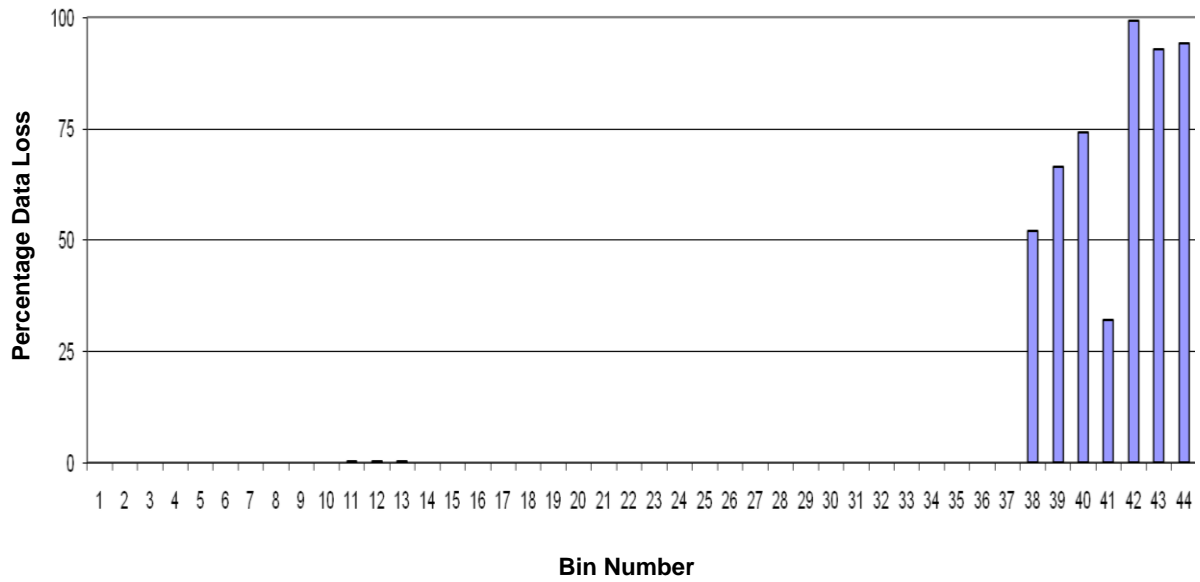
Figure 3.6: Percentage data loss for the inshore mooring. Bins 38 to 44 (the surface bins) had more than 25 % erroneous readings, and were thus excluded from data analysis.
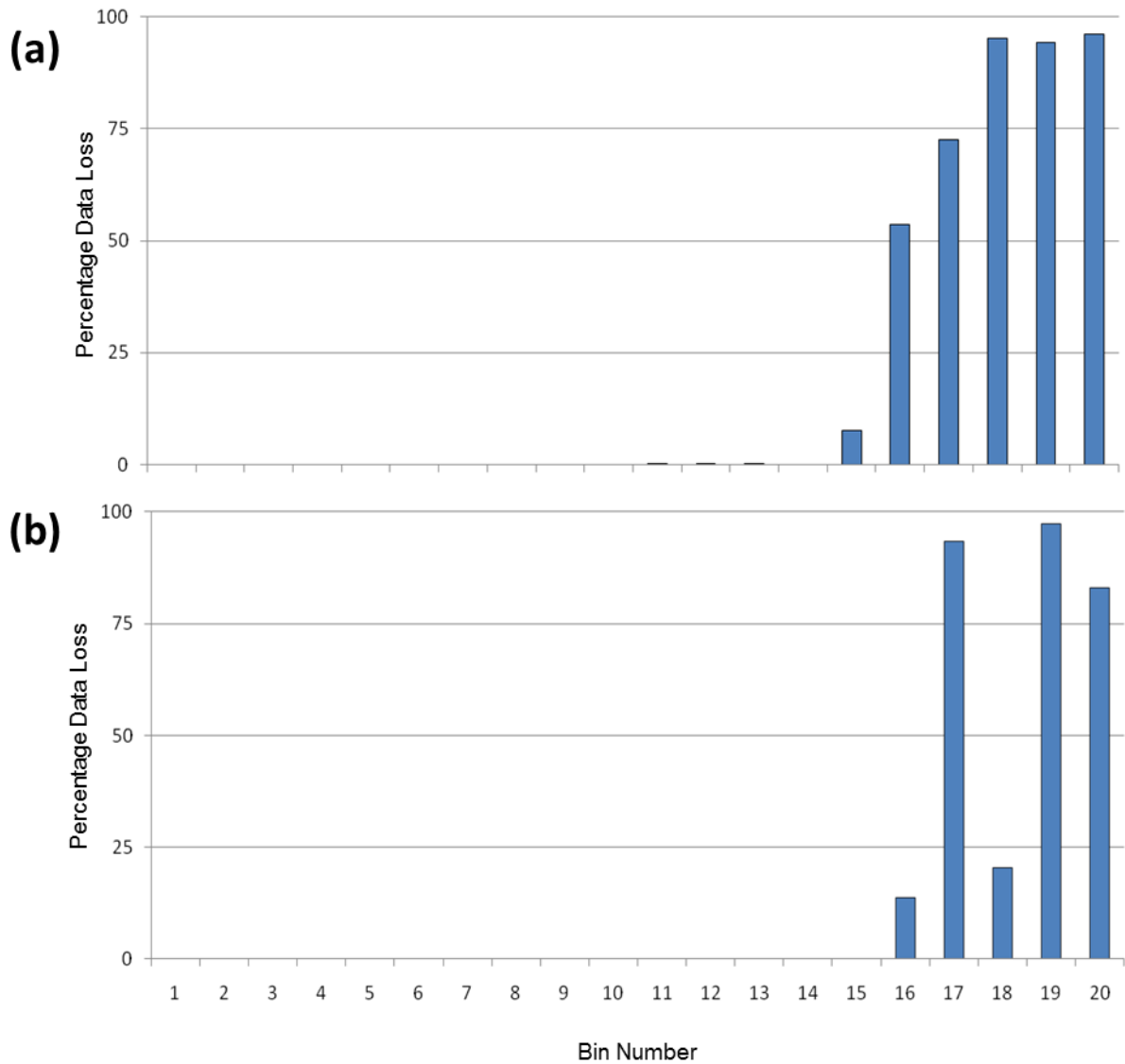
Figure 3.7: Percentage data loss for the two ADCPs on the slope mooring. (a) Bins 16 to 20 of the upward looking ADCP had more than 25 % erroneous readings, and were thus excluded from data analysis. (b) Percentage data loss for the downward looking ADCP. Bins 17, 19 and 20 had more than 25 % erroneous readings, and were initially excluded from data analysis. During data analysis, bins 18 and 16 were also excluded due to the presence of numerous inaccuracies during processing.
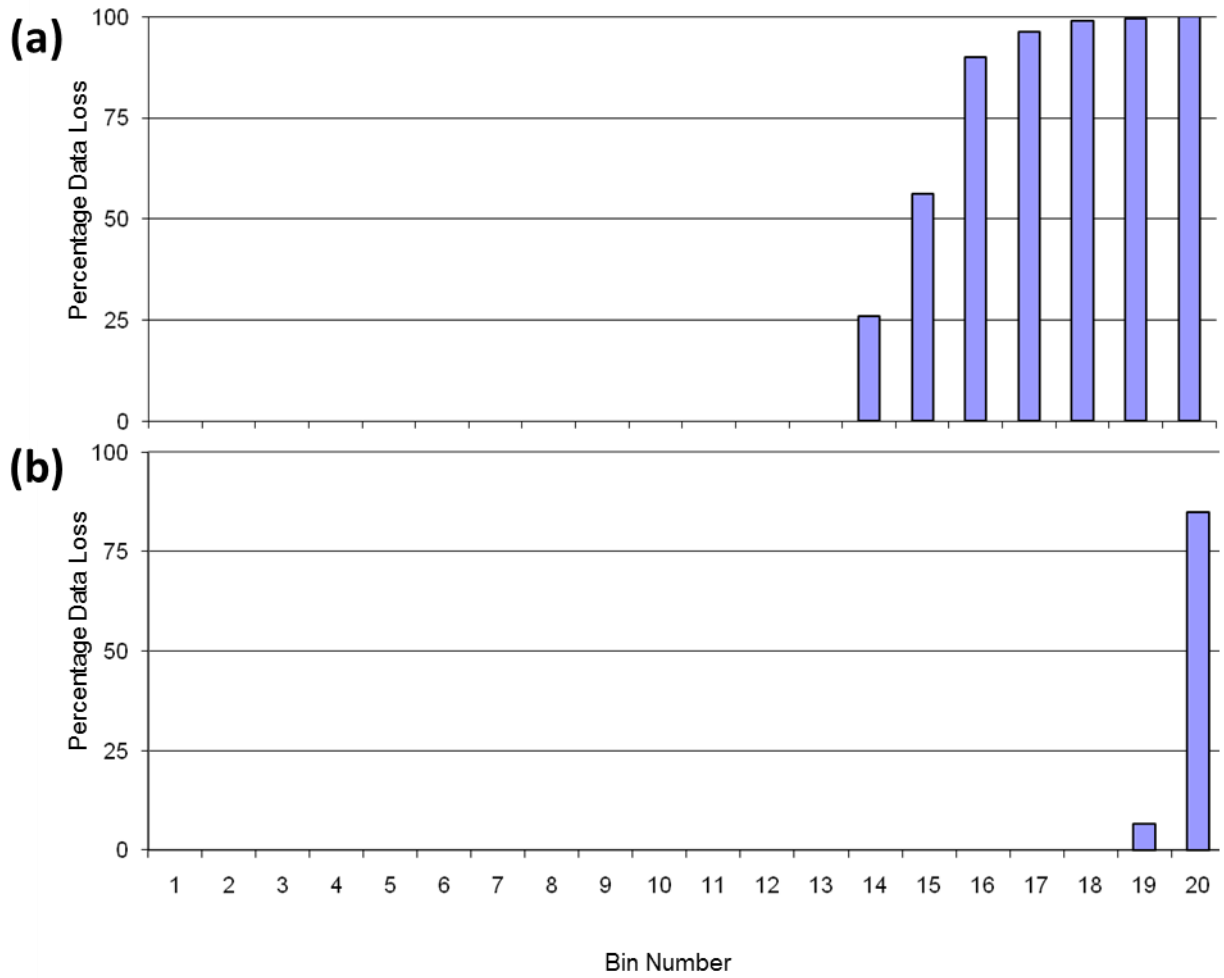
Figure 3.8: Percentage data loss for the (a) upward looking ADCP on the offshore mooring. Bins 14 to 20 were excluded from data analysis. (b) Percentage data loss for the downward looking ADCP on the offshore mooring. Only bin number 20 was excluded from data analysis.

3.4   Ship-based measurements

Ship-mounted Acoustic Doppler Current Profiler (S-ADCP) and CTD transects were conducted in order to obtain hydrographic measurements (temperature, salinity and dissolved oxygen) to describe the Agulhas Current and Agulhas Undercurrent on the same day the moorings were deployed and commenced their measurements.   These measurements were done to aid the description of the characteristics of the Agulhas Current obtained from the moorings.   Hydrographic data was collected along a transect perpendicular to the Port Edward coast, directly across the location of the ADCP moorings (Figure 3.9). These hydrographic data were collected using a SeaBird 9/11+conductivity-temperature-depth (CTD) and a Teledyne RD Instruments ship-mounted 75kHz Ocean Surveyor ADCP (S-ADCP). Due to the short cable length on the *RS Algoa*, a maximum depth of 1000 m was attained for CTD casts. The S-ADCP and CTD line extended ~55 nm offshore to the 3 000 m depth contour. The transect line aimed to intersect the Agulhas Current, the Agulhas Undercurrent and any cyclonic anomalies if they were present. Nine stations were sampled on the CTD line, with the inshore stations (1 to 4) being 1 nm apart for higher spatial resolution across the narrow shelf, and the deep stations (5 to 9) being 10 nm apart.
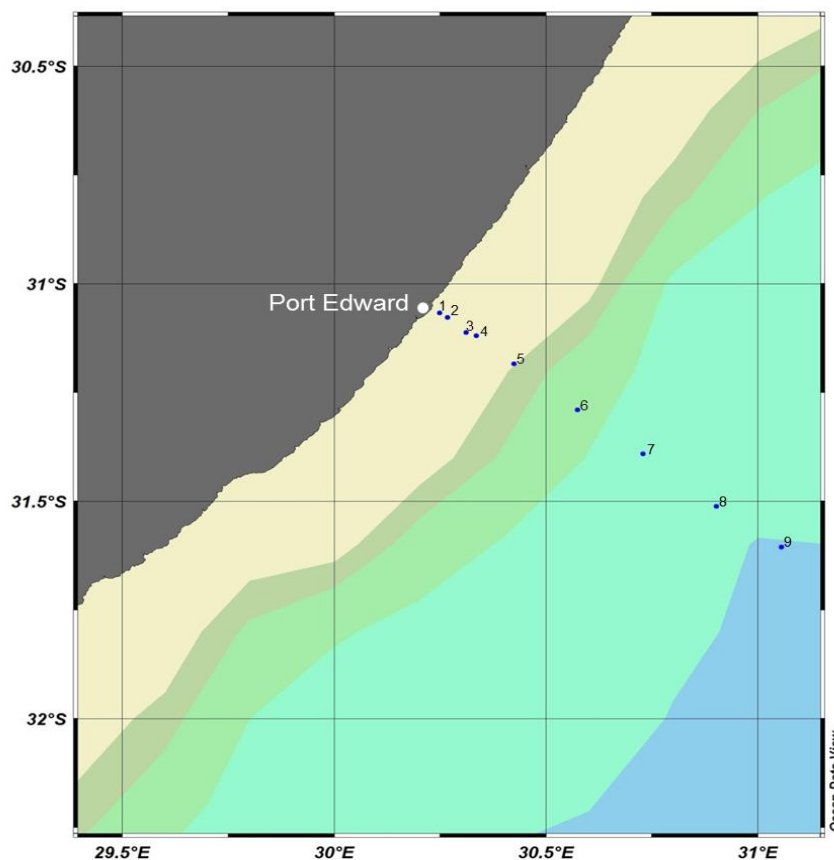
Figure 3.9: Position of the S-ADCP and CTD transect. The transect line runs perpendicular to the Port Edward coast. Colour shading represents the 500 m, 1000 m, 2000 m, and 3000 m bathymetry contours.

3.5   Satellite observations

3.5.1   Altimetry data

Maps of weekly Delayed Time (DT) Mean Sea Level Anomaly (MSLA), gridded at 1/3 degree resolution, produced by Ssalto/Duacs and distributed by AVISO, with support of CNES (ftp://ftp.aviso.oceanobs.com/duacs/) were used to identify and describe mesoscale features. Data from 21 July 2011 to 04 December 2011 were plotted using the Ocean Data View (ODV) software to analyse the area surrounding Port Edward.   The sea surface height anomaly (SSHA) data was obtained from the data of multiple satellites and merged to decrease mapping errors by up to 30 %.   The various institutions processing the data do so at a near real-time basis within 12 to 36 hours of the satellite's overflight.   For the best accuracy 7-day composite images were used.   In the case of Figure 4.4 where only a single day's SSHA was needed to compliment the S-ADCP transect, a single altimetry image was downloaded from the Colorado Centre for Astrodynamic Research (CCAR) near-real time altimetry site (http://argo.colorado.edu/~realtime/welcome/) for 21 July 2011.

3.5.2   Sea surface temperature (SST) and ocean colour (chlorophyll-*a*) data

MRSU compiles a database and displays images of sea-surface temperatures and chlorophyll-*a* for the African continent (http://www.afro-sea.org.za/mrsu/flags.php).   Data from 21 July 2011 to 04 December 2011 were used in this study. Chlorophyll-*a* and SST remotely sensed data are derived from optical and infra-red sensors. These operate at short wavelengths on the electromagnetic spectrum and radiation of these wavelengths cannot penetrate clouds. Ocean colour and SST images do however offer a complimentary and distinct view of oceanic circulation features such as filaments and eddies (Roberts *et al.*, 2010).

Chapter 4: Results

4.1   Ship-based observations

4.1.1   <u>CTD data</u>

The temperature profile presented in Figure 4.1a shows the gradual sloping of isotherms from an offshore location towards the continental shelf, typical of western boundary currents. Highest temperatures were recorded at the surface from station 6 to 9, roughly 40 km offshore.

Salinity in Figure 4.1b showed a similar pattern to that of the isotherms, i.e. sloping upwards as it approached the continental shelf. Higher salinities (35.2 psu – 35.4 psu) were found between 500 m depths and the surface at stations 1 to 5, while lower salinities (34.6 psu) were recorded along the continental slope, close inshore. Lower salinities only appeared below 800 m at the offshore stations.

Dissolved oxygen (Figure 4.1c) indicated a shallow minimum between 100 to 300 m depths. Below the oxygen minimum layer and roughly 20 km offshore, a layer of higher oxygen content occurred between 400 and 800 m. A second minimum dissolved oxygen layer at the foot of the continental slope between 500 m and 1000 m was observed, sloping to deeper depths in an offshore direction. These various hydrological minimums coincide with each other, i.e. lower temperatures and minimum salinity and oxygen values were all found at the foot of the continental slope.
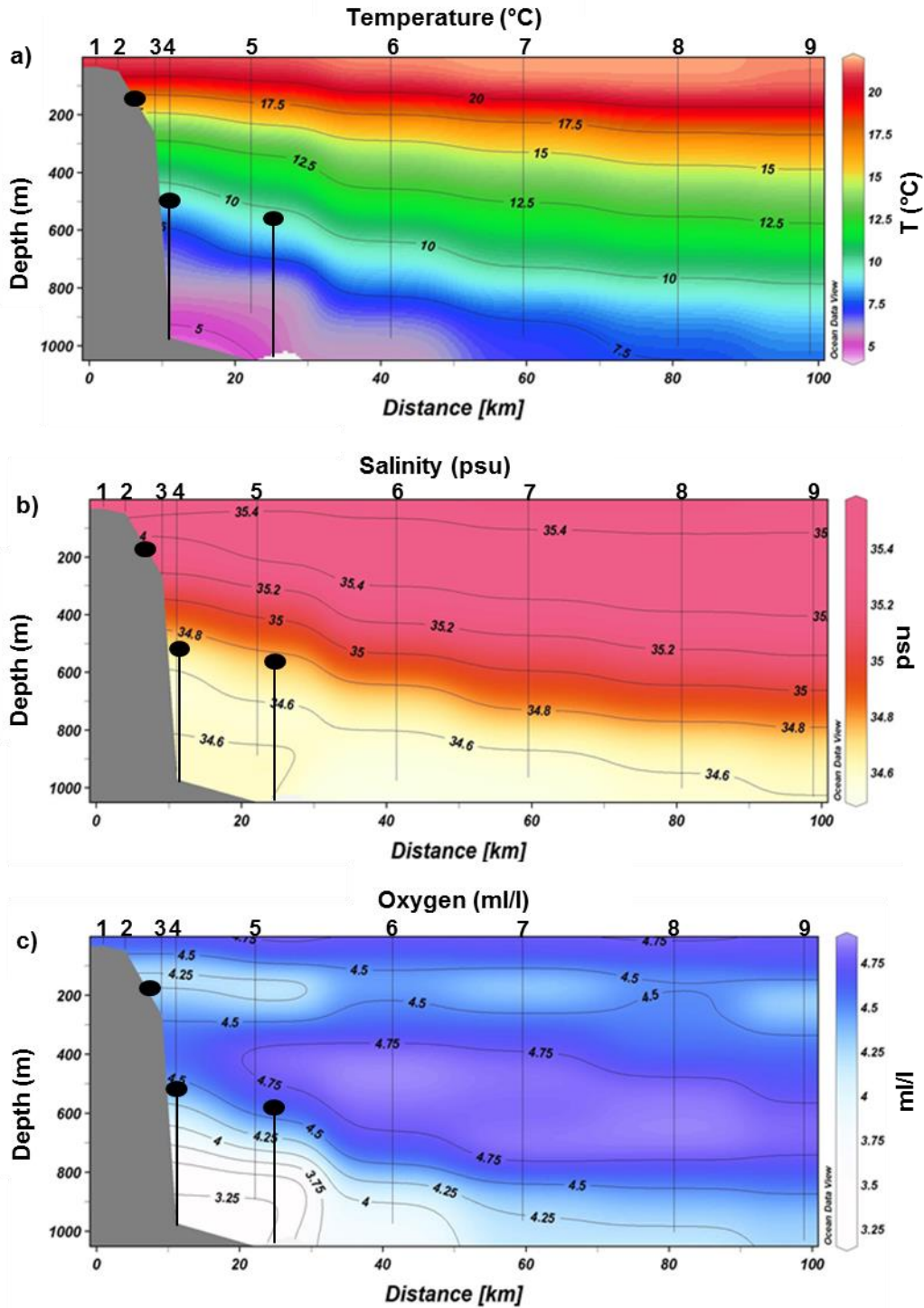
Figure 4.1: Vertical sections of the CTD transect conducted off Port Edward on 21 July 2011. Displayed are: a) temperature, b) salinity c) and dissolved oxygen. The three moorings are displayed as black lines and circles on all three images.

Figure 4.2 displays a temperature-salinity (T-S) graph for data collected on the CTD transect. The warm surface water was identified as Tropical Surface Water (TSW), which may be more specifically described as Indian Tropical Surface Waters (ITSW) (Lutjeharms *et al.*, 2000). ITSW displayed a characteristic winter temperature of 22 °C (Figure 4.2) and salinities of between 35.10 and 35.25 psu. Directly below the ITSW was South Indian Subtropical Surface Water (SISSW), identified by a salinity maximum of roughly 35.6 psu and a temperature of approximately 16 °C. South Indian Central Water (SICW) was shown by a line between 8-14 °C and 34.6 to 35.4 psu. Below the SICW, Antarctic Intermediate Water (AAIW) was found and possessed some of the lowest salinities (less than 34.6 psu). The sharp increase in salinity at the extreme depths of this study showed evidence of Red Sea Water (RSW).
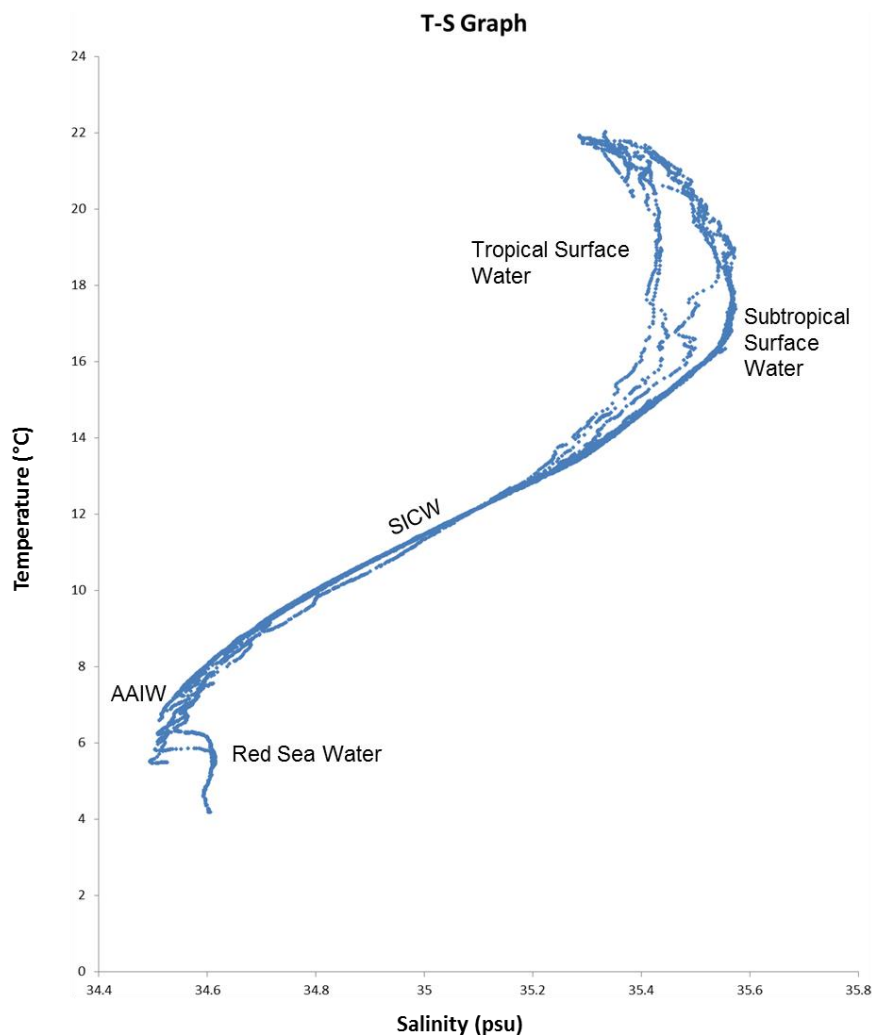
Figure 4.2: Temperature/salinity characteristics for all the stations on the Port Edward transect for 22 July 2011.

4.1.2   S-ADCP transect

Results obtained from the S-ADCP transect (Figure 4.3) on 21 July 2011 showed no evidence of cyclonic anomalies affecting a linear flowing Agulhas Current. Only the surface bin was used to indicate the general flow characteristics for 21 July 2011. The S-ADCP transect showed weaker currents inshore, increasing offshore until the core of the Agulhas Current between the 500-1000 m isobath. The Agulhas Current gradually weakens offshore. Strong southwestward currents flowing in excess of 50 cm/s were observed from the 200 m isobath up to the 3000 m isobath and extended to a depth of 700 m. The sharp diminishing current vectors over the shelf and shelf edge depicted the Agulhas Current inshore boundary to lie over the shelf edge.

An accompanying SSHA image for the 21 July 2011 is presented in Figure 4.4 and does not compliment the findings of the S-ADCP data.
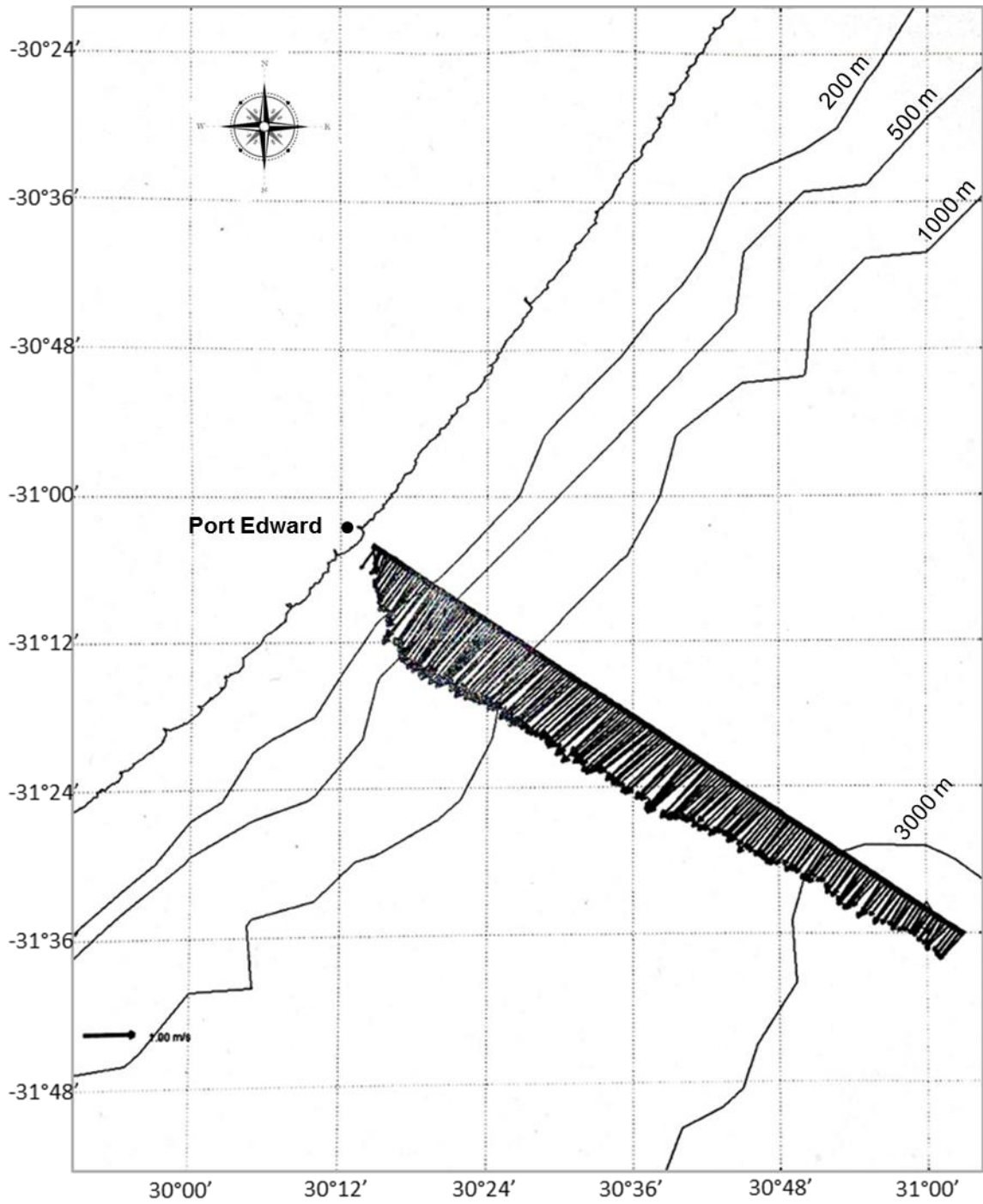
Figure 4.3: S-ADCP transect on 21 July 2011 across the Agulhas Current and directly over the three ADCP moorings. Current strength is displayed as vectors.
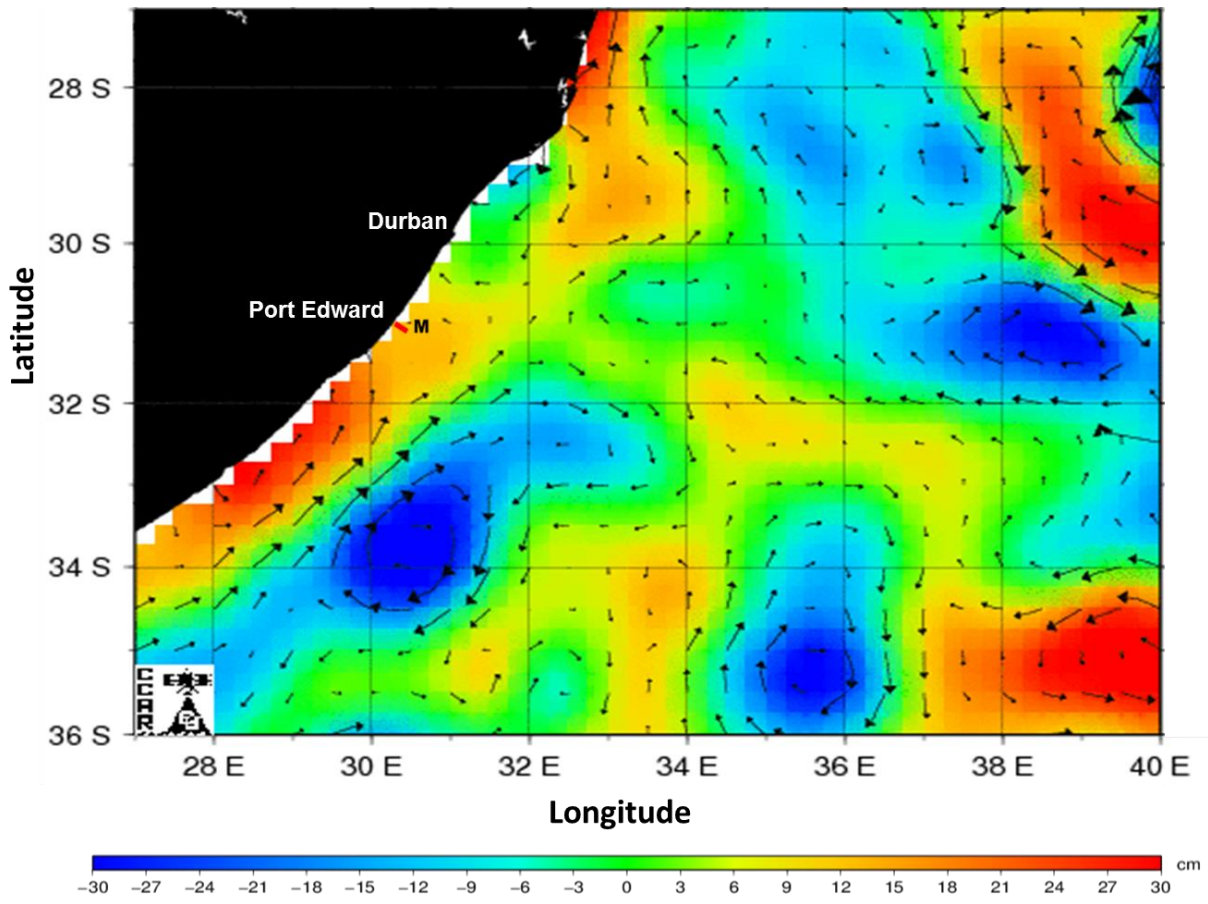
Figure 4.4: Satellite image representing SSHA with geostrophic velocities for 21 July 2011.

4.2 Moorings

4.2.1 Current direction

The general flow of the upper (shallower than 500 m) Agulhas Current in Figure 4.5 was shown to be in a southwestward direction (between 180° and 270°), intermittently reaching all the way to the sea floor at all moorings. This southwestward flow was occasionally interrupted by current reversals (0° to 90° and 270° to 360°) altering the directional flow of the water column. Three major current reversal events were visible at all three moorings and are highlighted in the black blocks (from right to left) as Events 1 to 3. These reversals occurred on 23 July 2011, 02 September 2011, and 11 October 2011 and lasted between one and four days. Also evident was a near constant northeastward flow at the seafloor, extending from 2000 m depth to the continental shelf at the inshore mooring.

Minor current reversals which do not reach the surface were also visible at all three moorings (indicated by 'X' in Figure 4.5). These events reached an average depth of 136 m beneath the surface on the continental shelf at the inshore mooring. The northward currents within these sub-surface reversals were largely concentrated at depths deeper than 100 m at the inshore mooring, 500 m at the slope mooring and 750 m at the offshore mooring.

Northeastward flow near the bottom to mid-water column was a persistent feature at the slope (1000 m) and offshore (2000 m) moorings. This northeastward flow was consistent with the definitions of Biastoch *et al.* (2009) and thus likely represented the Agulhas Undercurrent. The northeastward flow was absent after Event 2 at the offshore mooring, but exhibited northward flow after Event 1 and offshore (eastward) flow after Event 3. Occasionally when northeastward flow reached shallower depths at the slope mooring, concurrent, northeastward currents were also visible at the inshore mooring. These sub-surface current reversals may be representative of the movement of the Agulhas Undercurrent up the continental slope and onto the continental shelf. Fewer occurrences of northeastward flow were observed at the inshore mooring, and these occurred at shorter timescales.

The direction plot of the inshore mooring (Figure 4.5a) shows the dominant southwestward flow, but also the two major reversal events. The inshore mooring went offline in October

2011 and failed to capture data during the last two months of the deployment. At the surface, an average direction of 196° was found and close to the sea-floor the bottom layer showed an average current direction of 158°. Thus principal flow in the surface layer at the inshore mooring was in a southwestward direction. A maximum frequency of 66 % of current occurrences was found to flow in a southwestward direction (between 180° and 240°). A second, smaller maximum frequency of 26 % of current occurrences was found between 180° and 210°, representing a south to southwestward current direction in the surface layer. The remaining 8 % of currents occurred in each directional sector, with the highest of these minority values being 1.5 % in a northeastward direction (between 0° and 60°).

The direction plot of the slope mooring (Figure 4.5b) indicated the three major reversal events. The upper layers of the water column (shallower than 500 m) displayed an average direction of 202° (southwestward), while the bottom layers (500 to 1000 m depth) had an average of 138° (southeastward). The highest percentage frequency (66 %) of current measurements in the surface layer (<500 m) at the slope mooring was found in the 210° to 240° range (southwestward). An intermediate percentage of current direction (~25 %) were found to flow between 180° and 210°, indicating southward flow in the surface layer. The remaining currents (9 %) were found to travel in an offshore or onshore direction. The slope mooring indicated a net flow of currents in the bottom layers (500 to 1000 m) to have a northeastward direction (30° and 60°) 58 % of the time. Minor instances (20 %) of southwestward flow (180° to 270°) were present during the five month period. The remaining 22 % of currents were distributed between offshore and onshore directions.

The direction plot of the offshore mooring (Figure 4.5c) indicated the three major reversal events, with less variability in the surface layers (<500 m). The upward looking ADCP recorded an average current direction of 218° in the top 500 m of water. The bottom layers (500 m to 2000 m) as recorded by the downward facing ADCP and four of the five DVS single point current meters showed an average current direction of 203°. The highest percentage frequency of current measurements at the offshore mooring were found in the 210° to 240° range consisting of a maximum frequency percentage of 86 %. This indicated a surface current, travelling parallel to the coast in a southwestward direction, most likely the Agulhas Current. Second highest frequency (10 %) of current direction was recorded between 180° and 210°, which indicated southward flow as well. The remaining currents flowed from an offshore and onshore direction. The offshore mooring data indicated a more

varied current regime for the bottom layers (500 to 2000 m) with southwestward flow observed 49 %, and northeastward currents were found 27 % of the time. Currents flowing from an offshore and from an onshore direction account for the remaining 24 % of measurements.
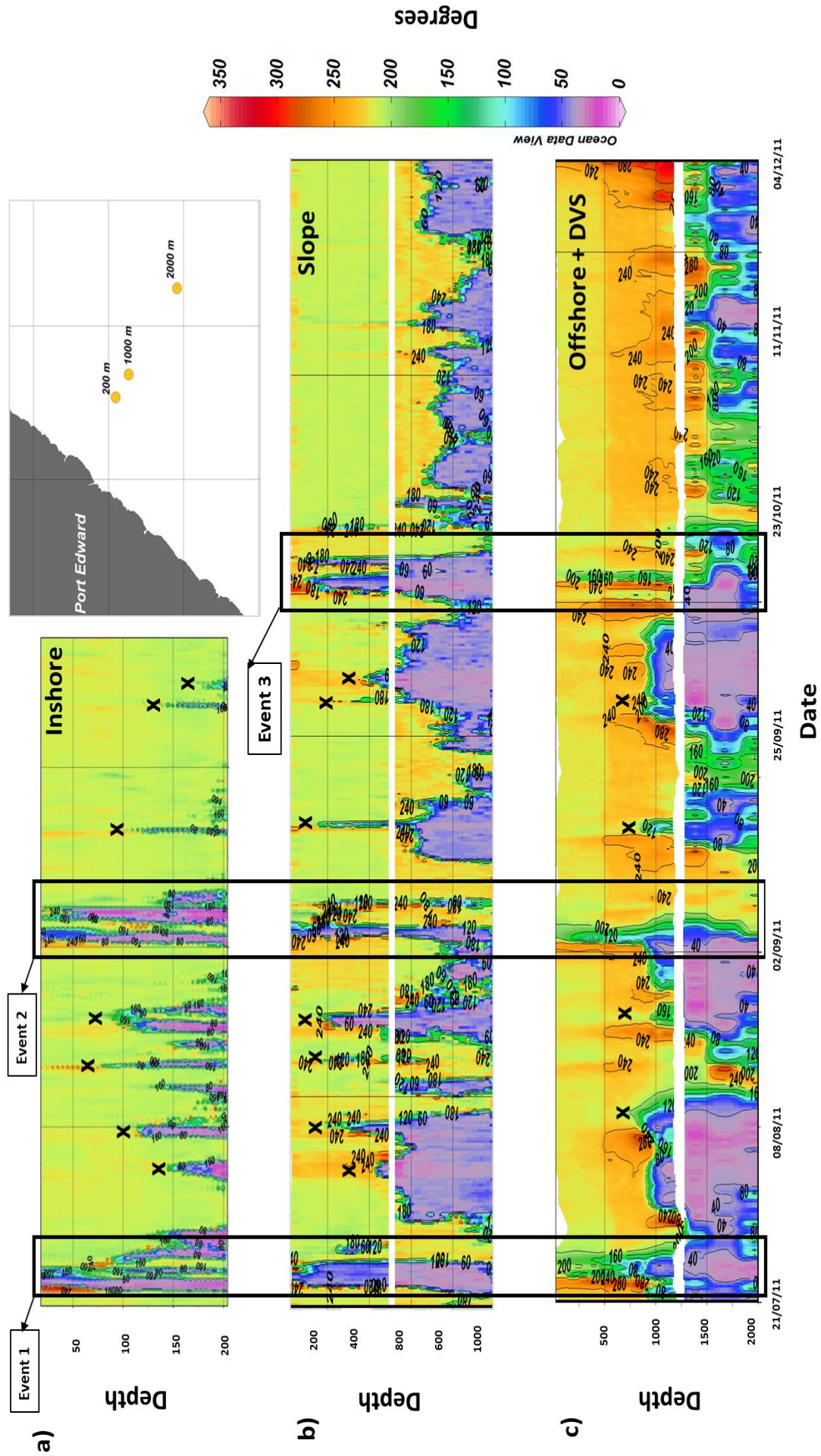
Figure 4.5: Depth profiles showing current direction for all three moorings from 21 July 2011 to 04 December 2011. Top panel a) shows the inshore mooring, middle panel b) the slope mooring and bottom panel b) the offshore mooring, which included the single point current meters (DVS). The inshore mooring stopped recording on 07 October 2011 due to technical problems. The blocks highlighted major reversal events. The 'X' indicates minor reversal events.

35

4.2.2 <u>Current velocity</u>

The time series of velocity at the three moorings are shown in Figure 4.6. Velocity was seen to decrease from the surface to the bottom layers.   The three current reversal events identified in Figure 4.5, were associated with decreases in current strength in the surface bins (Figure 4.6). As the Agulhas Current reached maximum velocities in the surface layers, velocities at greater depths (~500 m) increased correspondingly to values approaching 100 cm/s. Velocities in excess of 150 cm/s were recorded up to 375 m depths in the slope and offshore moorings. These velocities (>150 cm/s) were recorded at shallower depths of 125 m in the inshore mooring data. During current reversal events, surface velocities recorded ranged between 0 and 50 cm/s at all three mooring locations. Sub-surface reversal events lasting between 12 and 48 hours were reported by all three moorings simultaneously, with reduced velocities observed through the majority of the water column. These sub-surface peaks were marked by 'X's" in Figure 4.6.   Highest velocities were present directly after reversal events in the surface layers and penetrated to deeper depths than at other times during the study.   These peak velocities coincide with a current travelling in a southward direction throughout the water column. Bottom velocities were generally less energetic than at the surface layers and thus the effect of current reversals were not that pronounced in the bottom layers in terms of velocity.

Current velocity at the inshore mooring showed a maximum surface velocity of 213 cm/s and an average of 108 cm/s.   Majority of the surface currents (44 %) had velocities between 100 cm/s and 150 cm/s. The second highest peak (27 %) of currents in the surface layer was found between 50 cm/s and 100 cm/s. Fewer instances (18 %) of currents exceeded 150 cm/s, while the remaining 11 % of currents reported were between 0 cm/s and 50 cm/s. The average velocity for the bottom bin at the inshore mooring was 13 cm/s. A peak velocity of 69.0 cm/s and a minimum of 0.0 cm/s was recorded for the bottom layers at the inshore mooring.   The maximum frequency distribution of bottom velocity at the inshore mooring occurred between the 0 and 10 cm/s sector (49 %). A second intermediate peak of current velocity was recorded between 10 and 20 cm/s (31 %), with fewer measurements recorded between 30 and 70 cm/s (20 %).

The slope mooring exhibited higher incidences of current velocities above 150 cm/s in the surface layers than the inshore and offshore moorings. The maximum current velocity at the slope mooring was 203 cm/s, with average speeds of 98 cm/s. Currents between 0 cm/s and 50 cm/s were encountered 15 % of the time. Majority of the currents (42 %) recorded were between 50 cm/s and 100 cm/s and 36 % of currents occurred between 100 cm/s and

150 cm/s. Currents above 150 cm/s accounted for 7 % of the percentage frequency occurrences. Bottom velocities for the slope mooring indicated a maximum velocity of 56 cm/s, minimum of 0 cm/s and an average of 19 cm/s. A maximum percentage (51 %) of bottom current measurements observed at the slope mooring was recorded between the 0 and 10 cm/s range. A secondary peak (29 %) between 10 and 20 cm/s was reported and, as with the inshore mooring, fewer frequencies (20 %) of velocity measurements were recorded between 30 and 70 cm/s.

Surface velocities reached a maximum of 238 cm/s with an average of 123 cm/s at the offshore mooring. The offshore mooring exhibited a maximum velocity at the bottom layers of 30 cm/s and a minimum velocity of 0 cm/s was recorded. An average bottom velocity of 13 cm/s was recorded by the offshore mooring. Maximum frequency distributions (45 %) of current velocities recorded were between 10 and 20 cm/s in the bottom layer, with smaller peaks between 0 and 10 cm/s and between 20 and 30 cm/s also present.

Peak velocities of the Agulhas Undercurrent indicated the core to have been present between 1000 m and 600 m at the slope mooring on three occasions. The first occurrence of the Agulhas Undercurrent core was recorded on 06 August 2011, after Event 1. A second, less pronounced core was visible in the offshore mooring data during the same period. The second observable example of a swift flowing undercurrent core in the slope mooring data was recorded after Event 2 on 12 September 2011 (Figure 4.6). The third instance of an undercurrent core occurred on 01 October 2011, prior to Event 3 and exhibited weaker velocities than the previous two core velocities recorded, however it still displayed stronger velocities than the surrounding water (Figure 4.6).
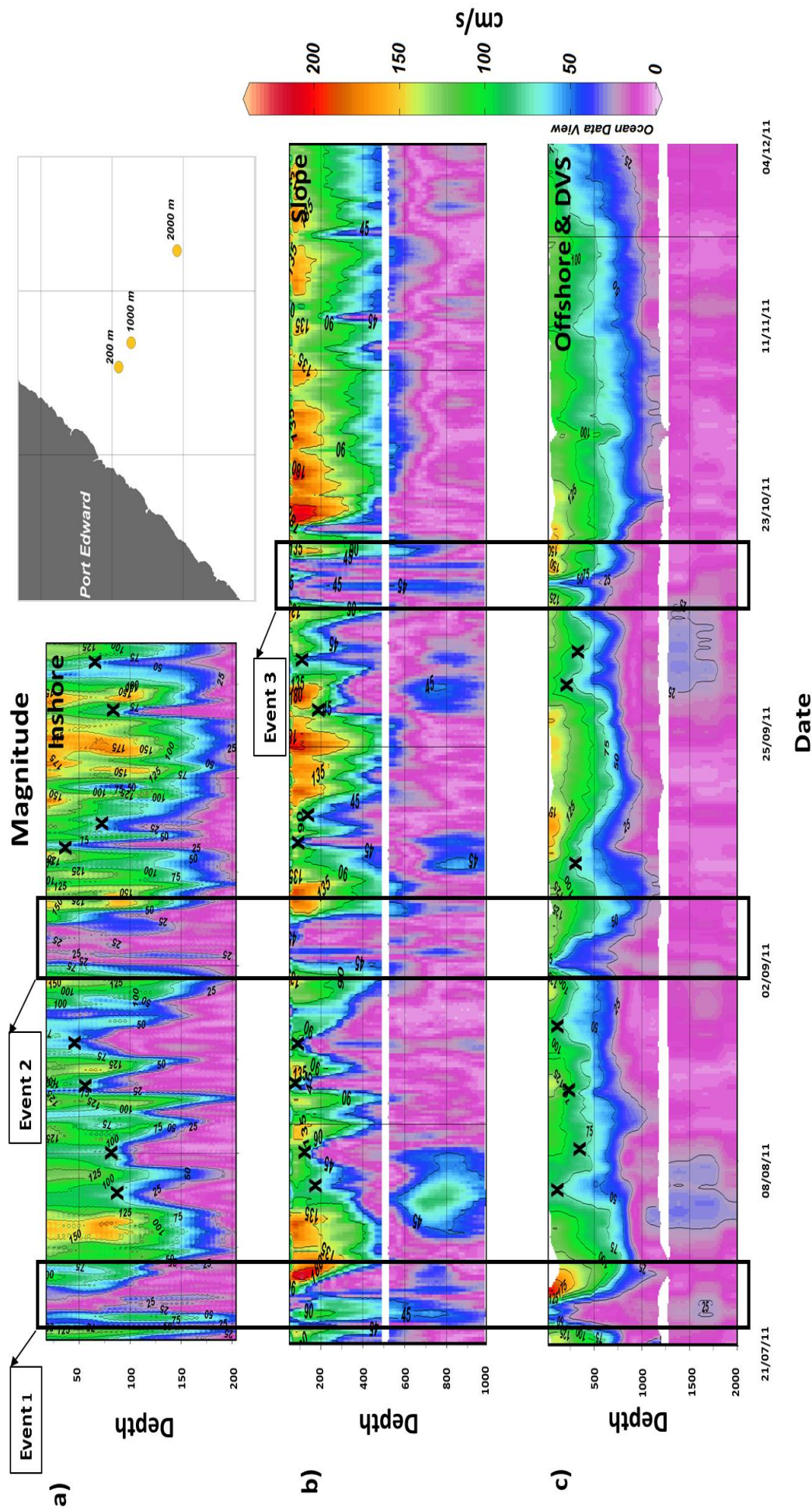
Figure 4.6: Depth profiles showing current velocity for all three moorings from 21 July 2011 to 04 December 2011. Top panel a) shows the inshore mooring, middle panel b) the slope mooring and the bottom panel c) the offshore mooring which included the single point current meters (DVS). The inshore mooring stopped recording on 07 October 2011 due to technical problems. The blocks highlighted major reversal events. The 'X' indicates minor reversal events.

4.2.3   Temperature time series

Temperature was measured at an average depth of 500 m from the ADCP's in both the slope and offshore moorings, while temperature measurements of the inshore mooring were taken at 200 m. Figure 4.7 is not a temperature depth profile, but rather the cross-stream temperature values as measured by the mooring line in an inshore/offshore extent. Concurrent decreases in temperature were evident in all three moorings and MicroCat data sets during the three major current reversal events. Temperature averages decreased from inshore to offshore stations. Temperature averages were in the order of 13 °C (± 0.91 °C) for the inshore mooring (Figure 4.7a), 10 °C (± 0.96 °C) for the slope mooring (Figure 4.7b) and 9 °C (± 0.77 °C) for the offshore mooring (Figure 4.7c). MicroCat 1 (661 m) recorded a temperature average of 9 °C (± 0.97 °C) (Figure 4.7d), MicroCat 2 (951 m) exhibited an average temperature of 5 °C (± 0.57 °C) (Figure 4.7e), MicroCat 3 (1241 m) recorded an average of 4 °C (± 0.23 °C) (Figure 4.7f), MicroCat 4 (1530 m) recorded an average of 3 °C (± 0.09 °C) (Figure 4.7g) and the deepest instrument, MicroCat 5 (1820 m), also reported an average of 3 °C (± 0.06 °C) (Figure 4.7h). Upwelling during Event 1 caused temperature declines of up to 6 °C at the inshore mooring during a four day period (23 July to 27 July).
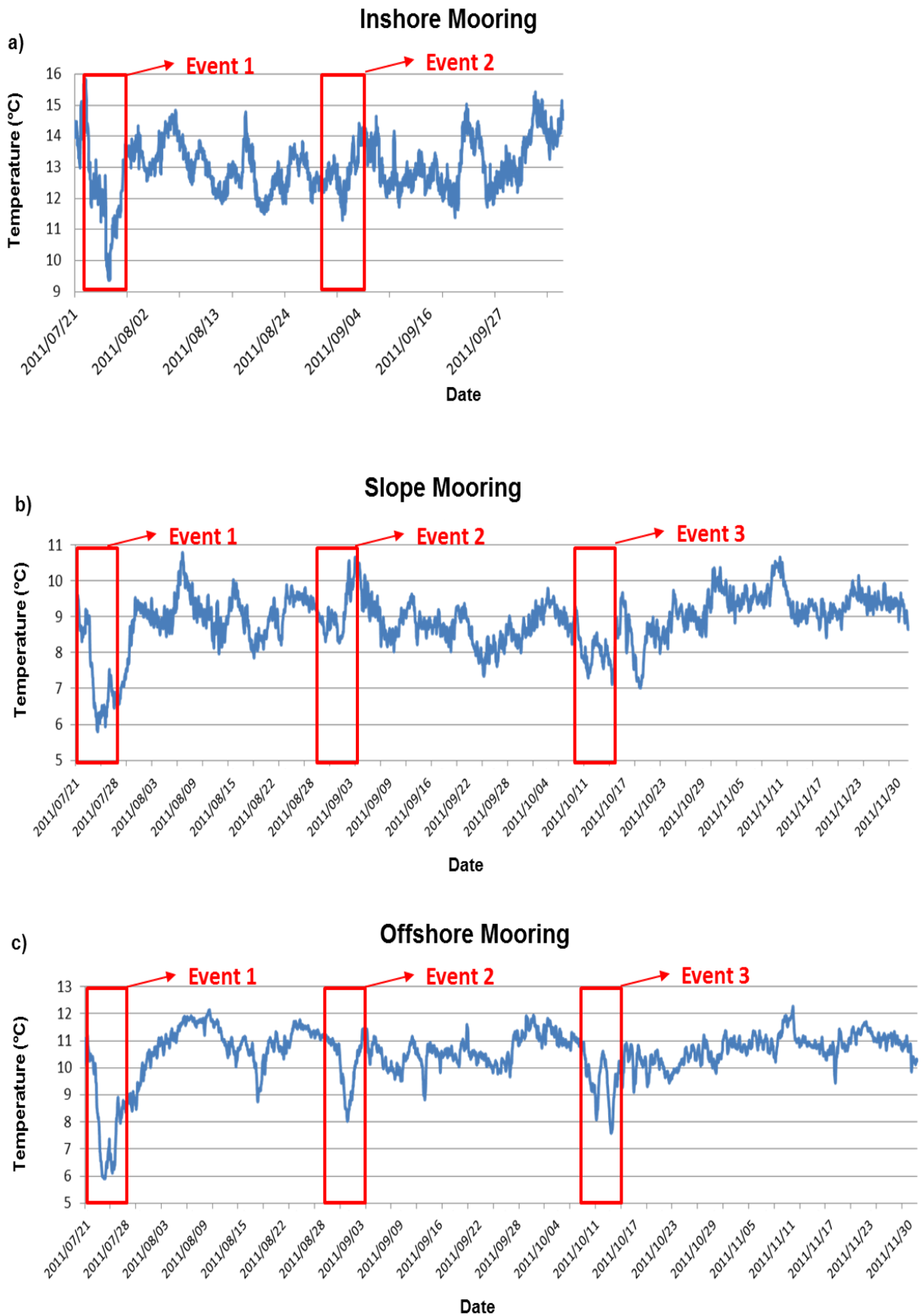
Figure 4.7: Temperature time series for (a) inshore mooring (b) slope mooring (c) offshore mooring (d) 661 m DVS (DVS1) (e) 951 m DVS (DVS2) (f) 1241 m DVS (DVS3) (g) 1530 m DVS (DVS4) and (h)1820 m DVS (DVS5). Temperature decreases during the three reversal events are highlighted by red boxes. Note: Difference in scales**.**
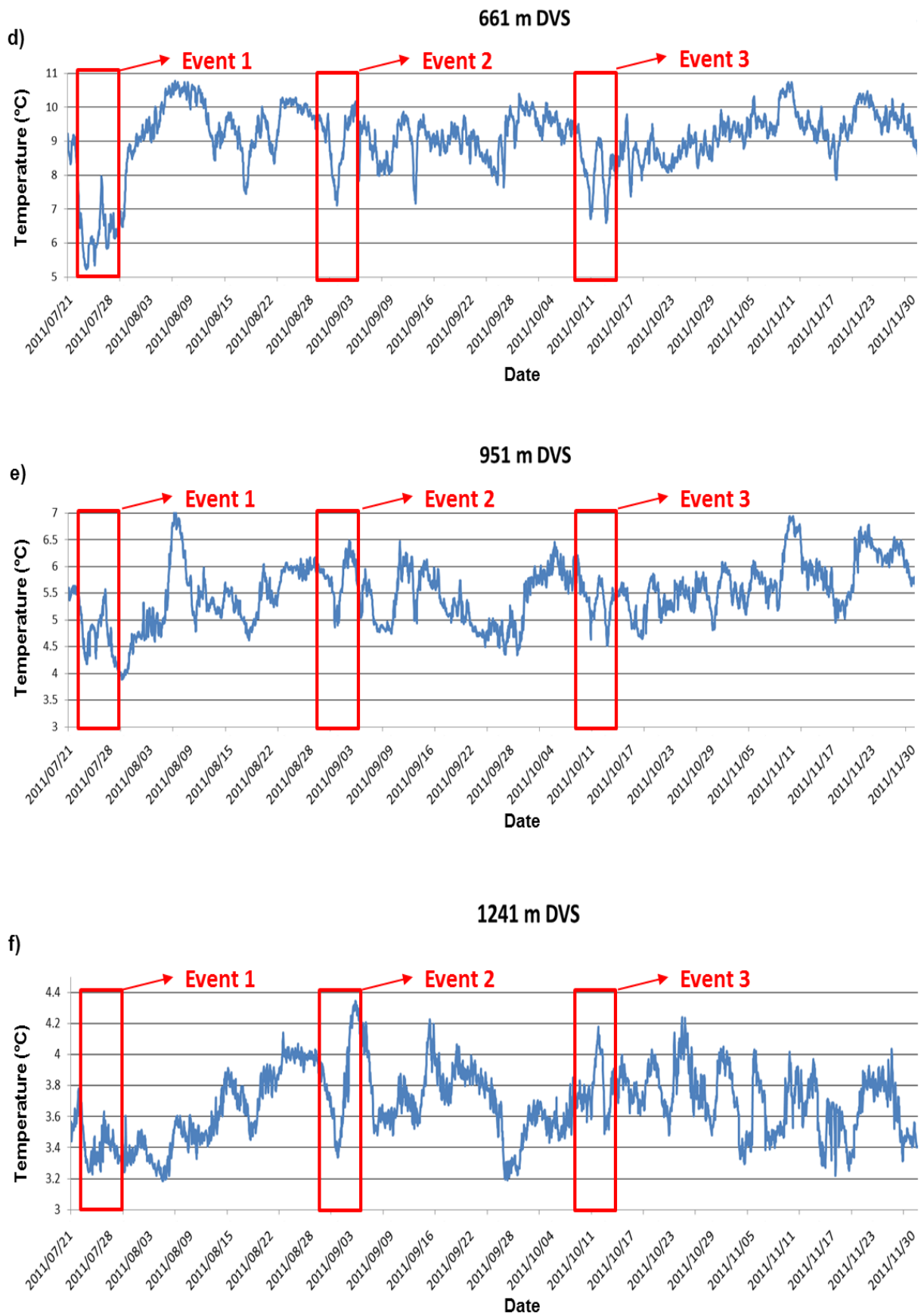
Figure 4.7 continued: : Temperature time series for (a) inshore mooring (b) slope mooring (c) offshore mooring (d) 661 m DVS (DVS1) (e) 951 m DVS (DVS2) (f) 1241 m DVS (DVS3) (g) 1530 m DVS (DVS4) and (h)1820 m DVS (DVS5). Temperature decreases during the three reversal events are highlighted by red boxes. Note: Difference in scales**.**

41
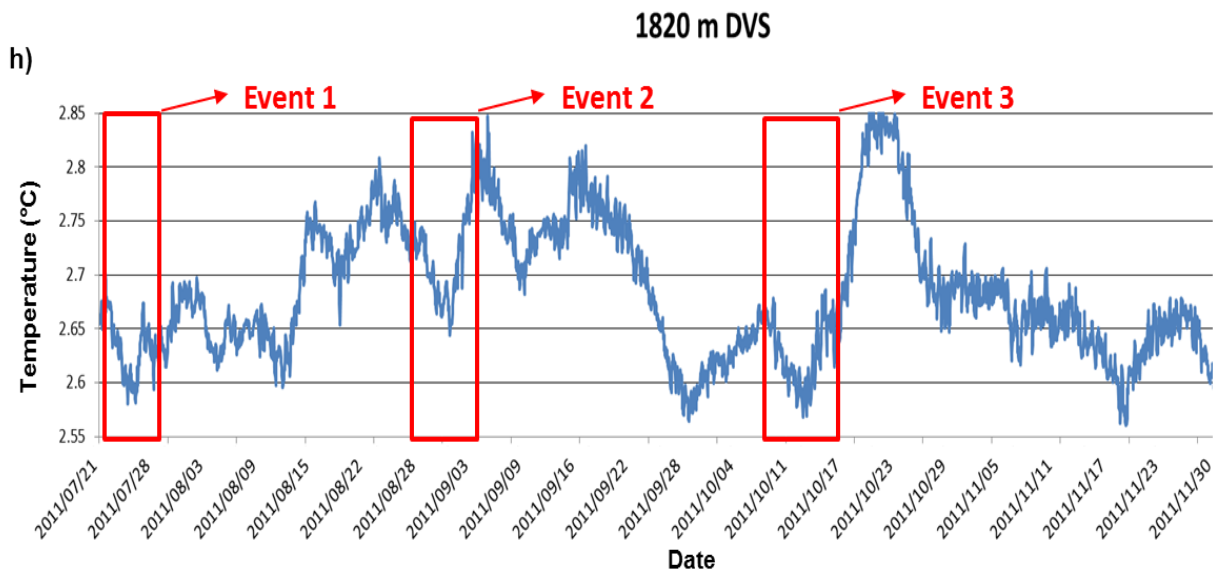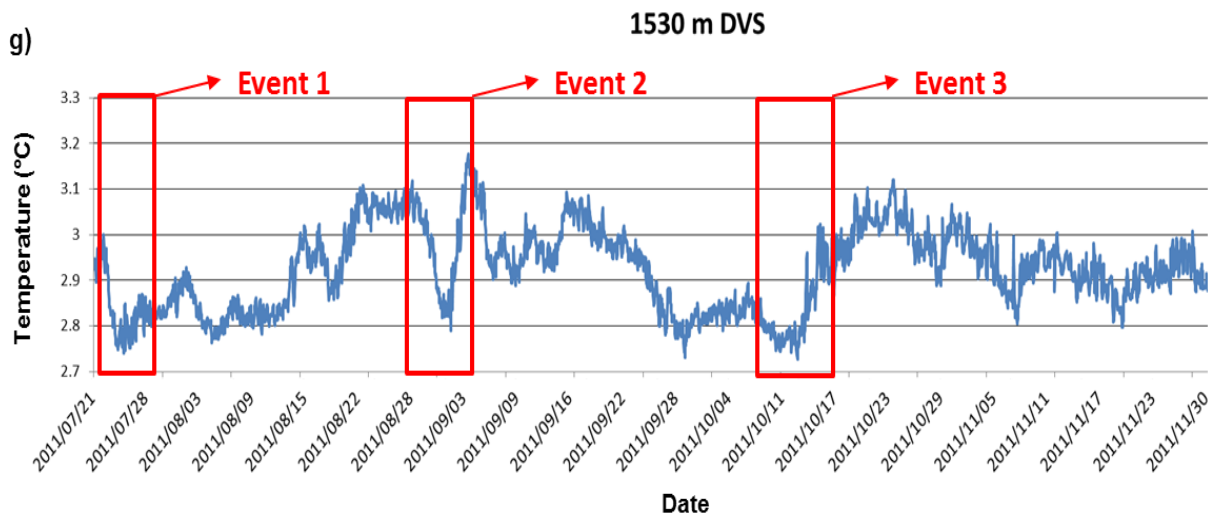
Figure 4.7 continued: Temperature time series for (a) inshore mooring (b) slope mooring (c) offshore mooring (d) 661 m DVS (DVS1) (e) 951 m DVS (DVS2) (f) 1241 m DVS (DVS3) (g) 1530 m DVS (DVS4) and (h)1820 m DVS (DVS5). Temperature decreases during the three reversal events are highlighted by red boxes. Note: Difference in scales.

4.3 Event investigations

In this section, the causes of the 3 major current reversals observed in Fig. 4.5 are investigated.

4.3.1 Event 1 – 23 July 2011

Figure 4.8 shows an expanded view of Event 1 from 22 July 2011 to 27 July 2011. Vertical plots for velocity and direction for all moorings are presented together with temperature measurements. Changes in the entire water column's direction during Event 1 were simultaneously accompanied by decreases in velocity and temperature. The effect of Event 1 was observed at all three mooring sites. Event 1 had a duration of three days, occurring from 23 July 2011 to 26 July 2011. The physical effects of Event 1 were reflected in the direction, velocity and temperature data.

Event 1 was more pronounced at the slope mooring than at the offshore mooring, as evident by the sustained period of northward current flow (0° - 90° and 270° to 360°). From the surface layer to a depth of 750 m, the current mainly flowed in an eastward (offshore) direction during the propagation of Event 1 at the offshore mooring. The bottom layers continued to flow in a northeastward direction, indicative of an undercurrent. Directional changes of the current at the inshore and offshore moorings firstly displayed a northwestward current (onshore) at the onset of Event 1. During Event 1 the offshore mooring indicated an eastward movement of water in the upper 1000 m of the water column and north to northeastward flow in the bottom 1000 m. The surface bins at the inshore and offshore moorings recorded two phases occurring within Event 1. With the onset of northward current reversals the velocity decreased and within a 12 hour period increased again. The increase in velocity lasted less than 24 h and once again decreased velocities (≤ 50 cm/s) were observed toward the end of Event 1. The slope mooring had a sustained period of northward flow and did not record a period of southwestward flow separating northeastward flow as did the inshore and offshore moorings.

Current reversals were associated with decreases in velocity from 100 – 150 cm/s to < 50 cm/s. Velocities within Event 1, at the inshore mooring were < 10 cm/s on 24 July 2011. The slope mooring recorded a current velocity range of 239 cm/s to 22 cm/s on 24 July

2011, at the surface layers. A maximum bottom velocity of 67 cm/s was recorded by the slope mooring and decreased to 0 cm/s during the core of Event 1. Reduced surface velocity was recorded at the offshore mooring on 24 July 2011. This delayed response suggested a 24 h lag between the inshore and slope moorings, and the offshore mooring. Majority of the current velocities for the surface layer at the inshore mooring were found between 80 and 160 cm/s. The high frequencies of peak velocities (>150 cm/s) were found during southward flow. Northward currents were associated with weaker velocities (≤ 50 cm/s) in the surface layers at the inshore mooring. The majority of velocity measurements in the bottom bin at the slope mooring were between 0 and 10 cm/s duration of Event 1.

All three moorings measured decreases in temperature during Event 1. With the onset of Event 1, the inshore mooring recorded a decrease in temperature from 16 °C to 10 °C. The slope mooring recorded a decrease from 11 °C to 6 °C and the offshore mooring recorded a decrease in temperature from 9 °C to 6 °C.
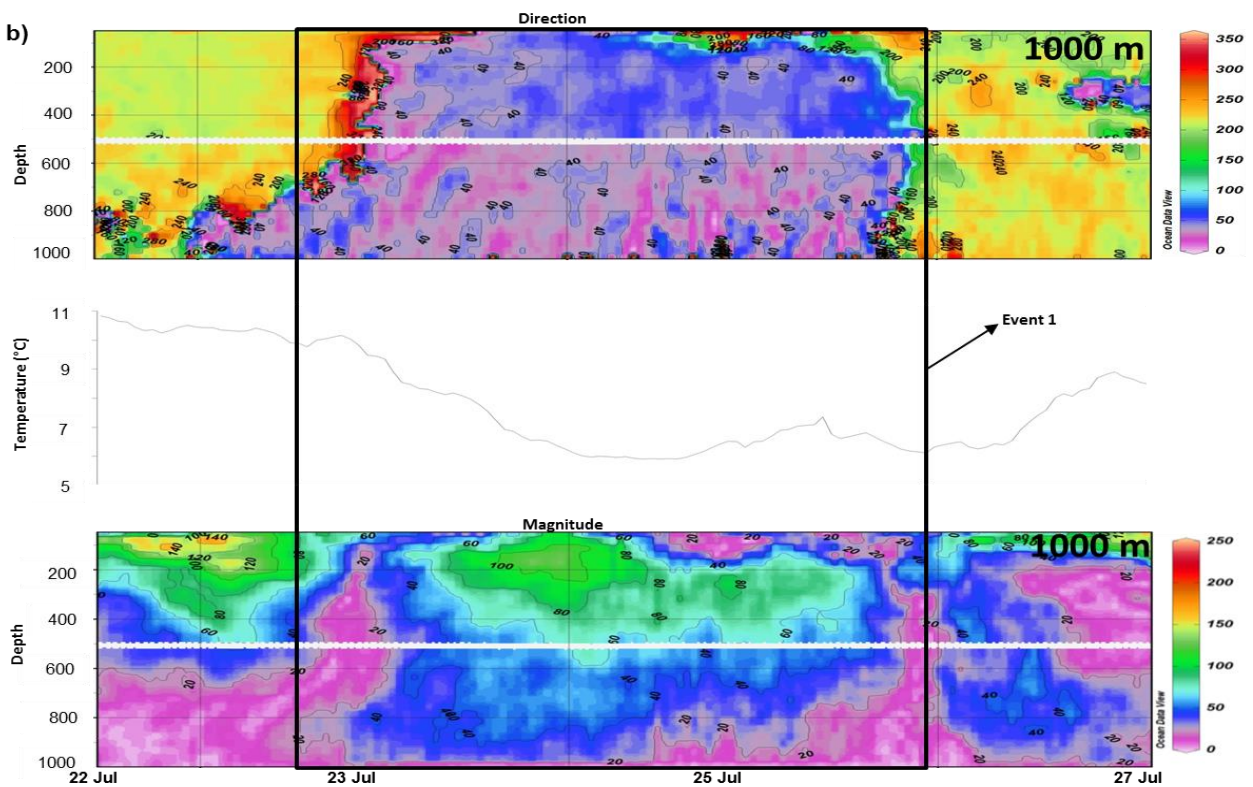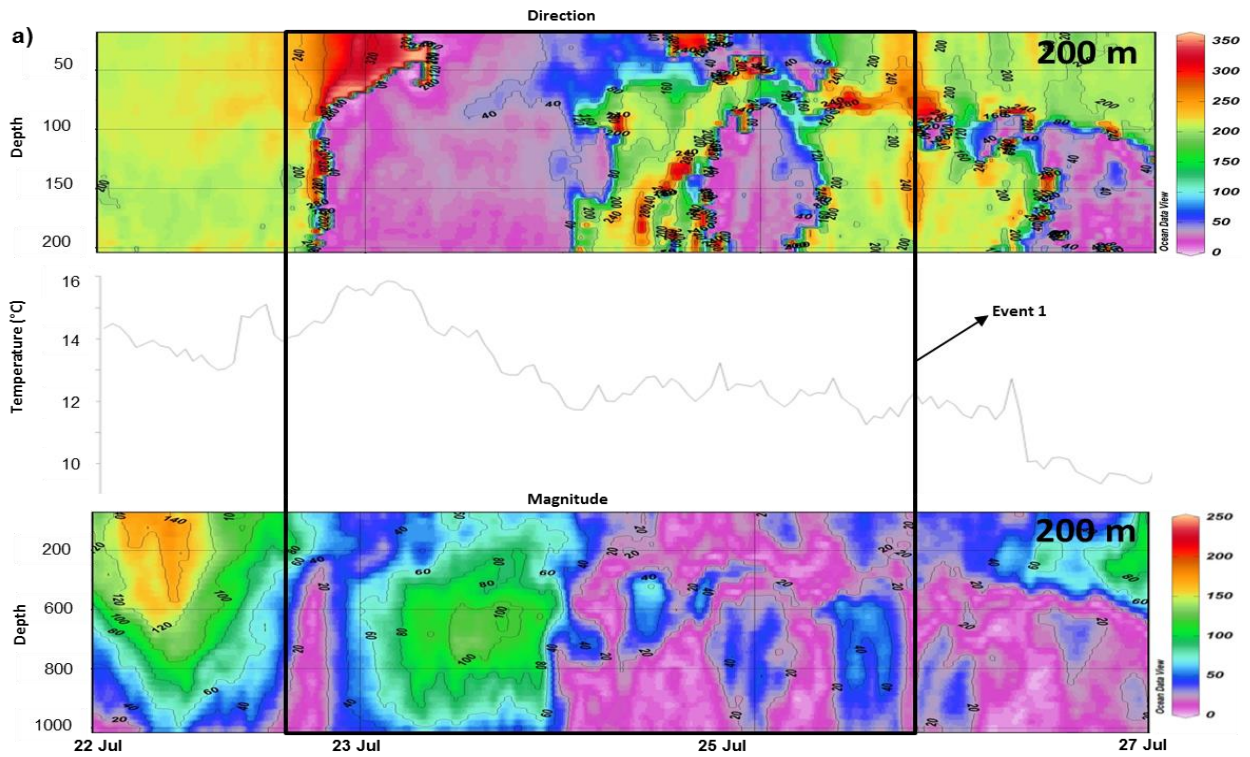
Figure 4.8: Current direction, velocity and temperature for all three moorings for the period from 22 July to 27 July 2011 at (a) inshore mooring (b) slope mooring and (c) offshore mooring. Note: Difference in scales. The black outline highlights Event 1.
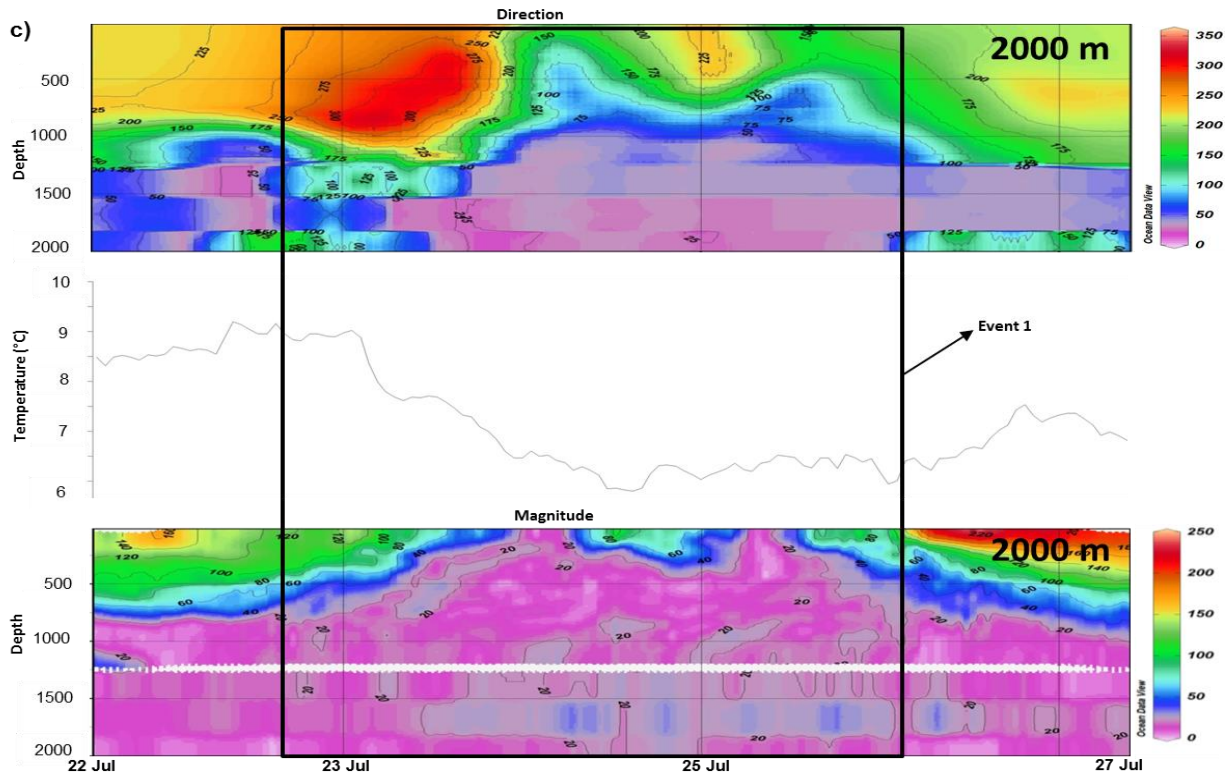
Figure 4.8 continued: Current direction, velocity and temperature for all three moorings for the period from 22 July to 27 July 2011 at a) inshore mooring b) slope mooring and c) offshore mooring. Note: Difference in scales. The black outline highlights Event 1.

Frequency histograms of current direction for the period 21 July 2011 to 21 August 2011 (Figure 4.9) showed current direction peaks between 180° and 240° for all three moorings (a, b and c). These values indicated south to southwestward flow. Disruptions to the southwestward currents were mainly due to currents with a northward component occurring during Event 1, where directions of between 0° and 30°, as well as 330° to 360° were recorded. Minor occurrences of onshore (shoreward) movement were reported by all three moorings and in both the surface and bottom bins. A more uniform distribution of northeastward and southwestward currents in the bottom layers were recorded by the inshore mooring. Two peak predominant directions occurred, the first between 0° and 30° indicating north to northeastward flow, and the second peak between 180° and 240° showing in a south to southwestward direction. The histogram representing the slope mooring's data displayed a similar pattern to that of the inshore mooring, with a high occurrence of southward and northward currents. Currents with a northward component were most prominent in the bottom bins. A principal current axis at the offshore mooring between 210° and 240° (southwestward) was recorded. Currents with a northward component were more frequent, yet minor frequencies of onshore (shoreward) and offshore

46

(eastward) currents were more prevalent at the offshore mooring than at the inshore and slope moorings.
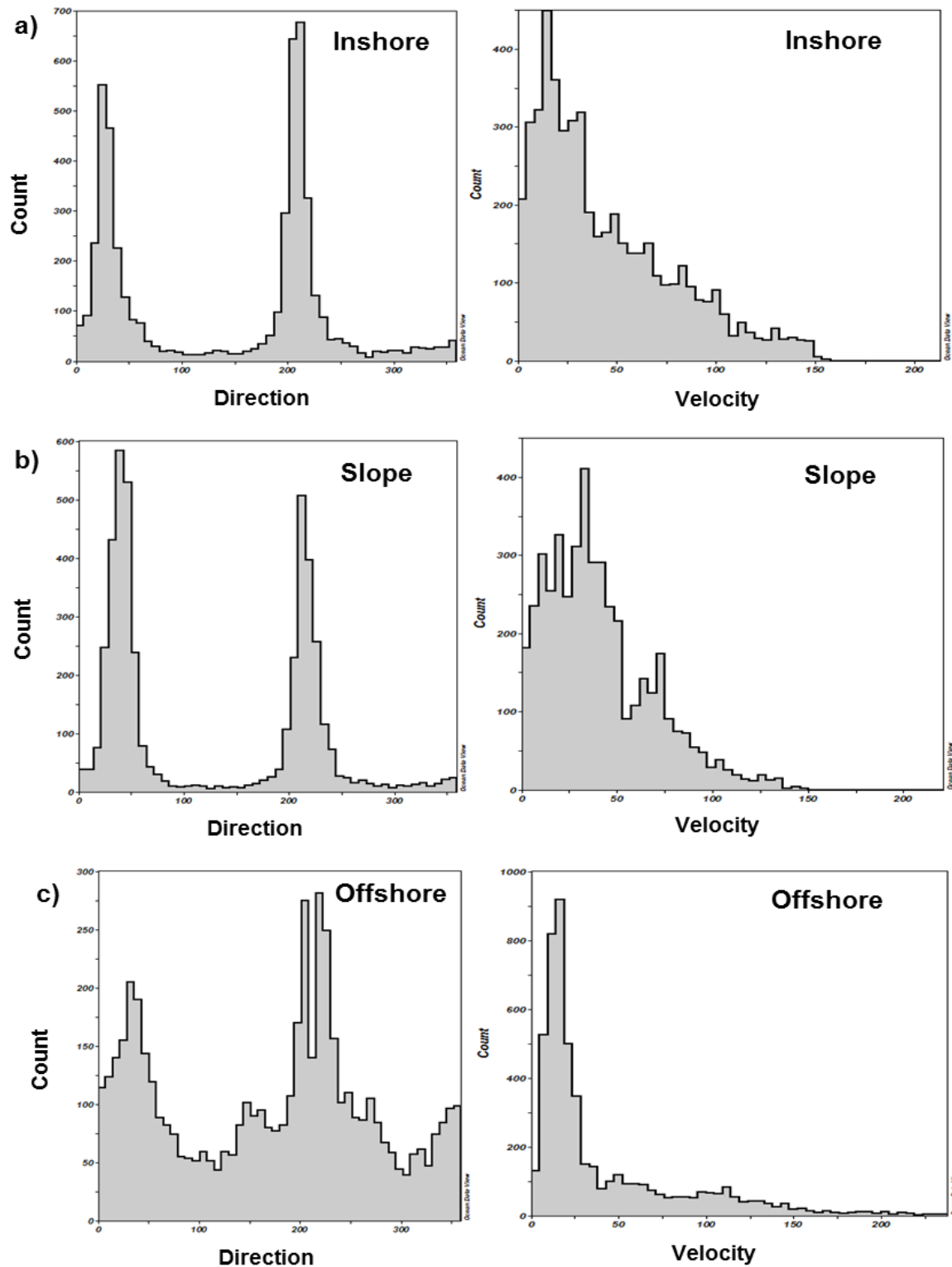
Figure 4.9: Percentage frequency histogram for direction (left column) and velocity (right column) for the (a) inshore mooring, (b) slope mooring and (c) offshore mooring during the period 21 July to 27 July 2011 (Event 1).

The composite altimetry data presented in Figure 4.10a showed the eddy field for 13 July 2011, 10 days before the start of Event 1. The depression situated in the Natal Bight region (blue) may be evidence of the Durban cyclonic eddy as a negative sea level anomaly as shown in Figure 4.10a. Flow around the Durban eddy was cyclonic, with the inshore boundary flowing in a northward direction. As the Durban cyclonic eddy migrated in a southwestward direction on 21 July 2011 (Figure 4.10b) the currents at Port Edward changed concurrently from a southwestward direction to a northeastward direction as depicted by the stick vector plots in Figure 4.10d. However, the offshore mooring recorded currents flowing in a westward direction (onshore). As the Durban cyclonic eddy propagated further south and past the mooring line on 26 July 2011 southwestward flow resumed at all the mooring locations. A positive sea level anomaly (E) was seen to migrate in a southwestward direction, located offshore of the depression around Durban.
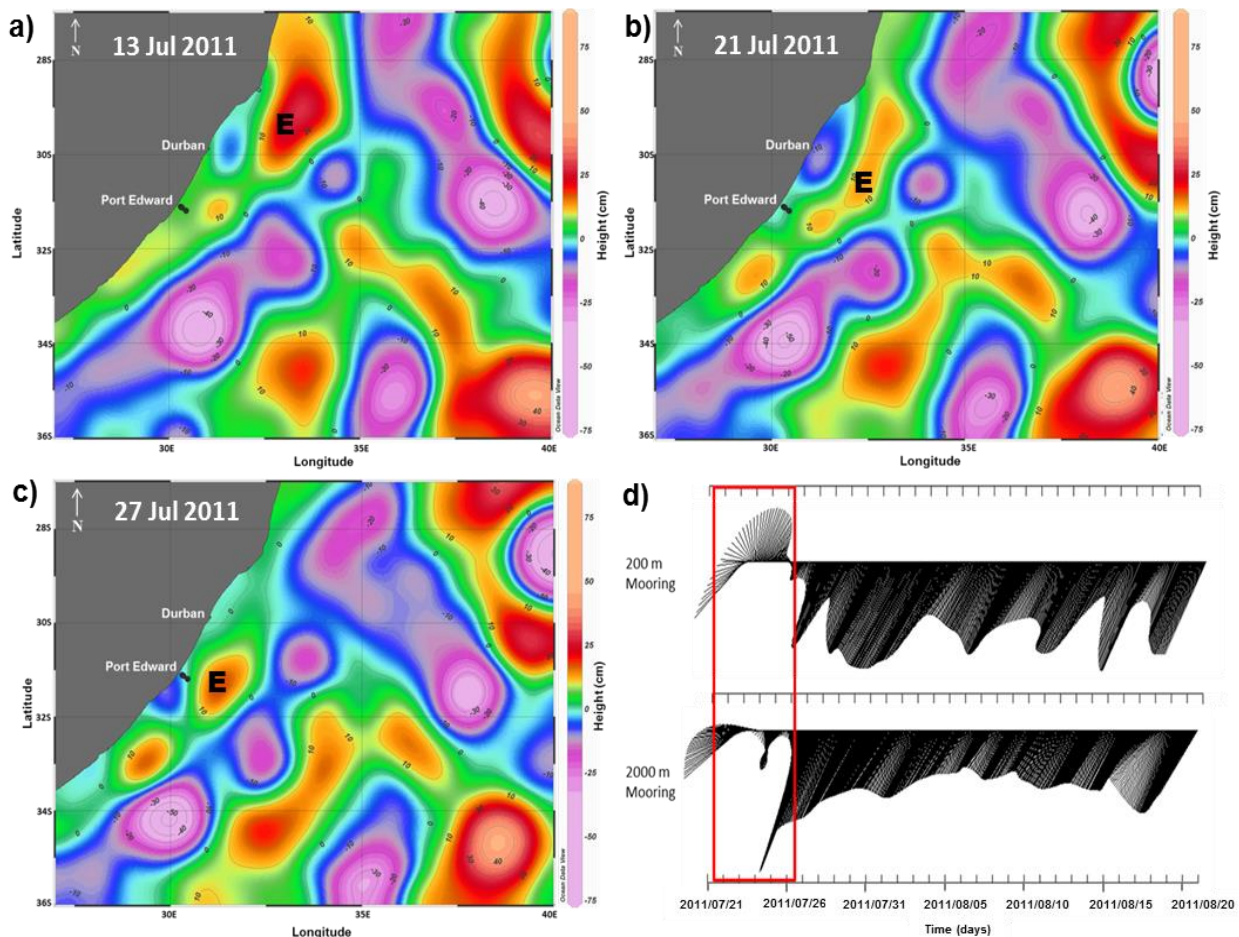
Figure 4.10: SSHA time series representing the period before a) 13 July 2011, upon initiation b) 21 July 2011 and after Event 1 c) 27 July 2011. Figure 4.14 d) displays accompanying velocity stick vector plots for Event 1. The mooring line position and offshore extent of the moorings are represented by the black dots.

The stick vector plots for the slope mooring displayed a similar pattern to that of the inshore and offshore moorings, but were omitted for brevity. Figure 4.10c shows the eddy field for 27 July 2011, three days after Event 1. Northward currents at Port Edward were absent at this time and current flow had resumed in a southwestward direction. From Figure 4.10c the cyclonic eddy responsible for current reversals had passed the moorings' position (31 °S), but was still situated on the inshore boundary of the Agulhas Current, south of Port Edward.

Sea surface temperature and ocean colour (satellite chlorophyll-*a*) data during this period was investigated, but overcast days during and preceding the occurrence of Event 1 hindered the process of identifying cyclonic anomalies in the ocean colour images. The depression which originated in the Natal Bight, as identified in the SSHA images was not clearly visible in the available ocean colour images. The cyclonic event responsible for reversals had not manifested in the satellite SST data set, most likely because differences between the thermal expression of the cyclonic event and the surrounding Agulhas Current were not apparent. For this reason, SST and chlorophyll-*a* images have not been shown for Event 1.

The evidence presented by the *in situ* and satellite data suggested that the cyclonic event responsible for current reversals at Port Edward on 23 July 2011 resembled that of the Durban cyclonic eddy, shedding from its point of origin in the Natal Bight region. The positive sea level anomaly may have triggered the generation of this eddy (Figure 4.10)

As with Event 1, the influence of Event 2 on the dynamics of the water column was observed in all three mooring data sets. The effects of Event 2 were more marked at the inshore and slope moorings (Figure 4.11) in terms of velocity and direction. Analyses of the inshore and slope mooring data suggested that Event 2 comprised two separate reversal phases, separated by a period of south to southwestward current flow.   During the period of southward flow which separated the two northward phases of Event 2, velocities remained between 0 and 50 cm/s and displayed an increase in temperature of 4 °C (Figure 4.11a). Event 2 had a duration of four days, occurring from 02 September 2011 to 06 September 2011.

Event 2 had produced currents with directions of between 0 and 90 degrees and between 300 and 330 degrees. Principal flow of the currents recorded was south to southwestward (180 to 240 degrees) at all three moorings and possessed sluggish velocities.   Minor manifestations of northward flow occurred between 0 and 30 degrees. Event 2 caused northward flowing currents at the inshore and slope moorings. Effects of Event 2 at the offshore mooring were not as distinct, only displaying an offshore movement of water which still contained a southward component. The inshore and slope mooring systems recorded two separate reversal phases embedded within Event 2 and consisted of one day of northward flow, one day of southward flow, followed once again by a day of northward flow. Northward and southward flow during Event 2 was observed throughout the water column. The offshore mooring provided a more stratified current regime in terms of direction, with northward flow only appearing deeper than 1000 m, underlying the shallower offshore currents.

Current reversals were associated with decreases in velocity from 150 cm/s to < 50 cm/s. Majority of the current velocity measurements for the surface layer at the inshore mooring were recorded between 100 and 150 cm/s. The high frequencies of peak velocities were found during southward flow.   Northward currents were usually associated with weaker velocities in the surface layer at the inshore mooring. A maximum surface velocity of 155 cm/s was recorded before the occurrence of Event 2, decreasing to <10 cm/s on 02 September 2011 upon its arrival at the moorings location. The velocities in the surface layer at the inshore mooring remained under 50 cm/s for the entire four day period. A maximum surface velocity of 45 cm/s was recorded after the first phase of northward flow, during the

two day period of southward flow. Velocities at the slope mooring were just over 100 cm/s before Event 2 had affected the dynamics at the mooring. Surface velocities here remained under 50 cm/s for the duration of Event 2, gradually increasing from 05 September 2011 to values in excess of 100 cm/s. Highest surface velocities were recorded from 07 September 2011. Bottom velocities remained consistently slow-moving below 600 m depth, with high variability in current strength from 600 m and shallower. Resultant flow at the offshore mooring during Event 2 was in an eastward direction from 1000 m to the surface (Figure 4.11). Deeper in the water column, flow was in a north to northwestward direction. Velocities were less than 50 cm/s between 600 m to 2000 m depth and between 50 and 75 cm/s from 600 m to the near surface bins. After the occurrence of Event 2 the bottom measurements showed northward flow to be absent until mid-September, when offshore and then northward flow resumed (Figure 4.11). Reductions in surface velocity had started manifesting at the offshore mooring on 01 September 2011. The velocity profile had displayed northward and eastward currents at the offshore mooring and weaker current velocities (≤ 50 cm/s) were present at the offshore mooring for a 24 h period.

All three moorings measured decreases in temperature during Event 2. With the onset of Event 2 the inshore mooring recorded a decrease in water temperature from 13 °C to 11 °C. The slope mooring recorded a decrease in water temperature from 11 °C to 8 °C and the offshore mooring had recorded a slight temperature decrease from 9 °C to 8 °C. Temperature traces for all the moorings increased gradually during the southward flowing phase and once again decreased when the second period of northward flowing currents were encountered within Event 2.
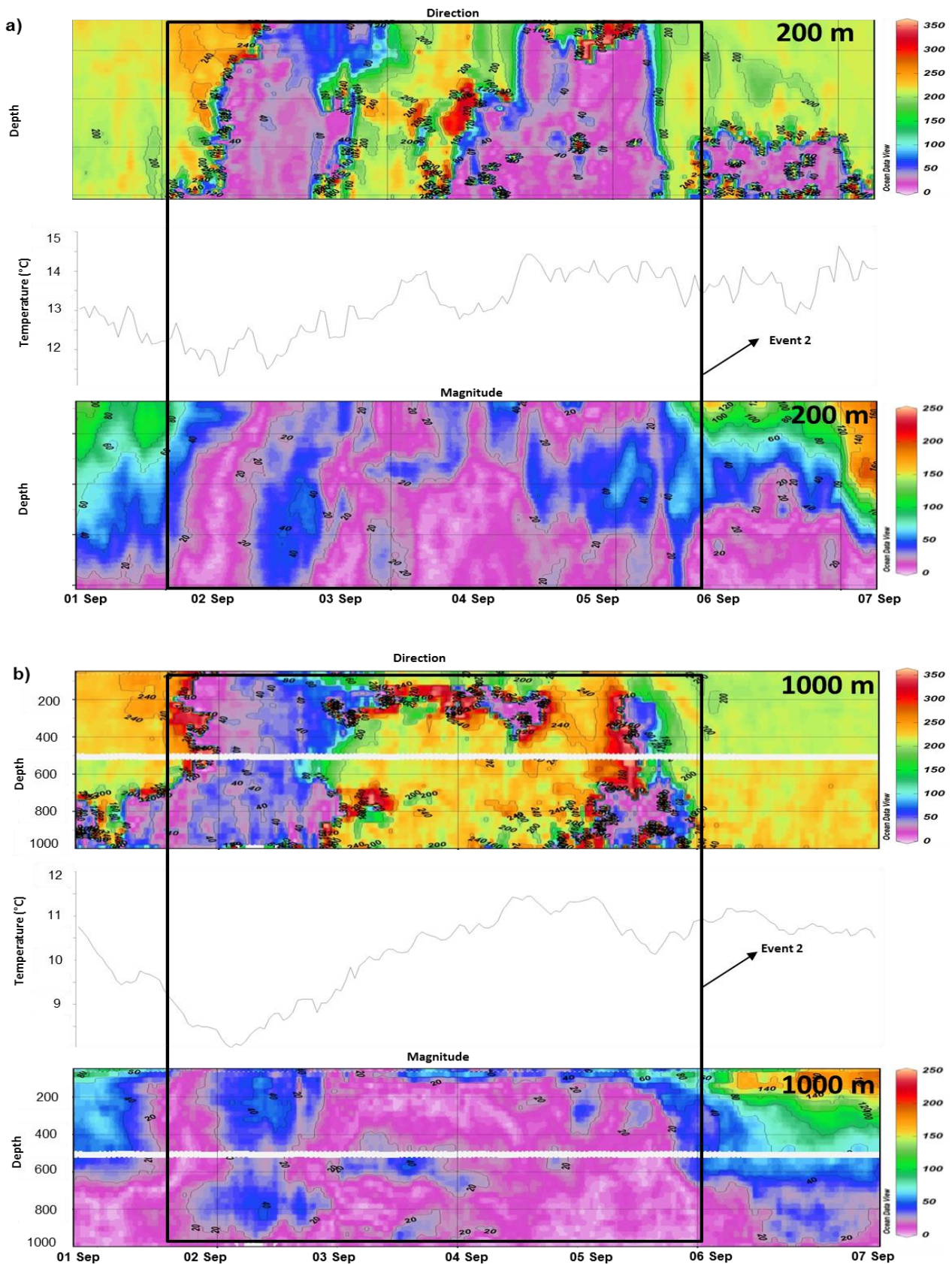
Figure 4.11: Current direction, velocity and temperature for the three moorings for the period 01 September 2011 to 07 September 2011 at a) inshore mooring b) slope mooring and c) offshore mooring. Note: Difference in scales. The black outline highlights Event 2.
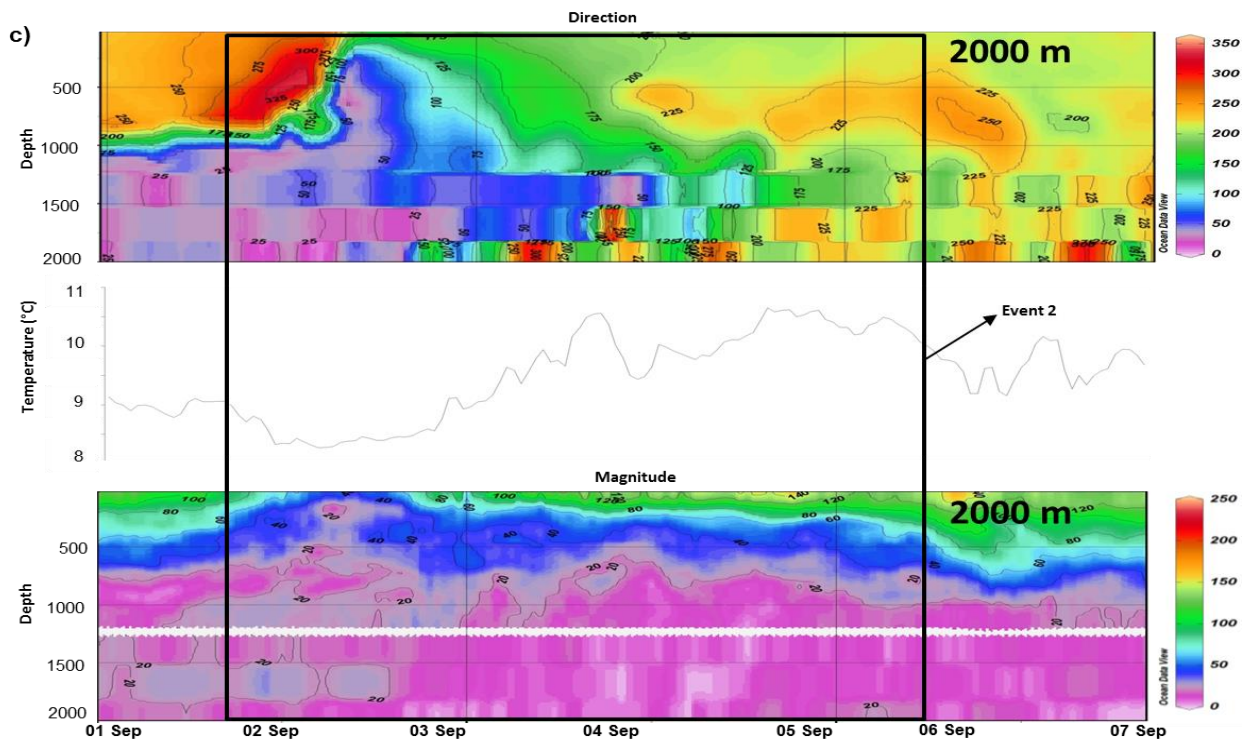
Figure 4.11 continued: Current direction, velocity and temperature for the three moorings for the period 01 September 2011 to 07 September 2011 at a) inshore mooring b) slope mooring and c) offshore mooring. Note: Difference in scales. The black outline highlights Event 2.

Frequency histograms representing the period for Event 2 for 01 September 2011 to 07 September are displayed in Figure 4.12. The moorings showed dominant south to southwestward flowing current. Currents were mainly recorded between 180 and 240 degrees. The inshore mooring recorded high instances of northward and offshore current flow during 01 September 2011 to 07 September 2011 (Figure 4.12a). Velocities below 50 cm/s were the most common at the inshore mooring, only increasing to 150 cm/s after the propagation of Event 2 (Figure 4.12a).

Principal flow at the slope moorings' bottom layer was in a north to northeastward direction (0 to 30 degrees). Velocities between 0 and 10 cm/s were the most common velocities recorded at the bottom layers of the slope mooring (Figure 4.12b).

The principal axis of the surface bin at the offshore mooring was recorded between 210 and 240 degrees (Figure 4.12c). A maximum current velocity of 182 cm/s was recorded and peak velocity frequencies were between 15 and 30 cm/s. Currents recorded within the bottom layer were more erratic, but a maximum frequency of 24 % flowed in a north to

northeastward direction. Compared to the previous two moorings, flow at the offshore mooring exhibited more onshore (westward) and offshore (eastward) movement.
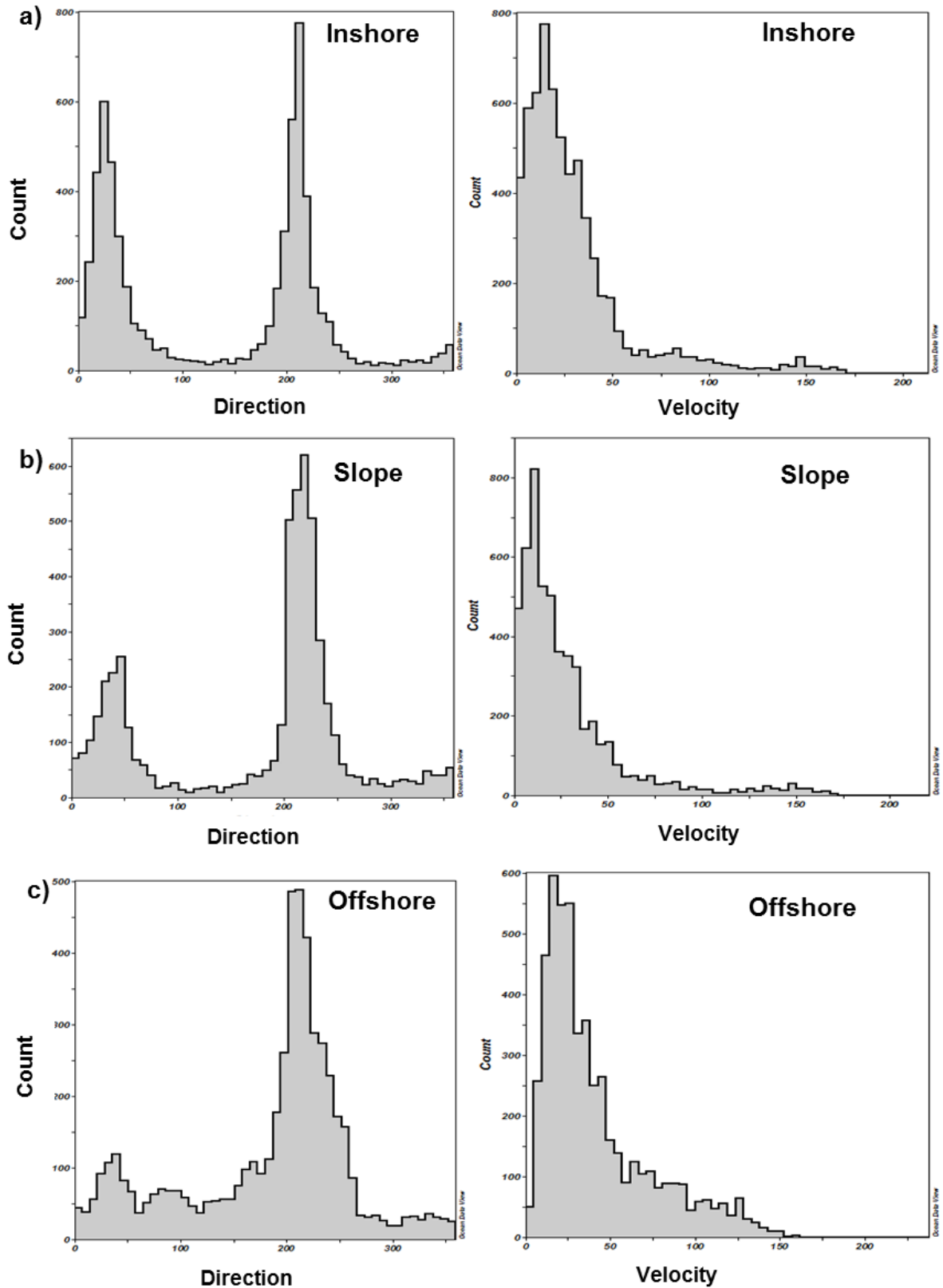
Figure 4.12: Percentage frequency histogram for direction (left column) and velocity (right column) for the (a) inshore mooring, (b) slope mooring and (c) offshore mooring during the period 01 September 2011 to 07 September 2011 (Event 2).

The SSHA in Figure 4.13 was produced for 31 August 2011, before Event 2 had been recorded by the moorings, until 14 September 2011. The SSHA images were weekly composites of satellite altimetry data. The onset of northward currents at the moorings was deemed to be the start of Event 2, occurring on 02 September 2011. Figure 4.13a suggested a level (0 cm) SSHA (green) at the moorings position on 31 August 2011. The yellow area north of the mooring's position and south of Durban displayed a higher sea level (10 cm). The SSHA image in Figure 4.13a illustrated the conditions before Event 2 and showed a lower comparative sea level than the surrounding area.

On 07 September (Figure 4.13b), four days after Event 2, the positive SSHA had migrated in a southwestward direction and was located over the mooring locations. Positive sea-surface heights of between 10 and 20 cm persisted in the Port Edward region into the next SSHA composite image on 14 September 2011 (Figure 4.13c).

According to the stick vector plots (Figure 4.13d), southwestward flow began to slow on 01 September 2011 and reversed to a northeastward direction by 02 September 2011. A positive sea level anomaly was positioned over the moorings' positions by 07 September 2011 and by that time southwestward currents had again started to flow. Stick vector plots indicated a northward current at the inshore (Figure 4.13d) and slope moorings (not shown) commencing on 01 September 2011. The same trend was not recorded at the offshore mooring (Figure 4.13d), only a decrease in current strength (compared to the previous day's velocity measurements) and continued southward flow was reported. The initial onset of northward flow at the inshore mooring was followed by a period of southward flow, then again northward flow. The lack of evidence for northward reversals at the offshore mooring suggested that Event 2 was limited to the inshore moorings. The effects on current direction and velocity at the offshore mooring were however still affected by Event 2. The positive anomaly identified in the SSHA did not correspond to the northward reversal observed in the mooring data. This may be due to the limited resolution of the SSHA data not being able to capture the smaller events on the inshore edge of the Agulhas Current.
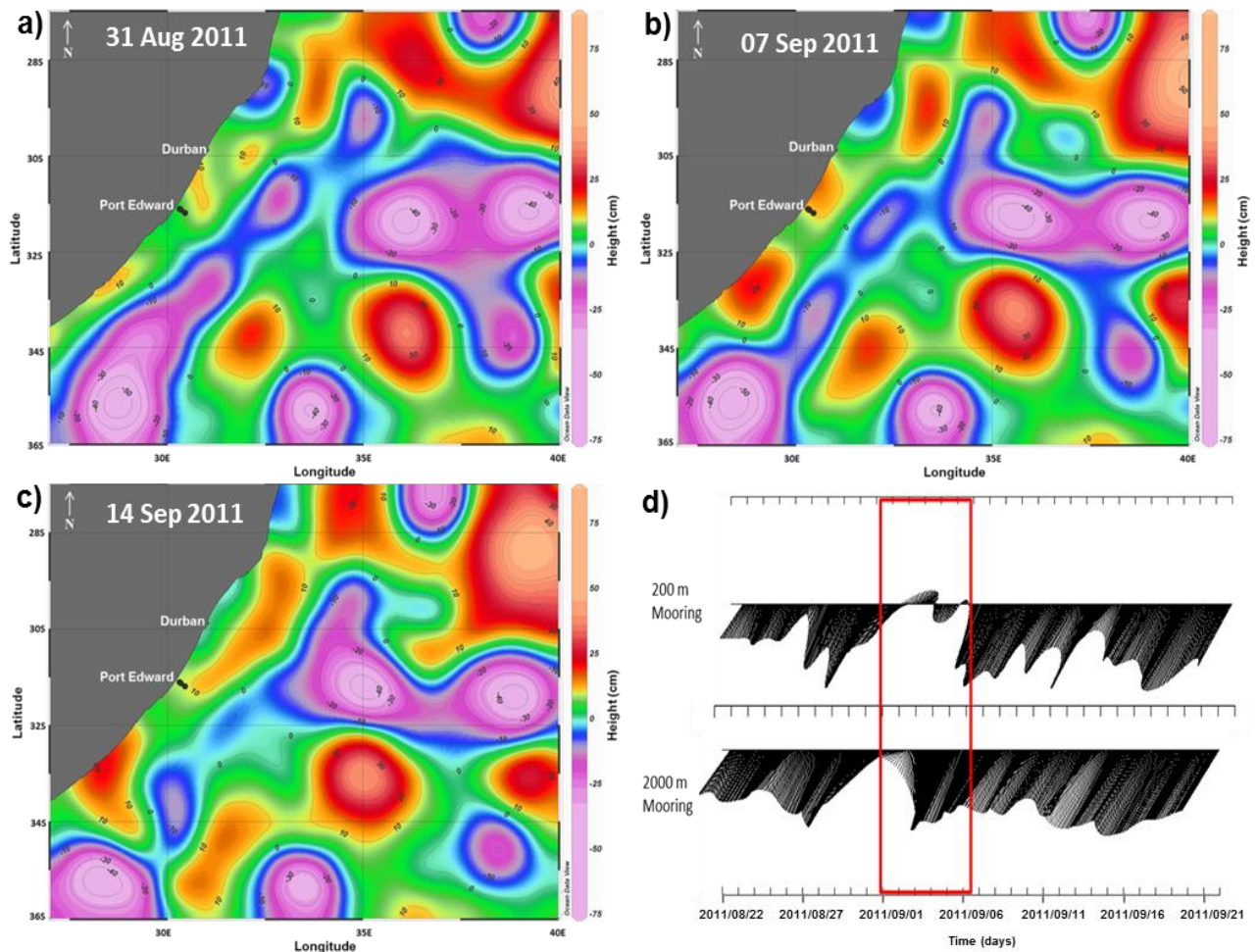
Figure 4.13: SSHA field representing the period before a) 31 Aug 2011, 5 days after b) 07 Sep 2011 and 12 days after Event 2 c) 14 Sep 2011. Figure 4.19 d) displays the velocity stick vector plots for a 30 day period which encompasses the occurrence of Event 2. Event 2 is highlighted in the stick vector plots. The position of the mooring line is represented by the black dots on the SSHA images.

Cloud cover was present over the majority of the study area on 01 September 2011 (Figure 4.14). A small 'window' of the region surrounding the study area was visible after persistent cloud cover during the latter stages of August 2011 and only two days of good data on 03 and 05 September 2011 were found. Analysis of the time series in Figure 4.14, showed the presence of a small cyclonic event positioned near the moorings on 03 September 2011. The cyclonic event dissipated further south of the mooring's position by 05 September 2011 and slight remnants of elevated chlorophyll-*a* concentration*s* formed a distinguishable silhouette of the event (Figure 4.14)
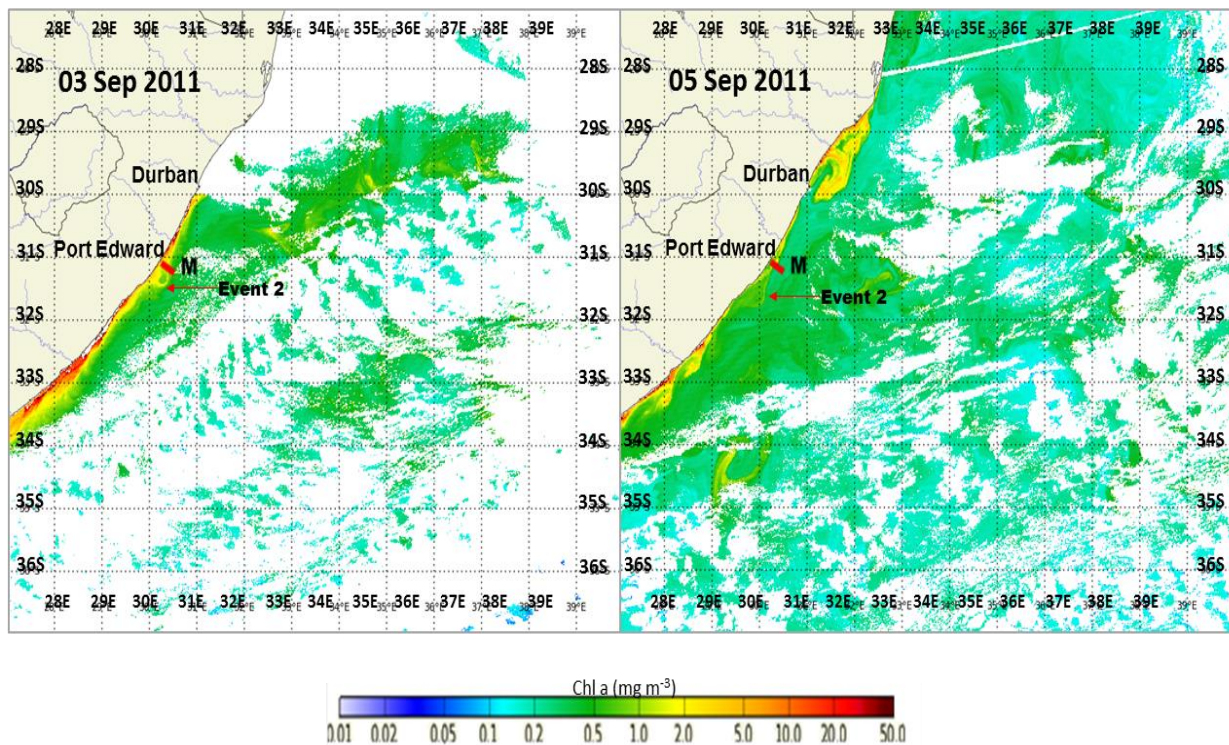
Figure 4.14: Ocean colour satellite image obtained from MRSU, depicting the moorings' positions (M) off Port Edward and the cyclonic event (Event 2) believed to have been the cause for current reversals on 02 September 2011.

The SST time series in Figure 4.15 indicated the presence of a cyclonic event with lower temperatures than the Agulhas Current moving in a southwestward direction, along the continental shelf close inshore. The cyclonic eddy's leading edge (southern end) started moving over the moorings' positions on 02 September 2011 south of 31° S. Changes in current direction and magnitude correspondingly started to appear on 02 September 2011 as shown by the stick vector plots in Figure 4.13d. The cyclone's northern edge was positioned over the moorings by 03 September 2011. During the ensuing days, the cyclonic event continued to propagate downstream in a southwestward direction and flow at the moorings' resumed in a southwestward direction as from 06 September 2011.

The evidence presented by the *in situ* and satellite data suggested that the event responsible for current reversals at Port Edward from 01 September 2011 resembled that of a Durban cyclonic eddy. Although the second reversal during Event 2 does not seem to be related to the Durban cyclonic eddy.
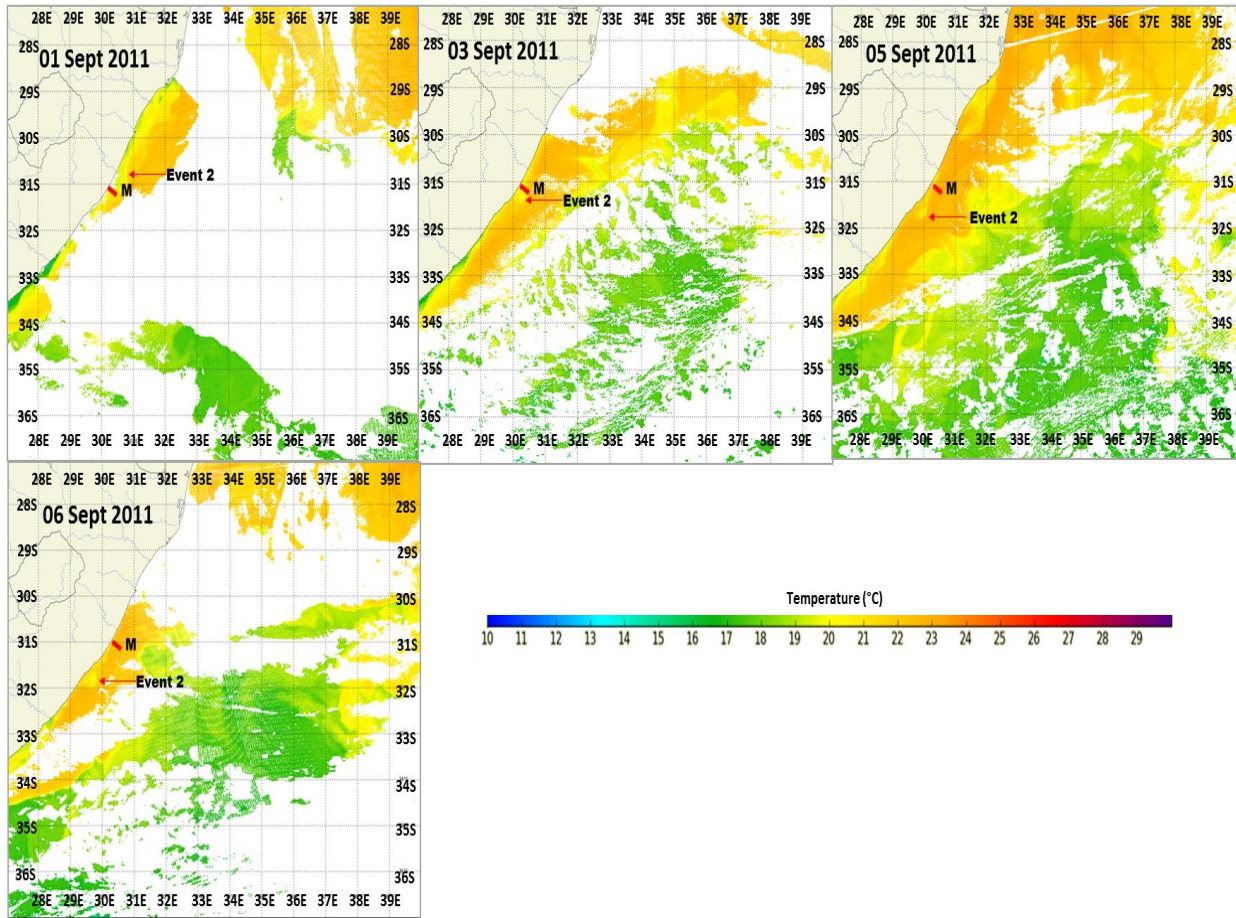
Figure 4.15: SST satellite image obtained from MRSU, depicting the moorings' positions (M) off Port Edward and the cyclonic event (Event 2) believed to have been the cause for current reversals on 02 September 2011.

4.3.3   Event 3 – 11 October 2011

According to Figure 4.16a, Event 3 consisted of two phases which affected the entire water column. Note that no observations were obtained at the inshore mooring for this event and thus only data for the slope and offshore moorings are presented in Figure 4.16. Event 3 started on 11 October 2011 and lasted 4 days, ending on 15 October 2011. On 12 October 2011 a southwestward current with higher velocities interrupted northward flow at the slope mooring. The second phase of current reversal during Event 3 then manifested northward currents at the slope mooring and eastward (offshore) currents at the offshore mooring. The first reversal phase was not very pronounced in the offshore mooring data, hinting at possible inshore sources for the current reversals.

The slope mooring had recorded two phases of prominent northward flow within Event 3 (Figure 4.16a).   The separation of these two phases by currents with a southward component lasted roughly 36 hours in the surface measurements and 5 hours at 500 m depth. Directional changes had not occurred in the bottom layers (≤ 500 m) and a sustained northward current was present leading up to and during Event 3. After Event 3 had moved past the mooring's location, northward flow ceased throughout the water column and was replaced by currents with a southward component.   From 19 October 2011 (Figure 4.5) northward flow resumed as part of a sub-sea reversal. This reversal extended from a depth of 1000 m to 140 m (Figure 4.5).

Event 3 was not as prominent at the offshore mooring than at the slope mooring. At the offshore mooring, Event 3 had only consisted out of one phase (Figure 4.16b), with a delayed onset. The reversal phase as recorded by the offshore mooring lasted for 24 hours and displayed an offshore movement of water with no northward currents in the upper layers to a depth of 1500 m.   The bottom layers had consistently displayed currents with a northward component before the onset of Event 3. During Event 3, northward currents were forced 500 m deeper and were found under a layer of eastward (offshore) moving currents. Each reversal phase produced a fast northward flowing core between 140 m and 1000 m depths, surrounded by lower velocities flowing in a northward direction as well. Velocities within the core ranged from 30 cm/s to 50 cm/s. Northward flow close to the sea-floor had receded once Event 3 had propagated southwestward and reappeared at depths greater than 1500 m by 19 October 2011 (Figure 4.5).

Current reversals were associated with decreased velocities at the moorings. At the onset of Event 3 on 11 October 2011, current velocity decreased from 150 cm/s to 40 cm/s at the slope mooring's surface layer. The offshore mooring recorded a similar decline in velocity as the slope mooring, but only towards the latter stages of Event 3 on 13 October 2011. Northward surface velocities toward the end of Event 3 were less than 10 cm/s. Velocity magnitude started to increase to over 50 cm/s at the offshore mooring on 15 October 2011.

During each reversal phase upwelling was evident, with a 3 °C decrease in temperature recorded over the initial 24 hour period at the onset of Event 3 as recorded by the slope mooring. During the commencement of southward flow between the two phases within Event 3, the slope mooring recorded a temperature increase of 3 °C (Figure 4.16a). When northward currents reappeared during the second phase of Event 3 temperature values again decreased by 3 °C (Figure4.16a), gradually rising as the event propagated in a southwestward direction, past the mooring. The offshore mooring recorded a temperature decrease of 1 °C during Event 3.

Direction frequency graphs for the slope mooring recorded a principal flow which occurred between 25 and 30 degrees (Figure 4.17). Surface current direction was mainly in a southwestward direction, altering during Event 3. Southwestward currents in the surface layer exhibited velocities between 100 and 150 cm/s. A maximum current velocity of 203 cm/s was recorded in the surface layer from 10 October 2011 to 16 October 2011 (Figure 4.17). A higher occurrence of northward currents was observed in the bottom layers at the slope mooring. A principal flow travelling in a northeastward direction was recorded, with 64% of currents travelling in this direction at the slope mooring. Maximum frequency of current velocity was recorded between 5 and 10 cm/s. A velocity peak of 37 cm/s had been recorded in the bottom layers by the slope mooring during Event 3 .

Southwestward flow was dominant at the offshore mooring. The principal flow at the offshore mooring was found between 210 and 240 degrees (southwestward). The Agulhas Undercurrent and Event 3 accounted for minor frequencies of northward current flow. Increases in onshore and offshore currents were recorded at the offshore mooring. A maximum velocity of 186 cm/s was recorded in the surface layer and the maximum frequency of velocities was between 15 and 25 cm/s. The bottom layer displayed currents which occurred in all directions. Most frequent velocities in the bottom layer were between 5

and 15 cm/s. From 10 October 2011 to 16 October 2011 a maximum current velocity of 26 cm/s was recorded in the bottom layers at the offshore mooring.
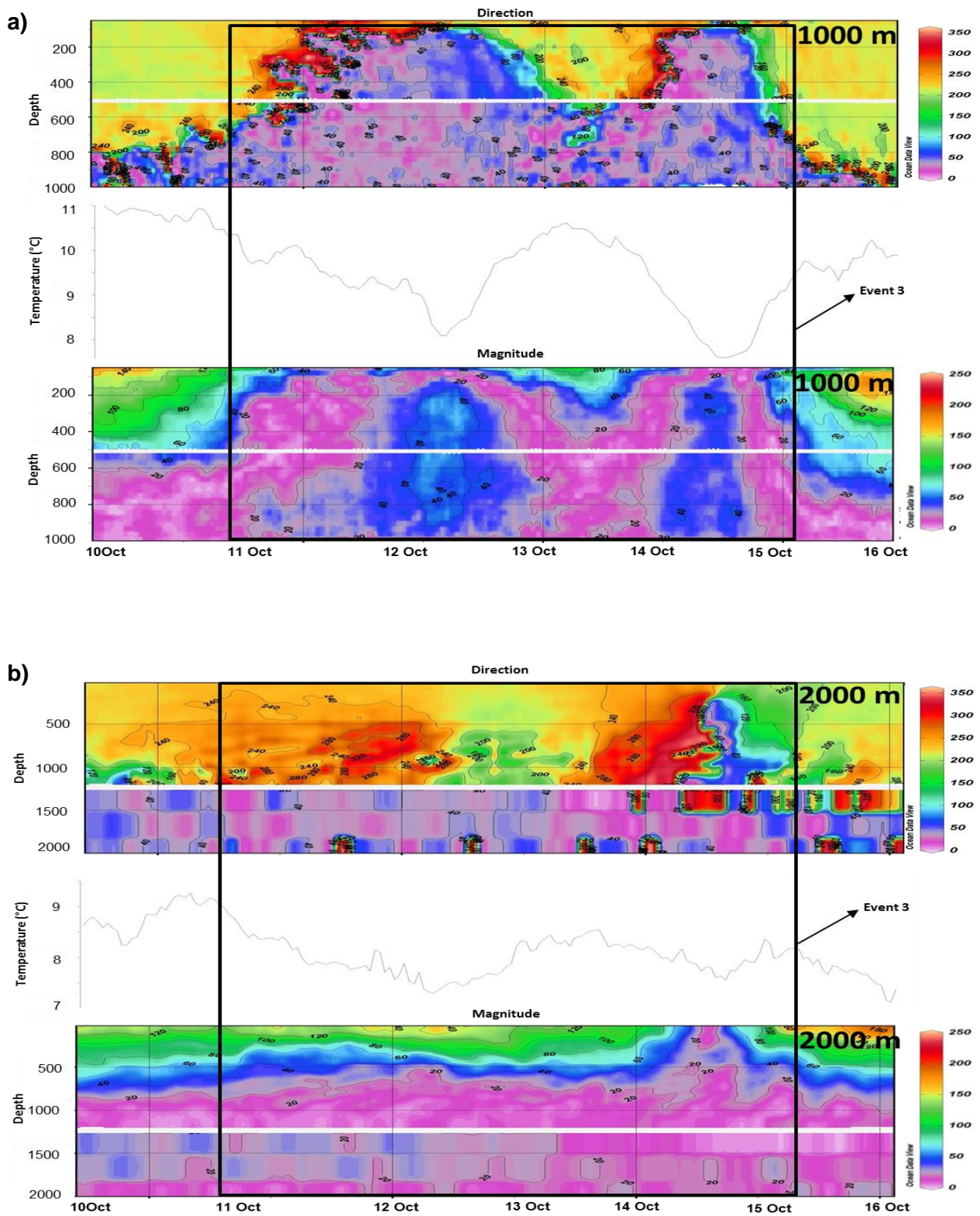
Figure 4.16: Current direction, velocity and temperature for the slope and offshore moorings for the period from 10 October 2011 to 16 October 2011 at a) slope mooring and b) offshore mooring. Note: Difference in scales. The black outline highlights Event 3.
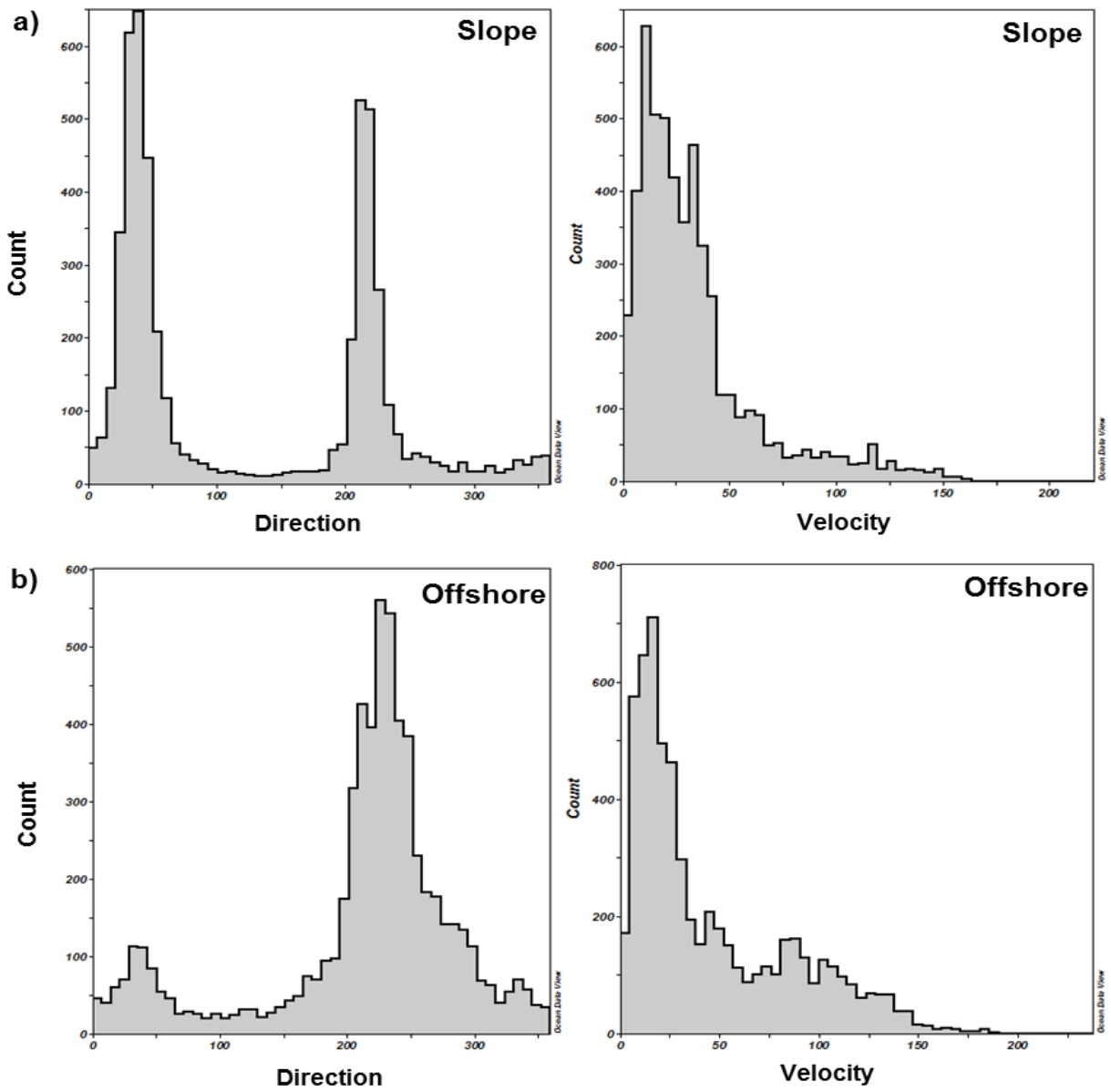
Figure 4.17: Percentage frequency histogram for direction (left column) and velocity (right column) for the a) slope mooring and b) offshore mooring during the period 10 October 2011 to 16 October 2011 (Event 3).

The SSHA image presented in Figure 4.18a showed a depression (A) that originated from the Natal Bight and migrated in a southwestward direction (Figure 4.18b), flattened and elongated while travelling close to the coast between Durban and Port Edward. The inshore cyclone moved in a southward direction and supposedly interacted with a deep sea cyclone (B) on 12 October 2011 (Figure 4.18a). From the SSHA image on 19 October 2011 (Figure 4.18b) the coastal depression was still present at the moorings' location, but southward flow had already resumed by 16 October 2011 which was the end of Event 3. On 19 October 2011 (Figure 4.18b) current flow at the moorings had resumed to flow in a southwestward direction, with northward currents not visible in the ADCP data (Figure 4.18d). Fourteen days after the commencement of Event 3, the Agulhas Current displayed a uniform structure and no inshore cyclonic anomalies were visible (Figure 4.18c). The slope mooring recorded the two phase structure of Event 3 in the stick vector plots, which consisted of two periods of northward currents separated by a period of weak southward currents (Figure 4.18d). After the occurrence of Event 3, southward currents were once again evident as depicted by the stick vectors in Figure 4.18d. There were no current reversals at the offshore mooring (Figure 4.18d), but there was however a decrease in current velocity by 13 October 2011. It is possible that the narrow depression along the coast in the SSHA (Figure 4.18) was associated with northward flow which was limited to the inshore mooring. However, this postulation cannot be confirmed since no data from the inshore mooring was obtained during Event 3.
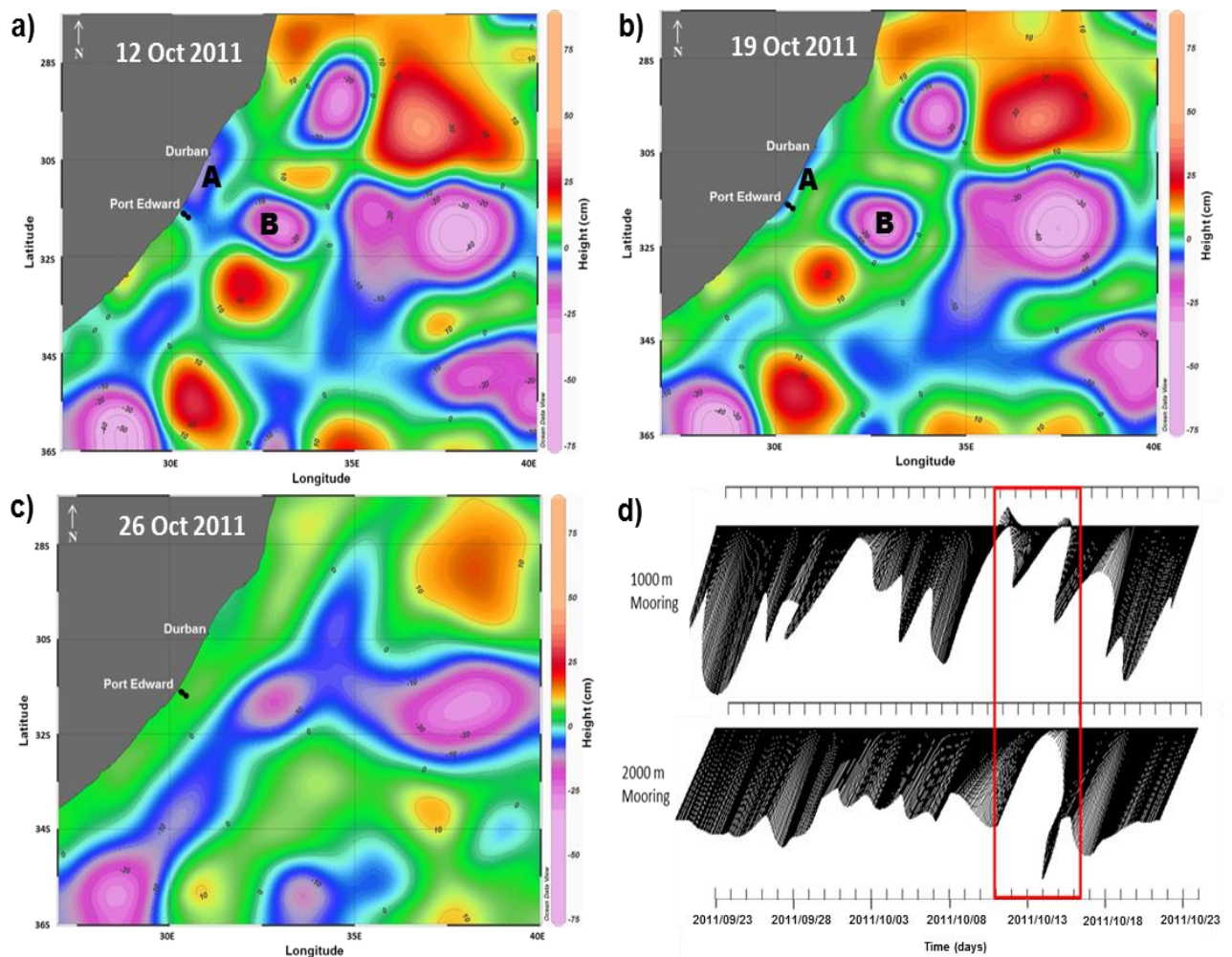
Figure 4.18: SSHA field representing a) 12 October 2011, b) 19 October 2011 and c) 26 October 2011. Figure 4.18 d) displays the velocity stick vector plots for a 30 day period which encompasses the occurrence of Event 3. The first appearance of current reversals at the moorings appeared on 10 October 2011 at the slope mooring.

The ocean colour time-series in Figure 4.19 shows the presence of the depression (A) south of Durban at 30.5° S on 07 October 2011. From Figure 4.19 this eddy (A) migrated and flattened along the coast reaching over the moorings position by 10 October 2011. The deep sea cyclonic eddy (B) was situated south of 31° S on 10 October 2011 and drew small filaments from the coast in a northeastward direction, toward the deep sea eddy matching its pattern of cyclonic flow (Figure 4.19). These filaments were still visible on 12 October 2011, but the cessation of these filaments could not be determined due to the lengthy overcast period following 12 October 2011.
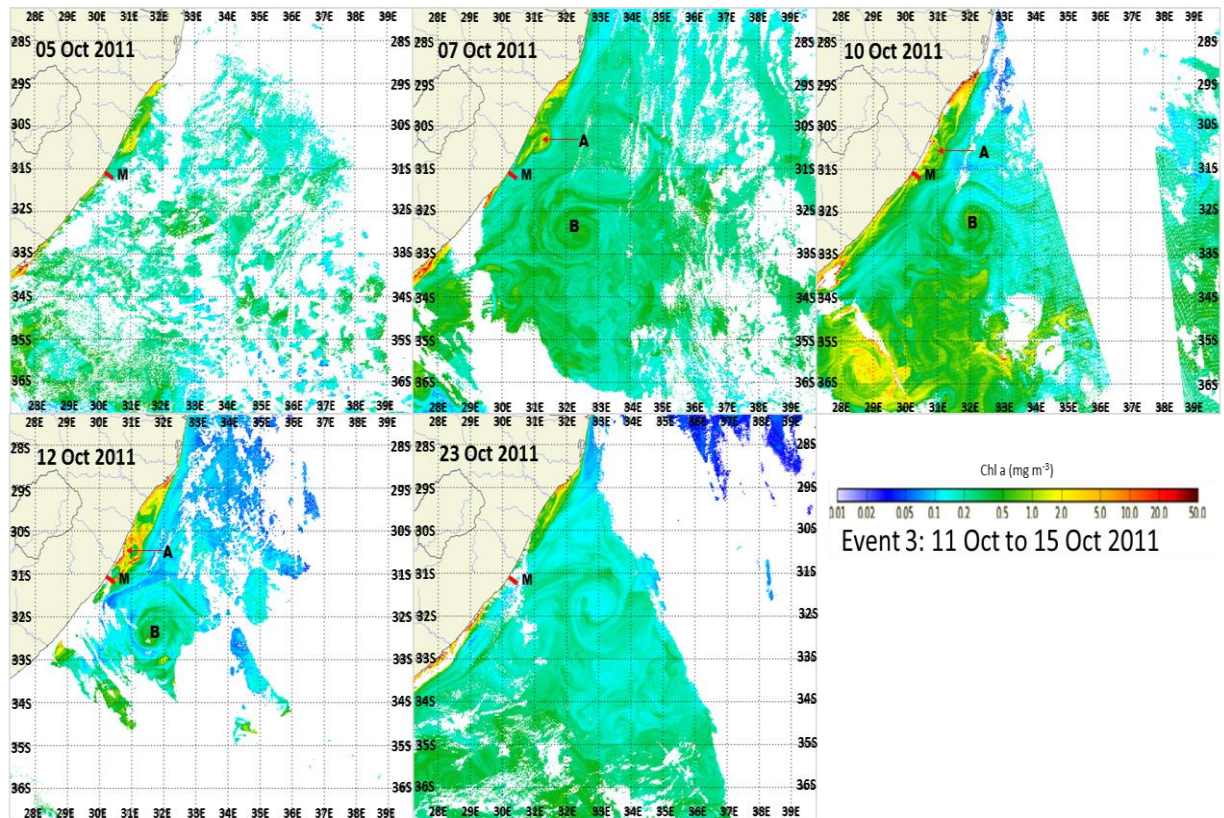
Figure 4.19: Ocean colour satellite time-series taken opportunistically for Event 3 for 05 October 2011 to 23 October 2011. Possible influences on the current dynamics at the moorings' positions (M) are labelled and these included a deep sea cyclone (B) and the Durban eddy (A).

The small window in the thermal infrared imagery of the Natal Bight region on 05 October 2011 showed an offshore movement of the Agulhas Current south of Durban, south of 30 °S (Figure 4.20). This offshore movement of the Agulhas Current near Durban was enlarged on 07 October 2011 as the cyclonic eddy intensified. This intensification was however short lived, as only a small, colder (~19 °C) cell remained north of the moorings' positions on 10 October 2011. Two days later, on 12 October 2011 a less intense cyclonic feature was visible at the moorings' positions. The deep sea cyclonic eddy identified earlier was visible from 07 October 2011 until the end of the SST time-series on 23 October 2011. The advection of filaments of coastal water in an offshore direction was not visible in the SST time-series in Figure 4.20.
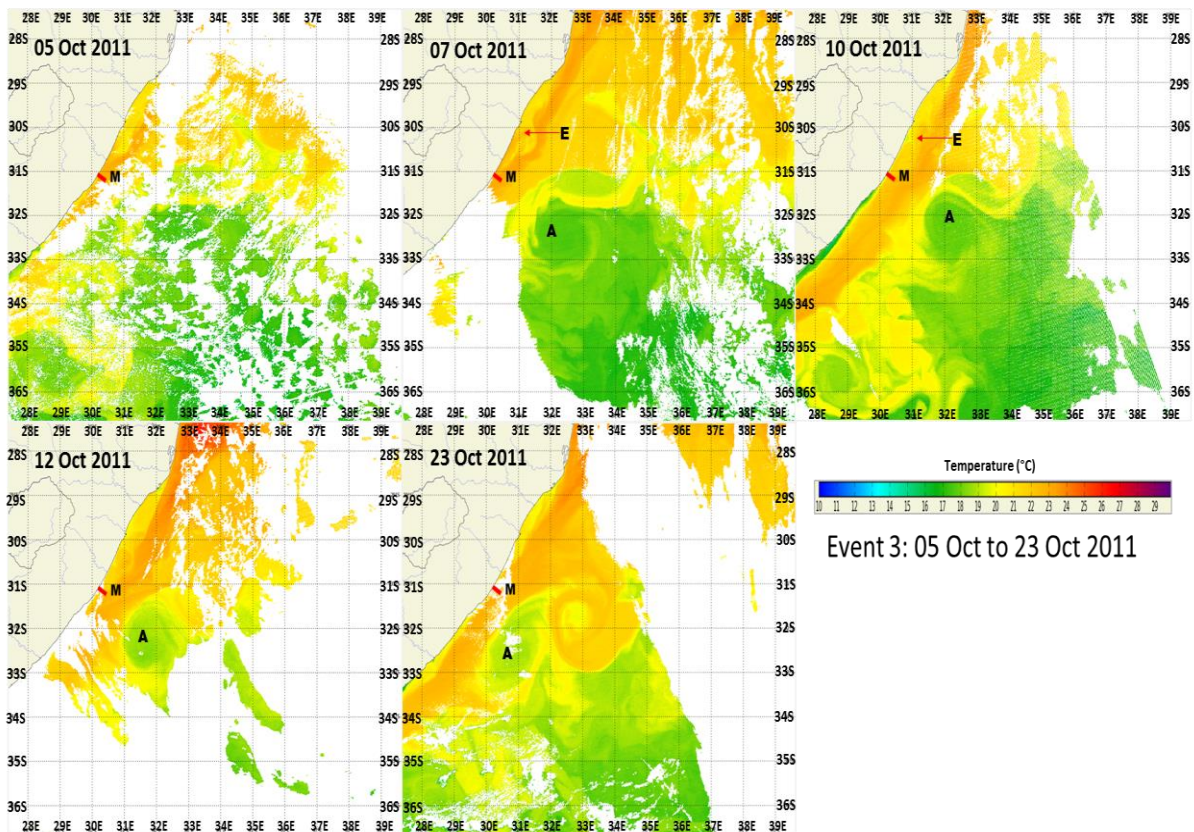
Figure 4.20: SST satellite imagery taken opportunistically for Event 3 for 05 October 2011 to 23 October 2011. The moorings positions (M), Durban eddy (E) and deep sea cyclone (A) are displayed.

Studying the accompanying satellite imagery on 12 October 2011 the cyclonic anomaly responsible for Event 3 resembled that of a Durban cyclonic eddy and its interaction with a deep sea cyclonic eddy.

Chapter 5: Discussion

To answer the key questions (1. Do the moorings capture the 'permanent' ocean currents, viz. the Agulhas Current and the Agulhas Undercurrent; 2. Are the moorings able to capture the transient features of the system, viz. Natal Pulses and Durban Eddies) proposed in this thesis, the discussion has been divided into sections which cover the various driving forces thought to influence the oceanic conditions around Port Edward. Firstly the general characteristics of the Agulhas Current will be discussed, followed by the Agulhas Undercurrent and cyclonic events as recorded by the line of moorings.

5.1   The Agulhas Current

The slope and offshore moorings had recorded a distinct stratified regime within the Agulhas Current, displaying a northeastward Agulhas Undercurrent and the southwestward Agulhas Current. The entire water column only flowed in a southwestward direction after reversal events. Highest velocities occurred shortly after reversal events in the surface layers and extended to deeper than usual depths. The *in situ* current direction and velocity data collected from 21 July to 04 December 2011, demonstrated the resilient nature of the Agulhas Current in the surface layers. These findings agree with work done by Lutjeharms and de Ruijter (1996) in that the Agulhas Current (southwestward flow) is extremely stable for 70 % of the time, intermittently interrupted by the irregular passage of meanders. According to Roberts *et al.* (2010), current meter mooring data showed an almost continuous south-westward current close to the coast off Port Edward. The findings by Roberts *et al.,* (2010) indicated a lack of regular instabilities and current reversals due to eddies and that the area surrounding Port Edward was strongly influenced by the Agulhas Current. Research conclusions by Roberts *et al.* (2010) and Schumann (1982), found the Agulhas Current core within 10 – 15 km offshore of Port Edward. Findings within this thesis showed that at the inshore mooring, the Agulhas Current exhibited its classic southwestward flow, with only 6 % of instances travelling in a northward direction and 5 % in an offshore direction. The Agulhas current was less variable at the slope mooring, with only 4 % of currents flowing in a northward direction. Northward flow at the offshore mooring (500 m and shallower) was negligible and the surface dynamics were strongly influenced by

68

southwestward currents. Surface velocities as recorded by the moorings within this study were in agreement with work done by Lutjeharms (2007) and Roberts *et al.* (2010), with average velocities in excess of 100 cm/s and peak velocities in the order of 200 cm/s recorded by the three moorings. Percentage histograms for direction showed that the Port Edward region was strongly influenced by southwestward currents, viz. the Agulhas Current.

The Agulhas Current was shown to have three primary zones (Lutjeharms, 2007) namely; a sharp, inshore, thermal frontal zone, the core of the current and a more disperse offshore front. Roberts *et al.*, (2010) defined the core boundary isotherm as the 24 °C isotherm, and delineates the inshore edged of the Agulhas Current. From the SST satellite imagery presented in this study, the Agulhas Current was seen close to the continental shelf on the east coast of South Africa during times of undisturbed linear flow. The core displayed highest temperature values and a sharp decrease in temperature values close inshore was observed. The primary driving force responsible for coastal zone dynamics off Port Edward was assumed to be the Agulhas Current. Similarly, Lutjeharms *et al.* (2000) found that the shelf circulation on the east coast of South Africa is strongly influenced by the proximity of the swiftly flowing Agulhas Current and with the aim of measuring the Agulhas Current the *in situ* data presented here concur with findings by Schumann (1987), that the Agulhas Current was found within a few kilometres of the coast at Port Edward. The current core is situated seaward of the 200 m isobaths, but does occasionally infiltrate the inshore zone to the 100 m isobaths (Pearce, 1977).

The water masses identified by the CTD data have specific origins and characteristic salinity/temperature relationships. The Indian Tropical Surface Water is generally found on the inshore boundary of the Agulhas Current (Gordon *et al.*, 1987; Biastoch *et al.*, 1999). It originates in the tropics and through an excess of precipitation over evaporation, possesses less saline waters (Lutjeharms *et al.*, 2000; Pearce, 1978). This water is believed to reach the Agulhas Current via the Mozambique Channel (Harris, 1972). The South Indian Subtropical Surface Water is found at a maximum depth of 150 m in the Agulhas Current and is shown to possess maximum salinity and dissolved oxygen contents and originates in the subtropical gyre of the South Indian Ocean (Wyrtki, 1971) where the evaporation rate exceeds that of precipitation (Lutjeharms and Ansorge, 2001). The water mass below this is the South Indian Subtropical Surface Water as presented in Figure 4.16. This water mass is fundamentally a mixture between the surface waters above and the Antarctic Intermediate Water below (Lutjeharms *et al.*, 2000). Antarctic Intermediate Water (AAIW) enters the Agulhas Current from the north and east via the south Indian Ocean subtropical gyre. Red Sea Water travels in a poleward direction, crossing the equator to eventually enter the Agulhas Current system (Beal, 2009).

5.2   The Agulhas Undercurrent

Definition of the Agulhas Undercurrent in this study follows work conducted by Biastoch *et al.* (2009) in that any north to northeastward flow below 1000 m across the entire mooring array was considered as evidence of the Agulhas Undercurrent.   According to Beal (2009), the undercurrent was defined only as northeastward flow over the continental slope, which often occurred on the inshore edge of the Agulhas Current.   The Agulhas Undercurrent was a persistent feature and average velocities between the line of moorings were in the order of 13.38 cm/s and 15.52 cm/s, increasing in an offshore direction.   The results reported in this study for the mean Agulhas Undercurrent velocity thus do not coincide with results of work done by Beal and Bryden (1999), Donohue *et al.* (2000) and van Aken *et al.* (2004), which showed the Agulhas Undercurrent to possess weaker velocity structures from 32° S towards the Mozambique Channel.   The mean current velocities reported by these authors were in the order of 4.3 cm/s, with 0.7% of instances displaying maximum velocities above 25 cm/s (van Aken *et al.*, 2004).   Beal (2009) found that the Agulhas Undercurrent is bottom intensified and possesses some of the highest velocities of a deep current in the world.

Sub-surface reversals were more prominent and regular at the inshore and slope moorings, thus concentrated inshore on the shelf and shelf edge.   The northward moving Agulhas Undercurrent was confined to a depth of 1000 m and deeper at the offshore mooring and showed numerous instances of offshore (eastward) flow rather than northeastward (Figure 4.5).   Agulhas Undercurrent velocity cores of peak speeds were recorded in the slope mooring's data between 1000 and 600 m depths.

Beal (2009) found that the dominant form of Agulhas Undercurrent variability matches that of the Agulhas Current which is a 50 -70 day meander mode related to so-called Natal Pulses. According to Roberts *et al.* (2010), Natal Pulses occur at a rate of 5 pulses per year which roughly correlates to the rate Beal (2009) described.   In this study there was evidence that occasionally reversals encroached up on to the continental shelf, resulting in northward flow and weaker velocities in the mid-water column of the shoreward side of the Agulhas Current. Periodic sub-surface reversals were evident ('X' in Figure 4.5 and Figure 4.6), which do not reach the surface, thus eliminating inferences drawn about possible cyclonic events as the cause for such events.   These sub-surface reversals were described by Roberts *et al.* (2010), but not identified as the Agulhas Undercurrent.   The results reported by the moorings in this study showed that on occasion the undercurrent was absent, thus not agreeing with

results reported by Bryden *et al.* (2005). Beal (2009) found the Agulhas Undercurrent to be absent less than 10 % of the time. A possible explanation is that the undercurrent may not be visible in the data due to an offshore movement and thus occurring in deeper waters (>2 000 m). The Agulhas Undercurrent is most notably absent after the propagation of cyclonic events. After reversal events the Agulhas Undercurrent was found to be absent or suppressed at all three moorings once the events had propagated in a southwestward direction. A possible explanation for the absence of northward currents after reversal events at the bottom layers found within this study was suggested by Bryden *et al.* (2005) who stated that during meander or cyclonic events, the Agulhas Current exhibits firstly, onshore movement, then offshore movement and then once again onshore movement. The onshore and offshore movement exhibits strengthening and weakening respectively and squeezes out the Agulhas Undercurrent at the slope during strengthening (Bryden *et al.,* 2005). During offshore movement of the Agulhas Current, the Agulhas Undercurrent strengthens and penetrates upwards, eventually returning to its position at the foot and along the continental slope at the time the Agulhas moves back onshore (Bryden *et al.,* 2005). Research by Beal (2009) concurs with that of Bryden *et al.* (2005) in saying that the Agulhas Undercurrent is replaced on the slope by southeastward currents as the Agulhas moves onshore. When the Agulhas Current moves offshore the Agulhas Undercurrent strengthens and penetrates upwards to shallower depths (Beal, 2009). The scenarios presented by Beal (2009) and Bryden *et al.* (2005) explain the absence of northward currents after the occurrence of reversal events. These two scenarios may relate the sub-surface reversals recorded within this study to the upward penetration and strengthening of the Agulhas Undercurrent as a result of the offshore movement of the Agulhas Current.

Antarctic Intermediate water was found in the upper layers of the Agulhas Undercurrent, possessing low salinity (≤34.6 psu) and high dissolved oxygen values (≥4.70 ml/l) (Figure 4.1). According to Lutjeharms (2007) the Agulhas Undercurrent consists largely of modified Red Sea water and so goes against the classic nature of Red Sea Water transport, the very existence of an Agulhas Undercurrent was disregarded by Toole and Warren (1993) because of the presence of this Red Sea Water. The horizontal movement in and out of water from the Agulhas Undercurrent mentioned here may explain the frequent occurrences of onshore and offshore movement observed in the frequency histograms of the deeper moorings and may also explain differences in the water masses observed in the Agulhas Undercurrent.

5.3   Cyclonic events

The current regime at Port Edward does not only follow the southwestward direction in which the Agulhas Current travels, or the northeastward direction in which the Agulhas Undercurrent travels, but movement up and down the continental slope as part of the entrainment and detrainment processes associated with the southward movement of cyclonic events on the inshore edge of the Agulhas Current.   This study reported the occurrence of three major cyclonic or reversal events between 21 July 2011 and 04 December 2011, occurring at roughly the same rate of pulse-like events reported by Roberts *et al.* (2010) and van der Vaart and de Ruijter (2001). Identification of the Natal Pulse on satellite derived images may be done by tracking them from their point of origin and characterising them by their physical features which include downstream speed (~20 km/d) and lateral growth (van Leeuwen *et al.,* 2000). Tracking cyclonic events using SST satellite imagery proved in some instances impossible, as they were not sufficiently different to the surrounding environment, but possessed similar thermal infra-red signatures as the surrounding Agulhas Current.   Altimetry data was more useful for the identification of cyclonic features, but even this failed to consistently match the *in situ* current reversals as a result of the limitations of the satellite technology close inshore.

During the southward movement of cyclonic events, occurrences of onshore and offshore flow, especially at the offshore mooring were recorded.   These onshore/offshore periods were never long-lived and may be attributed to the current flow dynamics as described by Bryden *et al.* (2005) regarding the onshore/offshore movement of the Agulhas Current.

Each of the three cyclonic events displayed evidence of eddy driven, slope upwelling.   The rate of upwelling and the types of water masses involved in the advection process is highly dependent on the efficiency of the upwelling induced by these cyclonic events (Lutjeharms *et al.*, 2000). Cyclonic events may originate from an offshore location and carry entrained cold deeper water towards the continental shelf and dispose these deeper waters on the shallower continental shelf, causing a decrease in shelf temperatures as part of an upwelling event (Lutjeharms *et al.*, 2003). According to Schumann (1988) upwelling on the shelf on the east coast of South Africa usually consisted out of central water.   In this study temperature measurements suggested South Indian Central Water (SICW) at the three mooring locations, thus corresponding to the results of Schumann (1988). However, the

observed temperature decreases correspond to cyclonic events originating in the Natal Bight, rather than cyclonic eddies originating from an offshore location.

The triggering mechanisms involved in the formation of eddies were not one of the objectives of this study, but a summary of work done by Oke and Griffin (2011) attributes the formation of mesoscale cyclonic eddies in western boundary current regimes to processes such as baroclinic instability (Boudra *et al.*, 1988; Oey, 1988; Lee *et al.*, 1991), barotropic instability (Jochum and Malanotte-Rizzoli, 2003; Bowen *et al.*, 2005) and mixed barotropic-baroclinic instability (Hurlburt *et al.*, 1996; Mata *et al.*, 2006). Topographically induced disturbances (Singer *et al.*, 1983; Lee *et al.*, 1991) and processes concerned with flow detachment (Penven *et al.*, 2001) are also possible generation mechanisms of these cyclonic events.

It has been postulated by Lutjeharms and de Ruijter (1996) that interactions between the Agulhas Current and deep sea eddies, whereby the Agulhas Current adsorbs these eddies on its seaward side may trigger the release of cyclonic events, specifically Natal Pulses, in the Natal Bight region. Event 1 was concentrated inshore and had prominent northward currents at the inshore and slope moorings. Mainly onshore flowing currents were found at the offshore mooring. Event 1 had increased in lateral dimensions as was shown by the satellite images (Figure 4.10c). Following definitions of the Natal Pulse by van der Vaart and de Ruijter (2001) and Roberts *et al.* (2010), Event 1 was not a Natal Pulse, but rather the Durban cyclonic eddy shedding from its point of origin. Schumann (1987) stated that current reversals close inshore, as was the case with Event 1, may also have been attributed to wind stress or shelf waves. The influences of wind stress and shelf waves were not investigated as possible causes of the current reversals observed in this study.

Event 2 was a small cyclonic eddy, different to that of a Natal Pulse (van der Vaart and de Ruijter, 2001; Roberts *et al.,* 2010). The place of origin of the cyclonic event causing current reversals during Event 2 was placed at the southern end of the Natal Bight. After propagating in a southwestward direction past the moorings off Port Edward it dissipated relatively quickly. Current reversals and decreases in velocity represented in the mooring data are synonymous with mesoscale events propagating over the moorings' positions. According to the evidence provided, Event 2 was considered to be a Durban cyclonic eddy, shedding from the Natal Bight.

Coastal dynamics at Port Edward during Event 3 were under the influence of a deep sea cyclonic eddy and a weaker Durban cyclonic eddy originating in the Natal Bight. The deep sea eddy and Durban eddy drew water from the shoreward boundary of the Agulhas Current in an offshore direction and was deemed as the cause for periods of northward and offshore currents and weaker velocities during Event 3.

5.4   Mooring performance

The results obtained from the mooring systems were consistent with previously described velocity, direction and hydrographic properties of the Agulhas Current (Lutjeharms, 2007 and Roberts *et al.*, 2010). Together with complimentary, remotely sensed data, characterisation of the mesoscale features affecting the coast off Port Edward was accomplished as described in sections 5.1 to 5.3. The moorings were proficient at capturing cyclonic events as they propagated in a southwestward direction. These ADCP mooring systems have been proven as reliable mechanisms in capturing ocean dynamics in the past.

The cross-shelf extent of the Agulhas Undercurrent too may be monitored with the line of moorings. Stringent scientific applications could not confidently make conclusions on the spatial variations using only one mooring. On the other hand, for short term real-time forecasting a single real-time mooring would be sufficient for the shipping industry and recreational users for current velocity and direction information. Side lobe interference is a problem that causes 5 to 10 % of surface measurement (direction and velocity) to be lost. This problem was linked to the acoustic technology employed to measure ocean currents and attempts are being made to decrease the effects of this in ADCP current data. In water depths of 1000 m the surface bins in the last 50 – 100 m were lost due to side lobe interference.

According to (Puryear *et al.,* 2009), usual factors which inhibit the efficiency of acoustic communication include multi-path interference, ambient noise and environmental conditions. The most restricting effect is that of multi-path interference which affects both baud rate and reliability (i.e. constant transmission). Multi-path interference might affect the quality of the data through reflections of the acoustic signal off the seafloor and sea-surface, reflections from objects near the receiving modem, thermal gradients and water turbulence. The last measurement bins (those close to the sea surface and seabed) of all three moorings were

discarded due to the interference effects of multipath interference. Multipath interference occurs when refraction and reflection cause the transmitted signal to reach the receiving transducer of the surface modem in two or more paths (Puryear *et al.*, 2009). Multipath is a constant problem in wireless data communication and mitigating its influence on signal transmission is still an area of research (Song *et al.*, 2007).

The moorings deployed in this study had sufficient buoyancy to counteract the extreme effects of velocity maximums within the Agulhas Current. Current induced mooring draw down values were exceptionally good for the inshore mooring and slope mooring as reflected in the data quality analysis (Figure 3.6 to Figure 3.8). The inshore mooring displayed a draw down depth range of 2.6 m, while the slope mooring displayed a draw down range of 14.1 m. Although not exceptional as the two shoreward moorings, the offshore mooring had a tolerable draw down range of 164.2 m. The maximum draw down values of the offshore mooring was achieved at times when the Agulhas Current displayed highest velocities in a southwestward direction.

Deploying a buoy system in a swift, warm western boundary current is one of the most difficult tasks in physical oceanography, but is important if we are to gain knowledge of the dynamics of these currents. The Agulhas Current on the east coast of South Africa is arguably the most powerful of the western boundary currents on the planet and controls much of the physical processes along the continental shelf. Monitoring of the Agulhas Current is therefore important if we are to understand its role in the oceanography of this region and importantly, the ecosystem. Moreover, it also strongly influences many marine activities such as oil and gas, maritime and port operations (Roberts *et al.*, 2011).

Because current measurements are difficult and risky endeavours, there have been several attempts to develop "remotely sensed' technology to measure velocity and direction of ocean currents. The latest of which is to utilize radar signals emitted from satellites – a technology referred to as Synthetic Aperture Radar (SAR). However SAR is still a new development and requires ground-truthing. These moorings will aid in acquiring real-time data for ocean research, prediction and to better understand local oceanic processes and the Indian Ocean on a basin scale.

Chapter 6: Conclusions and Recommendations

By deploying the line of moorings within the Agulhas Current system and capturing and describing the various macro and mesoscale features affecting the ocean dynamics off Port Edward, plans are to be made to deploy these mooring systems around the South African coast at key locations. These moorings will form part of scientific studies and provide data for operational, economic and recreational activities.

Three major current reversal events were identified in the 136 day time series collected by all three moorings, indicating a frequency of 45 days. All reversals observed throughout the water column were associated with the process of vortex shedding from the Natal Bight. These events were related to the shedding of the Durban Cyclonic Eddy from its origins in the Natal Bight as Roberts *et al.* (2010) discovered. Velocities decreased to below 50 cm/s at all three moorings during these reversal events. These reversal events were associated with cyclonic eddies which clearly impacted the direction and velocity of the Agulhas Current, thus having implications on its transport along the slope. Each reversal event was accompanied by periods of slope upwelling.

The Agulhas Undercurrent was a persistent feature at the slope and offshore moorings, absent only for a short period of time after reversal events. This deep Agulhas Undercurrent core was more developed at the slope mooring, with higher velocities occurring more frequently. Sub-surface reversal events suggested shoreward movement of the Agulhas Undercurrent.

The low directional variability in the surface layers at the offshore mooring and dominant southwestward flow, except during reversal events indicate the strong influence of the Agulhas Current in this region. The inshore mooring showed less occurrences of the Agulhas Undercurrent if northward flow in the bottom layers was to be considered as signs of the Agulhas Undercurrent. Flow here was intermittent and simultaneously appeared in the inshore mooring data at times when northward flow was prominent at shallower depths at the deeper moorings.

Data from the offshore mooring suggests that for Agulhas Current core dynamics, the offshore mooring was ideally placed. On the other hand the slope mooring was ideally placed in the Agulhas Undercurrent's core. Shelf dynamics were recorded adequately by the inshore mooring which was placed on the continental shelf, close to the shelf break.

Temperature readings were taken at 200 m for the inshore mooring and at 500 m for the slope and offshore moorings and displayed sufficient evidence of temperature decreases during upwelling events. Considerations will have to be made to equip all future moorings with a means to measure bottom and surface temperatures. Surface buoys accompanying a sub-surface real-time mooring can relay surface temperature readings in real-time for operational purposes.

References

Arhan, M., Mercier, H. and Park, Y. H. 2003. On the deep water circulation of the eastern South Atlantic Ocean. *Deep-Sea Research I.* **50**: 889 – 916.

Beal, L. M. 2009. A time series of Agulhas Undercurrent transport. *Journal of Physical Oceanography.* **39**: 2436 – 2450.

Beal, L. M. and Bryden, H. L. 1997. Observations of an Agulhas Undercurrent. *Deep-Sea Research I.* **44**(9-10): 1715 – 1724.

Beal, L. M. and Bryden, H. L. 1999. The velocity and vorticity structure of the Agulhas Current at 32° S. *Journal of Geophysical Research.* **104**: 5151 – 5176.

Biastoch, A., Beal, L. M., Lutjeharms, J. R. E. and Casal, T. G. D. 2009. Variability and coherence of the Agulhas Undercurrent in a high-resolution ocean general circulation model. *Journal of Physical Oceanography.* **39**: 2417 – 2435.

Biastoch, A. and Krauss, W. 1999. The role of mesoscale eddies in the source regions of the Agulhas Current. *Journal of Physical Oceanography.* **29**: 2303 – 2317.

Biastoch, A., Reason, C. J. C., Lutjeharms, J. R. E. and Boebel, O. 1999. The importance of flow in the Mozambique Channel to seasonality in the Agulhas Current system. *Geophysical Research Letters.* **26**: 3321 – 3324.

Boudra, D., Bleck, R. and Schott, F. 1988. A numerical model of instabilities in the Florida current. *Journal of Marine Research.* **46**(4): 715 – 751.

Bowen, M. M., Wilkin, J. L. and Emery, W. J. 2005. Variability and forcing of the East Australian current. *Journal of Geophysical Research.* **110**: C03019. doi:10.1029/ 2004JC002533.

Bryden, H. L. and Beal, L. M. 2001. Role of the Agulhas Current in Indian Ocean circulation and associated heat and freshwater fluxes. *Deep Sea Research I.* **48**: 1821 – 1845.

Bryden, H. L., Beal, L. M. and Duncan, L. M. 2005. Structure and transport of the Agulhas Current and its temporal variability. *Journal of Oceanography.* **61**(3): 479 – 492.

de Ruijter, W. P. M., van Leeuwen, P. J. and Lutjeharms, J. R. E. 1999. Generation and evolution of Natal Pulses: Solitary meanders in the Agulhas Current. *Journal of Physical Oceanography.* **29**: 3043 – 3055.

de Ruijter, W. P. M., Ridderinkhof, H., Lutjeharms, J. R. E., Schouten, M. and Veth, C. 2002. Observations of the flow in the Mozambique Channel. Geophysical Research Letters. **29**: L1502, doi:10.1029/2001GL013714.

Donohue, K. A., Firing, E. and Beal, L. M. 2000. Comparison of three velocity sections of the Agulhas current and Agulhas Undercurrent. *Journal of Geophysical Research*. **105**: 28585 – 28593.

Eden, C. and Olbers, D. 2010. Why western boundary currents are diffusive: A link between bottom pressure torque and bolus velocity. *Ocean Modelling.* **32**: 14 – 24.

Gordon, A. L., Lutjeharms, J. R. E. and Gründlingh, M. L. 1987. Stratification and circulation at the Agulhas retroflection. *Deep-Sea Research*. **34**: 565 – 599.

Gründlingh, M. L. 1980. On the volume transport of the Agulhas Current. *Deep Sea Research.* **27**: 557-563.

Gründlingh, M. L. 1983. On the course of the Agulhas Current. *South African Geographical Journal*. **65**(1): 49-57.

Harris, T. F. W. 1972. Sources of the Agulhas Current in spring of 1964. Deep Sea Research. **19**: 633 – 650.

Hoguane, A. M. 2011. *Proceedings of the Joint Nansen-Tutu Scientific Opening Symposium and OceansAfrica Meeting,* Cape Town, 7 – 9 December 2010, pp. 31 – 38.

Hurlburt, H. E., Wallcraft, A. J., Schmitz Jr., W. J., Hogan, P. J. and Metzger, E. J. 1996. Dynamics of the Kuroshio/Oyashio current system using eddy-resolving models of the North Pacific Ocean. *Journal of Geophysical Research.* **101**(C1): 941 – 976.

Jochum, M. and Malanotte-Rizzoli, P. 2003. On the generation of North Brazil current rings. *Journal of Marine Research*. **61**: 147 – 173.

Krug, M. and Tournadre, J. 2012. Satellite observations of an annual cycle in the Agulhas Current. *Geophysical Research Letters*. **39**: L15607. doi:10.1029/2012GL052335.

Lee, T.N., Yoder, J.A. and Atkinson, L.P. 1991. Gulf Stream frontal eddy influence on productivity of the southeast U.S. continental shelf. *Journal of Geophysical Research*. **96**: 22191 – 22205.

Lutjeharms, J. R. E. 2001. Agulhas Current. In *Encyclopedia of Ocean Sciences.* Academic Press, San Diego. Steele, J. H. (Editor-in Chief). 104 – 113.

Lutjeharms, J. R. E. 2006. *The Agulhas Current*. New York: Springer – Verlag Berlin Heidelberg.

Lutjeharms, J. R. E. 2007. Three decades of research on the greater Agulhas Current. Ocean Science. **3**: 129 – 147.

Lutjeharms, J. R. E. and Ansorge, I. J. 2001. The Agulhas Return Current. *Journal of Marine Systems.* **30**: 115 – 138.

Lutjeharms, J. R. E., Boebel, O. and Rossby, H. T. 2003. Agulhas cyclones. *Deep Sea Research II.* **50**: 13 – 34.

Lutjeharms, J. R. E. and Connell, A.D. 1989. The Natal Pulse and inshore counter-currents off the South African east coast. *South African Journal of Science.* **85**: 533-535.

Lutjeharms, J. R. E. and de Ruijter, W.P. 1996. The influence of the Agulhas Current on the adjacent coastal ocean: possible impacts of climate change. *Journal of Marine Systems.* **7**: 321-336.

Lutjeharms, J. R. E., Monteiro, P.M.S., Tyson, P.D. and Obura, D. 2001. The oceans around southern Africa and regional effects of global change. *South African Journal of Science.* **97**: 119-130.

Lutjeharms, J. R. E. and Roberts, H.R. 1988. The Natal Pulse; an extreme transient on the Agulhas Current. *Journal of Geophysical Research.* **93**(1): 631 – 645.

Lutjeharms, J. R. E., Valentine, H. R. and Van Ballegooyen, R. C. 2000. The hydrography and water masses of the Natal Bight, South Africa. *Continental Shelf Research.* **20**: 1907 – 1939.

Lutjeharms, J. R. E. and van Ballegooyen, R. C. 1988. Anomalous upstream retroflection in the Agulhas Current, Science. *Science.* **240**: 1770–1772.

Mata, M. M., Wijffels, S. E., Church, J. A. and Tomczak, M. 2006. Eddy shedding and energy conversions in the East Australian current. *Journal of Geophysical Research.* **111**: C09034. doi:10.1029/2006JC003592.

McPhaden, M. J. 2009. RAMA report. *Proceedings of the 2009 Conference of the CLIVAR/GOOS Indian Ocean Panel (IOP-6),* St Denis, 3 – 5 June 2009. La Reunion.

McPhaden, M. J., Meyers, G., Ando, K., Masumoto, Y., Murty, V. S. N., Ravichandran, M., Syamsudin, F., Vialard, J., Yu, L. and Yu, W. 2009. RAMA: The Research Moored Array for African-Asian-Australian Monsoon Analysis and Prediction. *Bulletin of the American Meteorological Society.* **90**: 459 - 480.

Meyer, A. A., Lutjeharms, J. R. E. and De Villiers, S. 2002. The nutrient characteristics of the Natal Bight, South Africa. *Journal of Marine Systems.* **35**(1-2): 11 – 37.

Nauw, J., van Aken, H., Lutjeharms, J. R. E., de Ruijter, W. and Webb, A. 2008. Observations in the southern East Madagascar Current and Undercurrent system. Journal of Geophysical Research. **113**: C08006, doi:10.1029/2007JC004639.

Nittis, K., Perivoliotis, L., Korres, G., Tziavos, C. and Thanos, I. 2006. Operational monitoring and forecasting for marine environmental applications in the Aegean Sea. *Progress in Marine Environmental Modelling.* **21**(2): 243 – 257.

Oey, L. 1988. A model of Gulf Stream frontal instabilities, meanders and eddies along the continental slope. *Journal of Physical Oceanography.* **18**(2): 211 – 229.

Oke, P. R. and Griffin, D. A. 2011. The cold-core eddy and strong upwelling off the coast of New South Wales in early 2007. *Deep Sea Research II.* **58**: 574 – 591.

Pearce, A. F. 1977. Some features of the upper 500m of the Agulhas Current. *Journal of Marine Research.* **35**: 731 – 753.

Pearce, A. F. 1978. Seasonal variations of temperature and salinity on the northern Natal continental shelf. *South African Geophysical Journal.* **60**: 135 – 143.

Penven, P., Lutjeharms, J. R. E., Marchesiello, P., Roy, C. and Weeks, S. J. 2001. Generation of cyclonic eddies by the Agulhas current in the lee of the Agulhas bank. *Geophysical Research Letters.* **27**: 1055 – 1058.

Puryear, A., Burton, L. J., Lermusiaux, P. F. J. and Chan, V. W. S. 2009. Underwater acoustic sparse aperture system performance: using transmitter channel state information for multipath and interference rejection, *OCEANS 2009-EUROPE, 2009.*

Rao, E. P. R., Satyanarayana, B. V. and Nayak, S. 2008. Ocean data and information system (ODIS) and web based services. *The International Archives of the Photogrammetry, Remote Sensing and Spatial Information Sciences.* **37**(B4): 697 – 702.

Roberts, M. J., Share, A., Johnson, A., Brundrit, G., Hermes, J., Bornman, T., Ansorge, I., Stander, J., Vousden, D., Valentine, H. and Rossouw, M. 2011. *Proceedings of the Joint Nansen-Tutu Scientific Opening Symposium and OceansAfrica Meeting,* Cape Town, 7 – 9 December 2010, pp. 49 – 62.

Roberts, M. J., van der Lingen, C. D., Whittle, C. and van den Berg, M. 2010. Shelf currents, lee-trapped and transient eddies on the inshore boundary of the Agulhas Current, South Africa: their relevance to the Kwazulu-Natal sardine run. *African Journal of Marine Science.* **32**(2): 423 – 447.

Robinson, J., Gerry, C. and Bijoux, J. 2009. Establishment of the Seychelles Ocean Temperature monitoring Network (SOTN). Paper presented at the United Nations Framework Convention On Climate Change, February 2009.

Rouault, M. J., Johannessen, J., Collard, F. and Bernard, S. 2009. Synthetic Aperture Radar Products for the African Marine Environment. *South African Journal of Science*. **105**: 85 – 86.

Rouault, M. J. and Penven, P. 2011. New perspectives on Natal Pulses from satellite observations. *Journal of Geophysical Research*. **116** (C7).

Schumann, E. H. 1981. Low frequency fluctuations off the Natal coast. *Journal of Geophysical Research*. **86**: 6499-6508.

Schumann, E. H. 1982. Inshore circulation of the Agulhas Current off Natal. *Journal of Marine Research*. **40**: 43 – 55.

Schumann, E. H. 1987. The coastal ocean off the east coast of South Africa. *Transactions of the Royal Society of South Africa*. **46**(3): 215 – 229.

Schumann, E. H. 1988. Physical oceanography off Natal. *In*: Coastal Ocean Studies Off Natal, South Africa. Schumann, E. H. (ed). Springer-Verlag, New York.

Schumann, E. H. 1998. The coastal ocean off southeast Africa, including Madagascar – coastal segment. *In:* Robinson, A. R. and Brink, K. H. (eds). *The Sea*. **11**: 557 – 577.

Shillington, E. H. 1992. East Coast Oceanography. In *Proceedings of the 2nd Linefish Symposium (Fish, Fishers and Fisheries),* volume Special Publication No. 2. The Oceanographic Research Institute.

Singer, J. J., Atkinson, L. P., Blanton, J. O. and Yoder, J. A. 1983. Cape Romain and the Charleston bump: historical and recent hydrographic observations. *Journal of Geophysical Research*. **88**(C8): 4685 – 4698.

Song, H., Hodgkiss, W. S. and Kuperman, W. A. 2007. MIMO time reversal communications. *In Proceedings of WuWNet '07*, New York, NY, USA. ACM Press: 5 – 10.

Toole, J. M. and Warren, B. A. 1993. A hydrographic section across the subtropical South Indian Ocean. *Deep-Sea Research I*. **40**: 1973 – 2019.

Tsugawa, M. and Hasumi, H. 2010. Generation and growth mechanism of the Natal Pulse. *Journal of Physical Oceanography*. **40**: 1597 – 1612.

van Aken, H. M., Ridderinkhof, H. and de Ruijter, W. P. M. 2004. North Atlantic Deep Water in the south-western Indian Ocean. *Deep-Sea Research I*. **51**: 755 – 776.

van der Vaart, P. C. F. and de Ruijter W. P. M. 2001. Stability of western boundary currents with an application to pulselike behaviour of the Agulhas Current. *Journal of Physical Oceanography.* **31**: 2625 – 2644.

van Leeuwen, P.J., de Ruijter, W.P.M. and Lutjeharms, J.R.E. 2000. Natal pulses and the formation of Agulhas rings. *Journal of Geophysical Research.* **105**: 6425-6436.

Veitch, J. and Backeberg, B. 2011. *Proceedings of the Joint Nansen-Tutu Scientific Opening Symposium and OceansAfrica Meeting,* Cape Town, 7 – 9 December 2010, pp. 35 – 38.

Vousden, D., Scott, L. E. P., Sauer, W., Bornman, T., Ngoile, M., Stapley, J. and Lutjeharms, J. R. E. 2008. Establishing a basis for ecosystem management in the western Indian Ocean. *South African Journal of Science.* **104**: 417 – 420.

Wyrtki, K. 1971. Oceanographic atlas of the International Indian Ocean Expedition. National Science Foundation, Washington, D.C.